320567-1-F

320567-1-F = RL-2526

EFFECT OF AN INTRUDER ON A SECURITY SYSTEM

Final Report

1 January - 31 May 1977

By

C.-M. Chu and S. Cho

Radiation Laboratory
Department of Electrical and Computer Engineering
The University of Michigan
Ann Arbor, Michigan 48109

Submitted to:

OMNI SPECTRA, Inc.
Security Products
1040 West Alameda Drive
Tempe, Arizona 85282

September 1977

I. INTRODUCTION

The analysis of the effect of an intruder on a security system using parabolic antennas has been carried out by T.B.A. Senior*. In his analysis, the far field pattern of the antenna is used, and by simulating an intruder with a thin rectangular plate, the effect of the intruder on the received signal was computed and agreed fairly well with experimental results in the far zone region. In the present work, antennas with rectangular apertures are considered, and the analysis is extended to the near field region, i.e., when the intruder is relatively close to the transmitting antenna.

For definiteness we assume from the outset that the incident wave is horizontally polarized; that the transmitting and receiving antennas are identical at the same height above the ground; that the ground plane is smooth, level and nearly perfectly conducting at the operating frequency.

For our theoretical analysis we choose the type of antenna with the rectangular aperture, the dimension of which is such that its far field pattern width in the boresight plane is much wider than that in the horizontal plane. We assume that the aperture field has a cosine amplitude-taper.

The essense of the method we employ in this work is as follows. In order to be able to evaluate the field in a region relatively close to the antenna, we divide the antenna aperture into a number of cell apertures; the smaller the cell aperture, the smaller the minimum Fraunhofer distance. Once

---

*T.B.A. Senior, "Effect of an intruder on a security system", University of Michigan, Radiation Laboratory Report No. 348330-1-F, July 1975.

the cell size is determined, then we find the minimum Fraunhofer distance allowed for all the cells. We choose a point P, say, whose distance to the cells is greater than the above minimum Fraunhofer distance.

We can now find the field at P due to one cell aperture field by carrying out the Fraunhofer analysis. This in turn leads us to find the current density induced by one cell aperture field on the scattering object at P. From the current density, the scattered field at any point in the free space Q, say, can be obtained by use of the Franz's formula. The ground effect on the scattering can be obtained by the usual image method. This is the essense of our method.

In section 2 we define various geometric quantities involved. In section 3 we derive the near field pattern function of the antenna as well as the far field pattern. In section 4, we derive the scattered field in the free space without the presence of the ground. In section 5 we obtain the field sensed by the receiving antenna in the presence of the ground. In section 6 some numerical results are presented for the pattern and the normalized field defined in section 5 for a set of input data of our interest. Finally, we present our concluding remarks in section 7.

2. SCATTERING GEOMETRY AND ANTENNA APERTURE

We set the fixed rectangular coordinate system (X, Y, Z) such that the Z = 0 plane coincides with the ground plane and the transmitting and receiving antenna lies, respectively, in the X = 0 plane and the X = d plane. The rectangular aperture of the antenna is assumed to be such that its y-dimension is several times longer than its z-dimension. Let the y- and the z-dimension of the aperture be denoted by L and ℓ_z, respectively. We divide the aperture into (2N + 1) equal cell apertures, each of which is ℓ_y by ℓ_z. Clearly, $L = \ell_y(2N + 1)$ for some positive integer N. See Figures 1 and 2 for the antenna aperture and the general view of the scattering system.

We introduce the following notations for various geometric quantities of the antenna height, aperture, the reflecting plate and observation point:

$\bar{r}_1$ = The center of the transmitting antenna.

$\bar{r}_2$ = The center of the receiving antenna.

$\overset{y}{0}$ = The center of the reflecting rectangular plate.

$\bar{r}'$ = Arbitrary point on the reflecting rectangular plate.

$\bar{r}$ = An observation point in the free space.

For the nth cell aperture of the transmitting antenna, for $-N \leq n \leq N$,

$\bar{r}^o_n$ = The center of the nth cell aperture.

$\bar{r}^s_n$ = Arbitrary point on the nth cell aperture.

To be specific, we denote

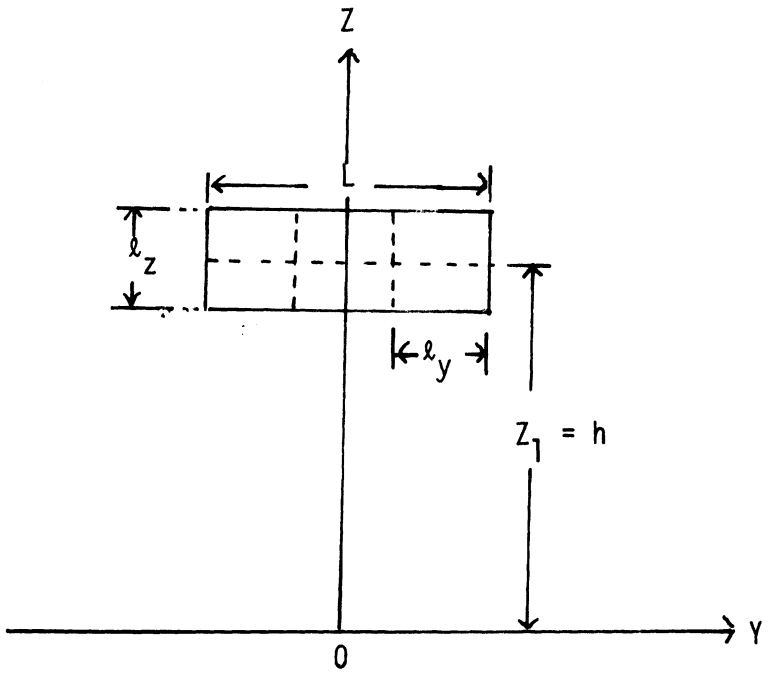

Figure 1. Antenna aperture with three ℓ_y X ℓ_z cells. The antenna is in the X = 0 plane.

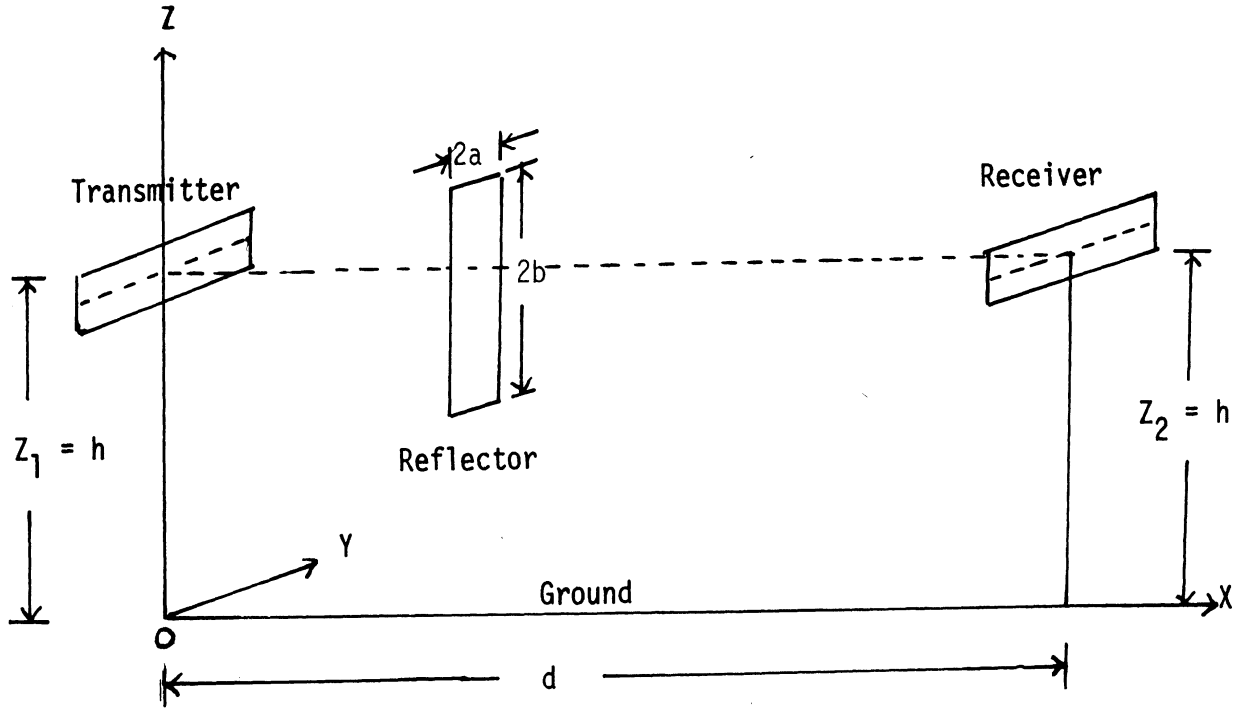

Figure 2. Cöordinate system and the general view of the scattering system.

$\bar{r}_1 = (o, o, z_1)$.

$\bar{r}_2 = (d, o, z_2)$.

$\overset{v}{0} = (x_o, y_o, z_o)$.

$\bar{r}' = (x_o, y', z')$.

$\bar{r} = (x, y, z)$.

$\bar{r}^o_n = (o, y^o_n, z_1)$.

$\bar{r}^s_n = (o, y^s_n, z^s)$.

Eventually we will set $z_1 = z_2 = h$. The y- and z-dimension of the reflecting retangular plate is denoted by 2a and 2b, respectively.

We also introduce the following notations denoting various distances:

$$R^o_n = |\bar{r}' - \bar{r}^o_n| = [x_o^2 + (y' - y^o_n)^2 + (z' - z_1)^2]^{1/2} .$$

$$\overset{vo}{R}_n = |\overset{v}{0} - \bar{r}^o_n| = [x_o^2 + (y_o - y^o_n)^2 + (z_o - z_1)^2]^{1/2} .$$

$$R^s_n = |\bar{r} - \bar{r}^s| = [x^2 + (y - y^s_n)^2 + (z - z^s)^2]^{1/2} .$$

$$R_2 = |\bar{r}_2 - \bar{r}'| = [(d - x_o)^2 + y'^2 + (z_2 - z')^2]^{1/2} .$$

$$\overset{vo}{R}_2 = |\bar{r}_2 - \overset{v}{0}| = [(d - x_o)^2 + y_o^2 + (z_2 - z_o)^2]^{1/2} .$$

We assume the following form of amplitude taper for the antenna:

$$A(y^s_n, z^s) = [1 + a_1 \cos\frac{\pi}{\ell_z}(z^s - z_1)]\,[1 + a_2 \cos(\frac{\pi y^s_n}{L})]. \qquad (1)$$

where a_1 and a_2 are some constants to be assigned. If the z-dimension of the antenna aperture is sufficiently small, then the aperture field over the z-dimension may be considered as uniform and one may then set $a_1 = 0$.

We note that, for all n, $-N \le n \le N$,

$$y^o_n = n\ell_y ,$$

$$-\ell_z/2 \le z^s - z_1 \le \ell_z/2,$$

$$-\ell_y/2 \le y^s_n - y^o_n \le \ell_y/2.$$

Therefore, if we define

$$\zeta = z^s - z_1, \qquad (2)$$

$$\eta_n = y^s_n - y^o_n, \qquad (3)$$

then

$$-\ell_z/2 \leq \zeta \leq \ell_z/2,$$

$$-\ell_y/2 \leq \eta_n \leq \ell_y/2.$$

For determination of the minimum Fraunhofer distance for the nth cell aperture, we write

$$R^s_n = R^o_n - \frac{\eta_n(y^s - y^o_n) + \zeta(z^s - z_1)}{R^o_n} + \frac{\eta_n^2 + \zeta^2}{2R^o_n} + \ldots$$

Then, for Fraunhofer analysis, we must require

$$\frac{2\ell^2}{\lambda} \lesssim R^o_n ,$$

where ℓ denotes the greater of ℓ_y, ℓ_z and λ the incident wavelength. For example, for $\lambda = 1.1214"$, $\ell_y = \ell_z = 4"$, we find $R^o_n \gtrsim 28.54"$. Then, similar restrictions must be applied to all the cell apertures.

If we place the reflecting rectangular plate so that $\bar{r}' = (x_o, y', z')$ is in the far zone for the nth cell, but in the near zone of the transmitting antenna, then the terms higher than the first order in y^s_n and z^s in R^s_n may be ignored for evaluation of the field at $\bar{r}'$. On the other hand, in evaluation of the scattered field due to the current induced on the reflecting plate at some point $\bar{r} = (x,y,z)$, the far zone criterion is determined by the linear dimension of the reflecting plate and the wavelength. For the typical rectangular plate we have in mind, the minimum Fraunhofer distance is in the orfer of 1,000 ft. for $\lambda = 1.1214"$. Therefore, the evaluation of the scattered field due to the reflecting plate does not permit us to employ the Fraunhofer analysis, but instead the Fresuel's analysis, since the antenna range of our interest does not exceed 500 ft.

Thus, in

$$R^o_n = x_o + \frac{(y' - y^o_n)^2 + (z' - z_1)^2}{2x_o} + \ldots , \tag{4}$$

$$R_2 = d - x_o + \frac{y'^2 + (z_2 - z')^2}{2(d-x_o)} , \tag{5}$$

for evaluation of the scattered field, we take the approximation of (4) and (5) as following:

as the distance factors,

$$R^o_n \simeq x_o,$$

$$R_2 \simeq d - x_o,$$

so that

$$\frac{1}{R^o_n R_2} \simeq \frac{1}{x_o(d - x_o)}; \tag{6}$$

on the other hand, as the phase factors, we need to retain up to the quadratic terms in y' and z'. When this is done, we find

$$k(R^o_n + R_z) \simeq kd + \frac{\pi}{\lambda d}(z_1 - z_2)^2 + \frac{\pi}{\lambda d}(y^o_n)^2 + q(z'-\delta)^2 + q(y' - \varepsilon_n)^2, \tag{7}$$

where

$$q = \frac{\pi d}{\lambda x_o(d - x_o)}, \tag{8}$$

$$\delta = z_1 - \frac{x_o}{d}(z_1 - z_2), \tag{9}$$

$$\varepsilon_n = y^o_n \left(1 - \frac{x_o}{d}\right), \quad -N \leq n \leq N. \tag{10}$$

In connection with the evaluation of the field pattern of the transmitting antenna, we define the elevation and the azimuth angles in the form

$$\sin\alpha'_n(\bar{r}') = \frac{z' - z_1}{R^o_n}, \tag{11}$$

$$\sin\beta'_n(\bar{r}') = \frac{y' - y^o_n}{R^o_n}. \tag{12}$$

As the point $\bar{r}'$ traverses the illuminated side of the reflecting plate, $\sin\alpha'_n(\bar{r}')$ and $\sin\beta'_n(\bar{r}')$ change accordingly. Now we make the key assumption that the variations of $\sin\alpha'_n(\bar{r}')$ and $\sin\beta'_n(\bar{r}')$ for all points of the reflecting plate are such that it is permissible to have $\{\sin\alpha'_n(\bar{r}')\}$ and $\{\sin\beta'_n(\bar{r}')\}$ be represented by a single $\sin\alpha_n$ and $\sin\beta_n$ of the "representative point" of all

the points on the plate, namely, $\overset{v}{0} = (x_o, y_o, z_o)$. In other words, we assume that

$$\sin\alpha'_n(\bar{r}') \simeq \sin\alpha_n \equiv \sin\alpha_n(\overset{v}{0}) = \frac{z_o - z_1}{R^{vo}_n} \tag{11-a}$$

$$\sin\beta'_n(\bar{r}') \simeq \sin\beta_n \equiv \sin\beta_n(\overset{v}{0}) = \frac{y_o - y_n}{R^{vo}_n} \quad . \tag{12-a}$$

The appropriateness of the above assumption clearly depends on the pattern function and the size of the reflecting plate. In other words, if the pattern does not radically vary over the reflecting plate, the assumption will be a valid one. Typically, the y-dimension of our reflecting plate is small compared with its z-dimension. Since the field pattern of the antenna we are considering here has a broad pattern width in the boresight plane, while the pattern width in the horizontal plane is narrow, the above assumption appears to be appropriate in the far zone. In the near zone, it is known in general that the near field pattern is more uniform than the far field pattern. In view of these observations, it seems that the above assumption is an acceptable one.

On the other hand, if the approximation (11-a) and (12-a) are not acceptable, then even within the framework of Fraunhofer analysis, the evaluation of the current density induced on the reflecting plate becomes quite involved and consequently a simple theoretical analysis which we have in mind is rendered impossible. Henceforth the elevation and the azimuth angles subtended by the points on the reflecting plate will be understood in the sense of equations (11-a) and (12-a), respectively.

For the receiving antenna which is sufficiently far from the rectangular plate, the elevation and the azimuth angles are given by

$$\sin\bar{\alpha} = \frac{z_o - z_2}{R^{vo}_2} , \tag{13}$$

$$\sin\bar{\beta} = \frac{y_o}{R^{vo}_2} , \tag{14}$$

$$R_o^{v\,2} = [(d - x_o)^2 + y_o^2 + (z_o - z_2)^2]^{1/2}.$$

We also introduce the following notations for later use; for the transmitting antenna,

$$Z_n = \frac{\pi \ell_z}{\lambda} \sin\alpha_n \equiv \frac{\pi \ell_z}{\lambda} \frac{z_o - z_1}{R_{o_n}^v}, \qquad -N \leq n \leq N \tag{15}$$

$$Y_n = \frac{\pi \ell_y}{\lambda} \sin\beta_n \quad \frac{\pi \ell_y}{\lambda} \frac{y_o - y_n^o}{R_{o_n}^v}; \tag{16}$$

for the receiving antenna,

$$\bar{Z} = \frac{\pi \ell_z}{\lambda} \sin\bar{\alpha} \equiv \frac{\pi \ell_z}{\lambda} \frac{z_o - z_2}{R_{o_2}^v}, \tag{17}$$

$$\bar{Y} = \frac{\pi L}{\lambda} \sin\bar{\beta} \quad \frac{\pi L}{\lambda} \frac{y_o}{R_{o_2}^v}. \tag{18}$$

Finally, we may now write R_n^s in the form

$$R_n^s \simeq R_n^o - (\zeta \sin\alpha_n + \eta_n \sin\beta_n). \tag{19}$$

3. FIELD PATTERNS

In this section we derive the near field pattern as well as the far field pattern. Dividing the transmitter aperture into cells, we choose an observation point $\bar{r} = (x,y,z)$ for the nth cell aperture such that

$$x \geq r_f ,$$

$$r_f \gtrsim \frac{2\ell^2}{\lambda} , \quad \ell \text{ being the greater of } \ell_y, \ell_z.$$

For the nth cell aperture, we consider the function

$$\psi_n(\bar{r}) = \iint_{\partial D_n} A(y^s_n, z^s) \frac{e^{ikR^s_n}}{R^s_n} dy^s_n \, dz^s, \quad -N \leq n \leq N \tag{20}$$

where ∂D_n denotes the area of the nth cell aperture and $A(y^s_n, z^s)$ is the amplitude tapering function given by equation (1). By use of equation (19), we write equation (20) in an approximate form as

$$\psi_n(\bar{r}) \underset{-N \leq n \leq N}{\simeq} \frac{e^{ikR^o_n}}{x_o} \int_{-\ell_z/2}^{\ell_z/2} d\zeta \, [1 + a_1 \cos(\tfrac{\pi\zeta}{\ell_z})] \, e^{-ik\zeta \sin\alpha_n}$$

$$\cdot \int_{-\ell_y/2}^{\ell_y/2} d\eta_n \, [1 + a_2 \cos\tfrac{\pi}{L}(\eta_n + y^o_n)] \, e^{-ik\eta_n \sin\beta_n} \tag{21}$$

$$\equiv \frac{e^{ikR^o_n}}{x_o} M_z(\alpha_n) \, M_y(\beta_n) , \tag{22}$$

where

$$M_z(\alpha_n) = \ell_z \left[\operatorname{sinc}(Z_n) + a_1 \frac{\pi}{2} \frac{\cos(Z_n)}{(\frac{\pi}{2})^2 - (Z_n)^2}\right] , \tag{23}$$

$$M_y(\beta_n) = \ell_y \left[\mathrm{sinc}(Y_n) + a_2 \frac{e^{i\frac{\pi}{L}y_0 n}}{2} \mathrm{sinc}\left(\frac{\pi \ell_y}{2L} - Y_n\right)\right.$$

$$\left. + a_2 \frac{e^{-i\frac{\pi}{L}y_0 n}}{2} \mathrm{sinc}\left(\frac{\pi \ell_y}{2L} + Y_n\right)\right] , \qquad (24)$$

$\mathrm{sinc}(u) = \sin(u)/u,$

$L = \ell_y (2N + 1), \; -N \leq n \leq N .$

The far field pattern can now be deduced from equations (23) and (24) as a special case. Thus, for $r \gtrsim R_f$, $R_f \gtrsim 2L^2/\lambda$,

$$r = \left[x^2 + y^2 + (z - z_1)^2\right]^{1/2} ,$$

we obtain

$$M_{zf}(\alpha) = \ell_z \left[\mathrm{sinc}(Z) + a_1 \frac{\pi}{2} \frac{\cos(Z)}{\left(\frac{\pi}{2}\right)^2 - (Z)^2}\right] , \qquad (25)$$

$$M_{yf}(\beta) = L \left[\mathrm{sinc}(Y) + a_2 \frac{\pi}{2} \frac{\cos(Y)}{\left(\frac{\pi}{2}\right)^2 - (Y)^2}\right] , \qquad (26)$$

where

$$Z = \frac{\pi \ell_z}{\lambda} \frac{z - z_1}{R} ,$$

$$Y = \frac{\pi L}{\lambda} \frac{y}{R} ,$$

$$R = \left[x^2 + y^2 + (z - z_1)^2\right]^{1/2} ,$$

$x \gtrsim R_f$.

In this far zone, a point in the boresight line of the antenna is $\bar{r} = (x, o, z_1 = z_2 = h)$, $x \gtrsim R_f$ and, at such point, equations (25) and (26) attain their maximum values. That is,

$$(M_{zf}(\alpha))_{max} = \ell_z \left(1 + a_1/\tfrac{\pi}{2}\right), \tag{25-a}$$

$$(M_{yf}(\beta))_{max} = L \left(1 + a_2/\tfrac{\pi}{2}\right) . \tag{26-a}$$

We define

$$P_{Mf} = (M_z)_{max} (M_y)_{max} = \ell_z L \left(1 + a_1/\tfrac{\pi}{2}\right) \left(1 + a_2/\tfrac{\pi}{2}\right). \tag{27}$$

Now, the normalized far field pattern of our antenna is defined by

$$P_f = M_{zf}(\alpha)\, M_{yf}(\beta)\, e^{ik(R-x)}/P_{Mf} , \tag{28}$$

where we imposed the condition that the maximum value of the far field pattern, P_f, be unity.

Let us now return to the derivation of the near field pattern of our antenna. From equation (22), we obtain the pattern function in the form

$$P_a = \frac{1}{P_{Mf}} \sum_{n=-N}^{N} M_z(\alpha_n)\, M_y(\beta_n)\, e^{ik(R_n^o - x)} \tag{29}$$

under the restriction

$$r_f \gtrsim \frac{2\ell^2}{\lambda} , \qquad \ell = \text{Max}\,(\ell_y, \ell_z),$$

$$x \gtrsim r_f .$$

The near field pattern (29) is computed for a set of variables and numerical results are presented in Section 6.1.

For later use, we define a quantity associated with equation (29) for the transmitting antenna. Thus

$$P_I(\alpha_n, \beta_n) = M_z(\alpha_n)\, M_y(\beta_n)/P_{Mf} \; ; \tag{30}$$

the corresponding quantity for the receiving antenna is

$$P_{II}(\bar{\alpha}, \bar{\beta}) = \bar{M}_z(\bar{\alpha})\, \bar{M}_y(\bar{\beta})/P_{Mf} \; , \tag{31}$$

where

$$\bar{M}_z(\bar{\alpha}) = \ell_z \left[\operatorname{sinc}(\bar{Z}) + a_1 \frac{\pi}{2} \frac{\cos(\bar{Z})}{(\frac{\pi}{2})^2 - (\bar{Z})^2} \right] , \tag{32}$$

$$\bar{M}_y(\bar{\beta}) = L \left[\operatorname{sinc}(\bar{Y}) + a_2 \frac{\pi}{2} \frac{\cos(\bar{Y})}{(\frac{\pi}{2})^2 - (\bar{Y})^2} \right] , \tag{33}$$

$$\bar{Z} = \frac{\pi \ell_z}{\lambda} \frac{Z - Z_2}{R_2} \; ,$$

$$\bar{Y} = \frac{\pi L}{\lambda} \frac{y}{R_2} \; ,$$

$$R_2 = [(d - x)^2 + y^2 + (Z_2 - Z)^2]^{1/2} \; .$$

4. SCATTERED E-FIELD IN THE FREE SPACE

We are now ready to derive the scattered field for the nth cell aperture field. Suppose a metallic rectangular plate of dimension 2a by 2b is placed in a far zone of the nth cell, but in a near zone of the whole antenna. By use of Ψ_n given by equation (22), we write the current density induced at $\bar{r}' = (x_o, y', z')$ on the reflecting plate in the form

$$\bar{J}_n(\bar{r}') = \hat{y}\, 2Y_o \frac{P_I(\alpha_n, \beta_n)}{x_o} e^{ikR_n^o} , \tag{34}$$

where $\hat{y}$ = unit vector in the Y direction,

$$Y_o = \sqrt{\frac{\varepsilon_o}{\mu_o}} = 1/Z_o .$$

Then, the scattered field at $\bar{r} = (x, y, z)$ in the free space is given by the Franz's formula which in our present case reduces to

$$\bar{E}_n^s(\bar{r}) = \frac{iZ_o}{4\pi k} \nabla \times \nabla \times \int\int_{\partial D_p} \bar{J}_n(\bar{r}') \frac{e^{ikR_2}}{R_2} dy'\, dz' , \tag{35}$$

where ∂D_p denotes the illuminated side of the metalic rectangular plate. Substituting (34) into (35) and carrying out the indicated differential operation, we obtain the approximate form

$$\bar{E}_n^s(\bar{r}) \simeq \hat{y} \frac{iq}{\pi d} P_I(\alpha_n, \beta_n) \int_{y_o-a}^{y_o+a} dy' \int_{z_o-b}^{z_o+b} dz'\, e^{ik(R_n^o + R_2)} . \tag{36}$$

Our next task is to carry out the integral in equation (36). For that purpose we employ the following form of the Fresnel's integral:

$$F(u) = \mathrm{sgn}(u)\frac{1}{\sqrt{2\pi}} \int_0^u \frac{e^{it}}{\sqrt{t}}\, dt$$

$$= \mathrm{sgn}(u)\sqrt{\frac{2}{\pi}} \int_0^{\sqrt{|u|}} e^{it^2}\, dt \qquad (37)$$

and, for notational convenience, suppress the signum henceforth. Then, by use of equation (7), Section 2, we find the scattered field at $\bar{r} = \bar{r}_2^{\,*} = (d, o, Z_2)$ in the free space in the form

$$\bar{E}_n^s(\bar{r}_2) \simeq \hat{y}\ \frac{e^{ikd}}{d} \cdot e^{i\frac{\pi}{\lambda d}(Z_1 - Z_2)^2} I_n(a)\, P_I(\alpha_n, \beta_n)\, I(b)\ , \qquad (38)$$

where

$$I_n(a) = \frac{i}{2} e^{i\frac{\pi}{\lambda d}(y_n^o)^2} \left\{ F[q(y_o + a - \varepsilon_n)^2] - F[q(y_o - a - \varepsilon_n)^2] \right\}, \qquad (39)$$

$$I(b) = F[q(Z_o + b + \delta)^2] - F[q(Z_o - b - \delta)^2]\ . \qquad (40)$$

Equation (38) represents the scattered electric field at $\bar{r}_2$ in the free space, due to the nth cell aperture field of the transmitting antenna. The scattered field at $\bar{r}_2$ due to the entire aperture field is then obtained by the linear superposition of the scattered fields due to the cell aperture field. That is:

---

* $\bar{r}_2$ is assumed to be in free space here.

$$\bar{E}^s(\bar{r}_2) = \sum_{n=-N}^{N} \bar{E}_n^s(\bar{r}_2)$$

$$= y \frac{e^{ikd}}{d} e^{i\frac{\pi}{\lambda d}} (Z_1 - Z_2)^2 \, I(b) \sum_{n=-N}^{N} I_n(a) P_I(\alpha_n, \beta_n) \, . \qquad (41)$$

In the next section, equation (41) will be specialized for various cases which arise in our scattering system. For that purpose, it will prove to be helpful to summarize the various quantities involved in equation (41). Thus,

$$\bar{r} = (x, y, z).$$

$$\bar{r}' = (x_o, y', z').$$

$$\bar{r}_n^{\,o} = (0, y_n^o, z_1).$$

$$\bar{r}_2 = (d, o, Z_2).$$

$$\bar{r}_o = (x_o, y_o, z_o).$$

$$R_n^{yo} = [x_o^2 + (y_o - y_n^o)^2 + (Z_o - Z_1)^2]^{1/2}. \quad -N \leq n \leq N$$

$$R_2^{yo} = [(d - x_o)^2 + y_o^2 + (Z_2 - Z_o)^2]^{1/2} \, .$$

$$q = \frac{\pi d}{\lambda x_o (d - x_o)} \, .$$

$$\delta = z_1 - \frac{x_o}{d} (z_1 - z_2) \, .$$

$$\epsilon_n = y_n^{\,o} (1 - \frac{x_o}{d}) \, , \quad -N \leq n \leq N$$

$$y_n^o = n\ell_y \, . \quad -N \leq n \leq N$$

$$L = \ell_y (2N + 1) \, .$$

$$\sin \alpha_n = \frac{z_o - z_1}{R_n^{yo}} \qquad -N \leq n \leq N$$

$$\sin \beta_n = \frac{y_o - y_n^{\,o}}{R_n^{yo}} \, .$$

$$Z_n = \frac{\pi \ell_z}{\lambda} \sin \alpha_n ,$$

$$-N \leq n \leq N$$

$$Y_n = \frac{\pi \ell_y}{\lambda} \sin \beta_n ,$$

$$\sin \bar{\alpha} = \frac{z_o - z_2}{R_2^{vo}} ,$$

$$\sin \bar{\beta} = \frac{y_o}{R_2^{vo}} ,$$

$$\bar{Z} = \frac{\pi \ell_z}{\lambda} \sin \bar{\alpha} ,$$

$$\bar{Y} = \frac{\pi L}{\lambda} \sin \bar{\beta} ,$$

$$P_{Mf} = \ell_z L \left(1 + a_1/\tfrac{\pi}{2}\right)\left(1 + a_2/\tfrac{\pi}{2}\right) ,$$

$$M_z(\alpha_n) = \ell_z \left[\operatorname{sinc}(Z_n) + a_1 \frac{\pi}{2} \frac{\cos(Z_n)}{(\frac{\pi}{2})^2 - (Z_n)^2} \right] ,$$

$$M_y(\beta_n) = \ell_y \left[\operatorname{sinc}(Y_n) + a_2 \frac{e^{i \frac{\pi}{L} y_n^o}}{2} \operatorname{sinc}\left(\frac{\pi \ell_y}{2L} - Y_n\right) \right.$$

$$\left. + a_2 \frac{e^{-i \frac{\pi}{L} y_n^o}}{2} \operatorname{sinc}\left(\frac{\pi \ell_y}{2L} + Y_n\right) \right] .$$

$$P_I(\alpha_n, \beta_n) = M_z(\alpha_n)\, M_y(\beta_n)/P_{Mf} , \qquad -N \leq n \leq N .$$

$$\bar{M}_z(\bar{\alpha}) = \ell_z \left[\operatorname{sinc}(\bar{Z}) + a_1 \frac{\pi}{2} \frac{\cos(\bar{Z})}{(\frac{\pi}{2})^2 - (\bar{Z})^2} \right],$$

$$\overline{M}_y(\overline{\beta}) = L\left[\operatorname{sinc}(\overline{Y}) + a_2 \frac{\pi}{2} \frac{\cos(\overline{Y})}{(\frac{\pi}{2})^2 - (\overline{Y})^2}\right] ,$$

$$P_{II}(\overline{\alpha}, \overline{\beta}) = \overline{M}_z(\overline{\alpha})\, \overline{M}_y(\overline{\beta})/P_{Mf} ,$$

$$I_n(a) = \frac{i}{2} e^{i \frac{\pi}{\lambda d} (y_n^o)^2} \left\{ F[q(y_o + a - \varepsilon_n)^2] - F[q(y_o - a - \varepsilon_n)]^2 \right\},$$

$$-N \leq n \leq a$$

$$I(b) = F[q(z_o + b - \delta)^2 - F[q(z_o - b - \delta)^2] .$$

It is instructive to note that, for the given antenna range and the reflector position, $I_n(a)$ depends only on the y coordinates of the cell apertures, the reflector and the y-dimension of the reflector, whereas I(b) depends only on the z-coordinates of the reflector, the z-dimension of the reflector and the antenna height. This means that it is only I(b), not $I_n(a)$, that changes its value for images of the transmitter and the reflector.

5. SCATTERING IN THE PRESENCE OF THE GROUND

The scattering system we wish to investigate in this section consists of a transmitting antenna and a receiving antenna (both assumed identical) positioned at the same height above the plane smooth ground and a metallic rectangular plate. Since the transmitter and the receiver are typically many wavelengths away from the reflector as well as the ground, the ordinary concept of the reflection coefficient applies and, therefore, we will employ the image method to account for the effect of the ground on the scattering. For horizontally polarized incident wave, we take the ground reflection coefficient as

$$\rho \simeq - 0.9472 \ . \tag{42}$$

Henceforth, we set $z_1 = z_2 = h$; since it is sufficient to consider the case of $y_0 \geq 0$ and $z_0 > 0$ by assumption, we note that all our geometric input data x_0, y_0, z_0, d and h are non-negative numbers.

5.1 Undisturbed Field

Let us first consider the field of the transmitter sensed by the receiver without being disturbed by the reflector.

The undisturbed field at the center of the receiving antenna $\bar{r}_2 = (d,o,h)$ due to the real transmitter aperture field can be obtained from

$$\bar{E}^i(\bar{r}_2) = - \hat{x} \times \hat{z} \, H_z(\bar{r}_2) \ ,$$

$$\bar{H}(\bar{r}_2) = \frac{1}{Y_o} \bar{J}(\bar{r}_2) , \qquad Y_o = \sqrt{\frac{\varepsilon_o}{\mu_o}} .$$

In view of the definition of the far field pattern, we obtain at once

$$\bar{E}^i(\bar{r}_2) = \hat{y} \frac{e^{ikd}}{d} . \tag{43}$$

We remark that, in the strict sense, equation (43) does not represent the electric field because it does not meet the physical dimensional requirement of the electric field. The dimensional discrepancy is due to the definition of ψ_n as given by equation (22). However, we are here concerned with the relative field variation caused by the presence of the scattering object and, therefore, the absolute sense of the physical dimension of the field is immaterial for our present purpose.

The undisturbed field at the receiving antenna due to the image transmitter can be found easily. Noting that $\bar{r}_1 = (0, 0, -h)$ and $\bar{r}_2 = (d, o, h)$, we find

$$\bar{E}_o^i(\bar{r}_2) \simeq \hat{y} \rho \frac{e^{ikd}}{d} \cdot e^{i \frac{4\pi}{\lambda d} h^2} \cdot (P_o^i)^2 , \tag{44}$$

where

$$P_o^i = \ell_z L(1 + a_2/\tfrac{\pi}{2}) \left[\operatorname{sinc}(Z_o^i) + a_1 \cdot \frac{\pi}{2} \cdot \frac{\cos(Z_o^i)}{(\frac{\pi}{2})^2 - (Z_o^i)^2} \right] / P_{Mf} , \tag{45}$$

$$Z_o^i = \frac{\pi \ell_z}{\lambda} \frac{2h}{\sqrt{(2h)^2 + d^2}} .$$

Therefore, the undisturbed field sensed by the receiving antenna is given by the sum of $\bar{E}^i(\bar{r}_2)$ and $\bar{E}_o^i(\bar{r}_2)$:

$$\bar{E}_t^i(\bar{r}_2) \simeq \hat{y}\ \frac{e^{ikd}}{d}\left[1 + \rho(P_o^i)^2\, e^{i\frac{4\pi}{\lambda d}h^2}\right]. \qquad (46)$$

Next, we will derive the scattered fields sensed by the receiving antenna.

5.2 Real Transmitter - Real Reflector - Receiver

In this case, $z_1 = h$, $z_2 = h$, $\overset{v}{0} = (x_o , y_o , z_o)$. From the list of the quantities summarized at the end of Section 4, we find

$$\delta = h ,$$

$$\sin \alpha_n^{(1)} = \frac{z_o - h}{(\overset{vo}{R}_n)_1} , \quad \sin \beta_n^{(1)} = \frac{y_o - y_n^o}{(\overset{vo}{R}_n)_1} , \quad -N \le n \le N$$

$$(\overset{vo}{R}_n)_1 = [x_o^2 + (y_o - y_n^o)^2 + (z_o - h)^2]^{1/2} ,$$

$$\sin \bar{\alpha}^{(1)} = \frac{z_o - h}{(\overset{vo}{R}_2)_1} , \quad \sin \bar{\beta}^{(1)} = \frac{y_o}{(\overset{vo}{R}_2)_1} ,$$

$$(\overset{vo}{R}_2)_1 = [(d - x_o)^2 + y_o^2 + (h - z_o)^2]^{1/2} ,$$

$$Z_n^{(1)} = \frac{\pi \ell_z}{\lambda} \sin \alpha_n^{(1)} , \quad Y_n^{(1)} = \frac{\pi \ell_y}{\lambda} \sin \beta_n^{(1)} , \quad -N \le n \le N ,$$

$$\bar{Z}^{(1)} = \frac{\pi \ell_z}{\lambda} \sin \bar{\alpha}^{(1)} , \quad \bar{Y}^{(1)} = \frac{\pi L}{\lambda} \sin \bar{\beta}^{(1)} ,$$

$$M_z^{(1)}(\alpha_n^{(1)}) = \ell_z \left[\operatorname{sinc}(Z_n^{(1)}) + a_1 \frac{\pi}{2} \frac{\cos(Z_n^{(1)})}{(\frac{\pi}{2})^2 - (Z_n^{(1)})^2}\right] ,$$

$$M_y^{(1)}\left(\beta_n^{(1)}\right) = \ell_y \left[\operatorname{sinc}\left(Y_n^{(1)}\right) + a_2 \frac{e^{i\frac{\pi}{L} y_n^o}}{2} \operatorname{sinc}\left(\frac{\pi \ell_y}{2L}\right) - Y_n^{(1)} \right.$$

$$\left. + a_2 \frac{e^{-i\frac{\pi}{L} y_n^o}}{2} \operatorname{sinc}\left(\frac{\pi \ell_y}{2L} + Y_n^{(1)}\right) \right] ,$$

$$P_I^{(1)}\left(\alpha_n^{(1)}, \beta_n^{(1)}\right) = M_z^{(1)} M_y^{(1)} / P_{Mf} , \quad -N \leq n \leq N \tag{47}$$

$$\bar{M}_z^{(1)}\left(\bar{\alpha}^{(1)}\right) = \ell_z \left[\operatorname{sinc}\left(\bar{Z}^{(1)}\right) + a_1 \frac{\pi}{2} \frac{\cos\left(\bar{Z}^{(1)}\right)}{\left(\frac{\pi}{2}\right)^2 - \left(\bar{Z}^{(1)}\right)^2} \right],$$

$$\bar{M}_y^{(1)}\left(\bar{\beta}^{(1)}\right) = L \left[\operatorname{sinc}\left(\bar{Y}^{(1)}\right) + a_2 \frac{\pi}{2} \frac{\cos\left(\bar{Y}^{(1)}\right)}{\left(\frac{\pi}{2}\right)^2 - \left(\bar{Y}^{(1)}\right)^2} \right],$$

$$P_{II}^{(1)}\left(\bar{\alpha}^{(1)}, \bar{\beta}^{(1)}\right) = \bar{M}_z^{(1)} \bar{M}_y^{(1)} / P_{Mf} , \tag{48}$$

$$I^{(1)}(b) = F\left[q(z_o + b - h)^2\right] J - F\left[q(z_o - b - h)^2\right] . \tag{49}$$

q, ε_n and $I_n(a)$ remain unchanged as in Section 4. The scattered field is then found to be

$$\vec{E}_1^s\left(\bar{r}_2\right) \simeq \hat{y} \frac{e^{ikd}}{d} P_{II}^{(1)} I^{(1)}(b) \sum_{n=-N}^{N} I_n(a) P_I^{(1)}\left(\alpha_n^{(1)}, \beta_n^{(1)}\right) . \tag{50}$$

5.3 Real Transmitter - Image Reflector - Receiver

$$z_{o1} = h , \quad z_2 = h , \quad \overset{\vee}{0} = (x_o , y_o , -z_o) ;$$

$$\delta = h .$$

$$\sin \alpha_n^{(2)} = -\frac{z_o + h}{(R_n^{vo})_2} \quad , \quad \sin \beta_n^{(2)} = \frac{y_o - y_n^o}{(R_n^{vo})_2} \quad , \quad -N \leq n \leq N$$

$$(R_n^{vo})_2 = [\, x_o^2 + (y_o - y_n^o)^2 + (z_o + h)^2]^{1/2} \quad ,$$

$$\sin \bar{\alpha}^{(2)} = -\frac{z_o + h}{(R_n^{vo})_2} \quad , \quad \sin \bar{\beta}^{(2)} = \frac{y_o}{(R_2^{vo})_2} \quad ,$$

$$(R_2^{vo})_2 = [(d - x_o)^2 + y_o^2 + (h + z_o)^2\,]^{1/2} \quad ,$$

$$Z_n^{(2)} = \frac{\pi \ell_z}{\lambda} \sin \alpha_n^{(2)} \quad , \quad Y_n^{(2)} = \frac{\pi \ell_y}{\lambda} \sin \beta_n^{(2)} \quad , \quad -N \leq n \leq N \quad ,$$

$$\bar{Z}^{(2)} = \frac{\pi \ell_z}{\lambda} \sin \bar{\alpha}^{(2)} \quad , \quad \bar{Y}^{(2)} = \frac{\pi L}{\lambda} \sin \bar{\beta}^{(2)} \quad ,$$

$$M_z^{(2)}(\alpha_n^{(2)}) = \ell_z \left[\operatorname{sinc}(Z_n^{(2)}) + a_1 \frac{\pi}{2} \frac{\cos(Z_n^{(2)})}{(\frac{\pi}{2})^2 - (Z_n^{(1)})^2} \right],$$

$$M_y^{(2)}(\beta_n^{(2)}) = \ell_y \left[\operatorname{sinc}(Y_n^{(2)}) + a_2 \frac{e^{i\frac{\pi}{L} y_n^o}}{2} \operatorname{sinc}(\frac{\pi \ell_y}{2L} - Y_n^{(2)}) \right.$$

$$\left. + a_2 \frac{e^{-i\frac{\pi}{L} y_n^o}}{2} \operatorname{sinc}(\frac{\pi \ell_y}{2L} + Y_n^{(2)}) \right], \quad -N \leq n \leq N$$

$$P_I^{(2)}(\alpha_n^{(2)}, \beta_n^{(2)}) = M_z^{(2)} M_y^{(2)} / P_{Mf} \quad , \quad -N \leq n \leq N \qquad (51)$$

$$\bar{M}_z^{(2)}(\bar{\alpha}^{(2)}) = \ell_z \left[\operatorname{sinc}(\bar{Z}^{(2)}) + a_1 \frac{\pi}{2} \frac{\cos(\bar{Z}^{(2)})}{(\frac{\pi}{2})^2 - (\bar{Z}^{(2)})^2} \right],$$

$$\bar{M}_y^{(2)}\left(\bar{\beta}^{(2)}\right) = L\left[\operatorname{sinc}\left(\bar{\gamma}^{(2)}\right) + a_2 \frac{\pi}{2} \frac{\cos\left(\bar{\gamma}^{(2)}\right)}{\left(\frac{\pi}{2}\right)^2 - \left(\bar{\gamma}^{(2)}\right)^2}\right],$$

$$P_{II}^{(2)}\left(\bar{\alpha}^{(2)}, \bar{\beta}^{(2)}\right) = \bar{M}_z^{(2)}\, \bar{M}_y^{(2)}/P_{Mf}\,, \tag{52}$$

$$I^{(2)}(b) = F\left[q(-z_o + b - h)^2\right] - F\left[q(-z_o - b - h)^2\right], \tag{53}$$

Now the scattered field is given by

$$\bar{E}_2^s\left(\bar{r}_2\right) \simeq \hat{y}\, \rho^2\, \frac{e^{ikd}}{d} P_{II}^{(2)}(b)\, I^{(2)}(b) \sum_{n=-N}^{N} I_n(a)\, P_I^{(2)}\left(\alpha_n^{(2)}, \beta_n^{(2)}\right). \tag{54}$$

5.4 Image Transmitter - Real Reflector - Receiver

$$z_1 = -h\,, \quad z_2 = h\,, \quad \overset{v}{0} = (x_o\,, y_o\,, z_o)\,.$$

We find that

$$\delta = -\hat{\delta}\,, \quad \text{where}$$

$$\hat{\delta} = h\left(1 - \frac{2x_o}{d}\right); \tag{55}$$

$$\sin \alpha_n^{(3)} = \frac{z_o + h}{\left(R_n^{vo}\right)_2} = -\sin \alpha_n^{(2)}\,,$$

$$-N \leq n \leq N$$

$$\sin \beta_n^{(3)} = \sin \beta_n^{(2)}\,,$$

$$\sin \bar{\alpha}^{(3)} = \sin \bar{\alpha}^{(1)}\,, \quad \sin \bar{\beta}^{(3)} = \sin \bar{\beta}^{(1)}\,,$$

$$M_z^{(3)}(\alpha_n^{(3)}) = M_z^{(2)}(\alpha_n^{(2)}) ,$$

$$M_y^{(3)}(\beta_n^{(3)}) = M_y^{(2)}(\beta_n^{(2)}) ,$$

$$P_I^{(3)}(\alpha_n^{(3)}, \beta_n^{(3)}) = P_I^{(2)}(\alpha_n^{(2)}, \beta_n^{(2)}) , \tag{56}$$

$$\bar{M}_z^{(3)}(\bar{\alpha}^{(3)}) = \bar{M}_z^{(1)}(\bar{\alpha}^{(1)}) ,$$

$$\bar{M}_y^{(3)}(\bar{\beta}^{(3)}) = \bar{M}_y^{(1)}(\bar{\beta}^{(1)}) ,$$

$$P_{II}^{(3)}(\bar{\alpha}^{(3)}, \bar{\beta}^{(3)}) = P_{II}^{(1)}(\bar{\alpha}^{(1)}, \bar{\beta}^{(1)}) , \tag{57}$$

$$I^{(3)}(b) = F[q(z_o + b + \hat{\delta})^2] - F[q(z_o - b + \hat{\delta})^2]. \tag{59}$$

The scattered field is

$$\bar{E}_3^s(\bar{r}_2) \simeq \hat{y}\, \rho\, \frac{e^{ikd}}{d}\, e^{i\frac{4\pi}{\lambda d}h^2}\, P_{II}^{(1)}\, I^{(3)}(b) \sum_{n=-N}^{N} I_n(a)\, P_I^{(2)}(\alpha_n^{(2)}, \beta_n^{(2)}) . \tag{60}$$

5.5 Image Transmittor - Image Reflector - Receiver

$$z_1 = h , \quad z_2 = h , \quad \overset{v}{0} = (x_o , y_o , -z_o) .$$

$$\delta = -\hat{\delta} ,$$

$$\sin \alpha_n^{(4)} = - \frac{z_o - h}{(R_n^{v_o})_1} = - \sin \alpha_n^{(1)} ,$$

$$-N \leq n \leq N$$

$$\sin \beta_n^{(4)} = \sin \beta_n^{(1)} ,$$

$$\sin \bar{\alpha}^{(4)} = \sin \bar{\alpha}^{(2)} , \quad \sin \bar{\beta}^{(4)} = \sin \bar{\beta}^{(2)} ,$$

$$M_z^{(4)} (\alpha_n^{(4)}) = M_z^{(1)} (\alpha_n^{(1)}) ,$$

$$-N \leq n \leq N$$

$$M_y^{(4)} (\beta_n^{(4)}) = M_y^{(1)} (\beta_n^{(1)}) ,$$

$$P_I^{(4)} (\alpha_n^{(4)} , \beta_n^{(4)}) = P_I^{(1)} (\alpha_n^{(1)}, \beta_n^{(1)}) ; \tag{61}$$

$$\bar{M}_z^{(4)} (\bar{\alpha}^{(4)}) = \bar{M}_z^{(2)} (\bar{\alpha}^{(2)}) ,$$

$$M_y^{(4)} (\bar{\beta}^{(4)}) = \bar{M}_y^{(2)} (\bar{\beta}^{(2)}) ,$$

$$P_{II}^{(4)} (\bar{\alpha}^{(4)}, \bar{\beta}^{(4)}) = P_{II}^{(2)} (\bar{\alpha}^{(2)}, \bar{\beta}^{(2)}) , \tag{62}$$

$$I^{(4)}(b) = F [q(-z_o + b + \hat{\delta})^2] - F [q(-z_o - b + \hat{\delta})^2] . \tag{63}$$

The scattered field is

$$\bar{E}_4^s (\bar{r}_2) \simeq \hat{y} \rho \frac{e^{ikd}}{d} e^{i\frac{4\pi}{\lambda d} h^2} P_{II}^{(2)} I^{(4)}(b) \sum_{n=-N}^{N} I_n(a) P_I^{(1)} (\alpha_n^{(1)}, \beta_n^{(1)}) . \tag{64}$$

5.6 Normalized Field

We have obtained the scattered electric field for four different combinations of the transmitters and reflectors. The total scattered field is the sum of these. That is,

$$\bar{E}_t^s(\bar{r}_2) = \sum_{n=1}^{4} \bar{E}_n^s(\bar{r}_2)$$

$$= \hat{y}\,\frac{e^{ikd}}{d}\left\{ P_{II}^{(i)} \sum_{n=-N}^{N} I_n(a)\left[P_I^{(1)}\, I^{(1)}(b) + \rho\, e^{i\frac{4\pi}{\lambda d}h^2} P_I^{(2)} I^{(3)}(b)\right]\right.$$

$$\left. + \rho\; P_{II}^{(2)} \sum_{n=-N}^{N} I_n(a)\left[\rho\, P_I^{(2)} I^{(2)}(b) + e^{i\frac{4\pi}{\lambda d}h^2} P_I^{(1)} I^{(4)}(b)\right]\right\} \quad . \qquad (65)$$

An examination of the form of equation (65) shows that, for computation of the total scattered field, we need to evaluate the following quantities for each given position of the reflector and the antenna range:

$$\{I_n(a)\} \quad , \qquad -N \le n \le N \quad \text{once for all 4 cases ,}$$

$$\left.\begin{array}{l} P_I^{(1)} \;,\; P_I^{(2)} \;, \\ \\ P_{II}^{(1)} \;,\; P_{II}^{(2)} \;, \end{array}\right\} \quad -N \le n \le N$$

$$I^{(1)}(b) \;,\; I^{(2)}(b) \;,\; I^{(3)}(b) \;, I^{(4)}(b) \;.$$

Having obtained the total undisturbed field and the total scattered field, the total electric field sensed by the receiving antenna is the sum of these. In order to obtain the effect of the scattering object on the undisturbed field, we evaluate the normalized field:

$$\left|\bar{E}_N\ (\bar{r}_2)\right|^2 = \left|1 + \bar{E}_t^s\ (\bar{r}_2)/\bar{E}_t^i\ (\bar{r}_2)\right|^2 . \qquad (66)$$

Equation (66) will be computed for the following set of data:

(1) λ : incident wavelength

(2) h, d : antenna height, range

(3) ℓ_z, L : antenna paerture dimension

(4) 2N + 1 : total number of cell apertures

(5) ℓ_y : y-dimension of the cell aperture, $\ell_y = L/(2N + 1)$

(6) a_1, a_2 : aperture tapering parameters.

(7) a, b : reflector plate half dimension

(8) (x_o , y_o , z_o) : center coordinates of the reflector plate. The minimum allowable x_o is restricted by

$$x_o \gtrsim \frac{2\ell^2}{\lambda} , \quad \ell = \text{Max}\ (\ell_y , \ell_z).$$

6. NUMERICAL RESULTS

In this section we present some sample numerical results for the pattern and the normalized field. Throughout the section, we assume that

λ = 1.1214 inches,

ρ = -0.9472,

polarization = horizontal,

h = 30 inches.

6.1 Antenna Patterns

We have computed the near field patterns as well as the far field patterns for two antennas, the Antenna-I and Antenna-II:

Antenna-I	Antenna-II
L = 12"	L = 15"
ℓ_z = 4"	ℓ_z = 3" ,

10 dB cosine amplitude taper is assumed across L.

The knowledge of the antenna pattern is necessary not only for evaluation of the current density which the antenna aperture field induces on the scattering object, but also for the determination of the ability of the receiving antenna to sense the scattered field in the given direction. The pattern

function Pa, equation (29), was derived by synthesis of the fields due to the cell aperture fields. The far field pattern, P_f, equation (28), was also derived independently by taking the antenna aperture as a whole. It follows then that, in the far zone, the pattern described by equation (29), Pa, should agree with the pattern described by equation (28). It also follows that, at a point in the near zone, determined by the cell aperture size, the pattern described by equation (29), Pa, should agree with another pattern Pa which is obtained with an smaller cell aperture size. To see this, we divide Antenna-I and Antenna-II into two different ways:

Antenna-I (3)	Antenna-I (5)
ℓ_z = 4"	ℓ_z = 4"
ℓ_y = 4"	ℓ_y = 2.4"
L = 12"	L = 12"
NC = 3	NC = 5 ,

where NC denotes the number of cells; similarly,

Antenna-II (5)	Antenna-II (7)
ℓ_z = 3"	ℓ_z = 3"
ℓ_y = 3"	ℓ_y = 2.14"
L = 15"	L = 15"
NC = 5	NC = 7 .

Figures PA-1 and PA-2 represent, respectively, the near field pattern (x_0 = 28.54" - plane) on the E- and H-plane for Antenna-I (3). The solid curve is our near field pattern, Pa. The dotted curve representing P_f (equation (28)) on the x_0 = 28.54" - plane is superimposed here to show the degree of discrepancy between Pa and P_f in this near zone. Needless to say, P_f is not valid in the near zone.

It is seen that the near field pattern strength decreases to one-half of its maximum value at x_0 = 28.54", z = 30" at

$$\beta \simeq 9^0 \quad \text{in the E-plane,}$$
$$\alpha \simeq 11^0 \quad \text{in the H-plane.}$$

Considering the aperture dimension of 12" in the E-plane and 4" in the H-plane, we observe that the pattern widths in both planes do not differ as much as the far field pattern widths would.

It is also seen that the near field pattern strength is weaker, but more uniform, than that of the far field pattern.

Figures PA-3 and PA-4 represent the far field pattern (x_0 = 260" - plane). We note the close agreement between the patterns described by equation (29) and equation (28), as they should. We see that the far field pattern strength decreases to one-half of its maximum strength at

$$\beta \simeq 4^0 \quad \text{in the E-plane,}$$
$$\alpha \simeq 9.5^0 \quad \text{in the H-plane,}$$

showing the narrower pattern width in the E-plane as expected.

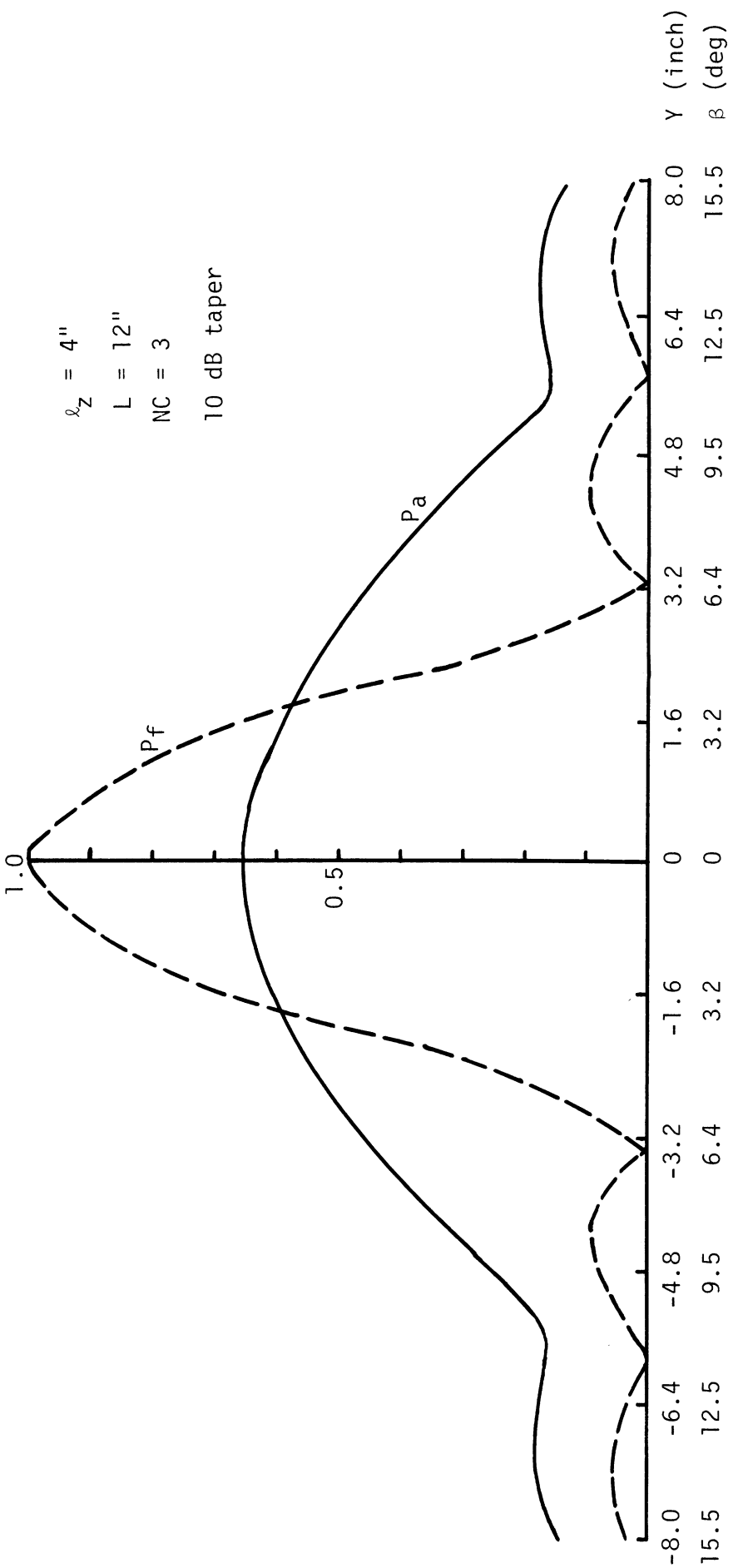

Figure PA-1 Near field pattern on E-plane (z = 30", x = 28.54").

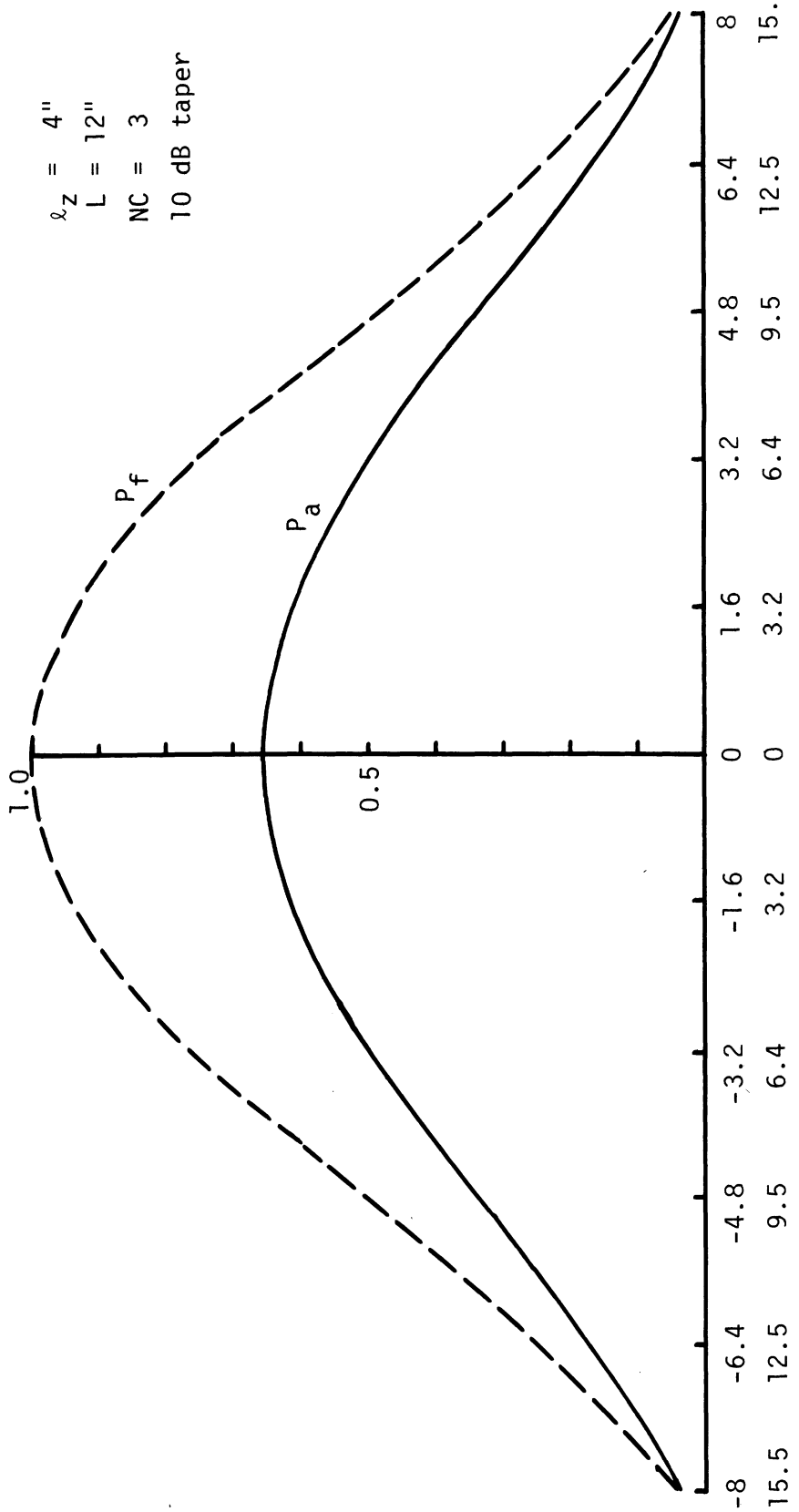

Figure PA-2: Near field pattern on H-plane (Y = 0, x = 28.54").

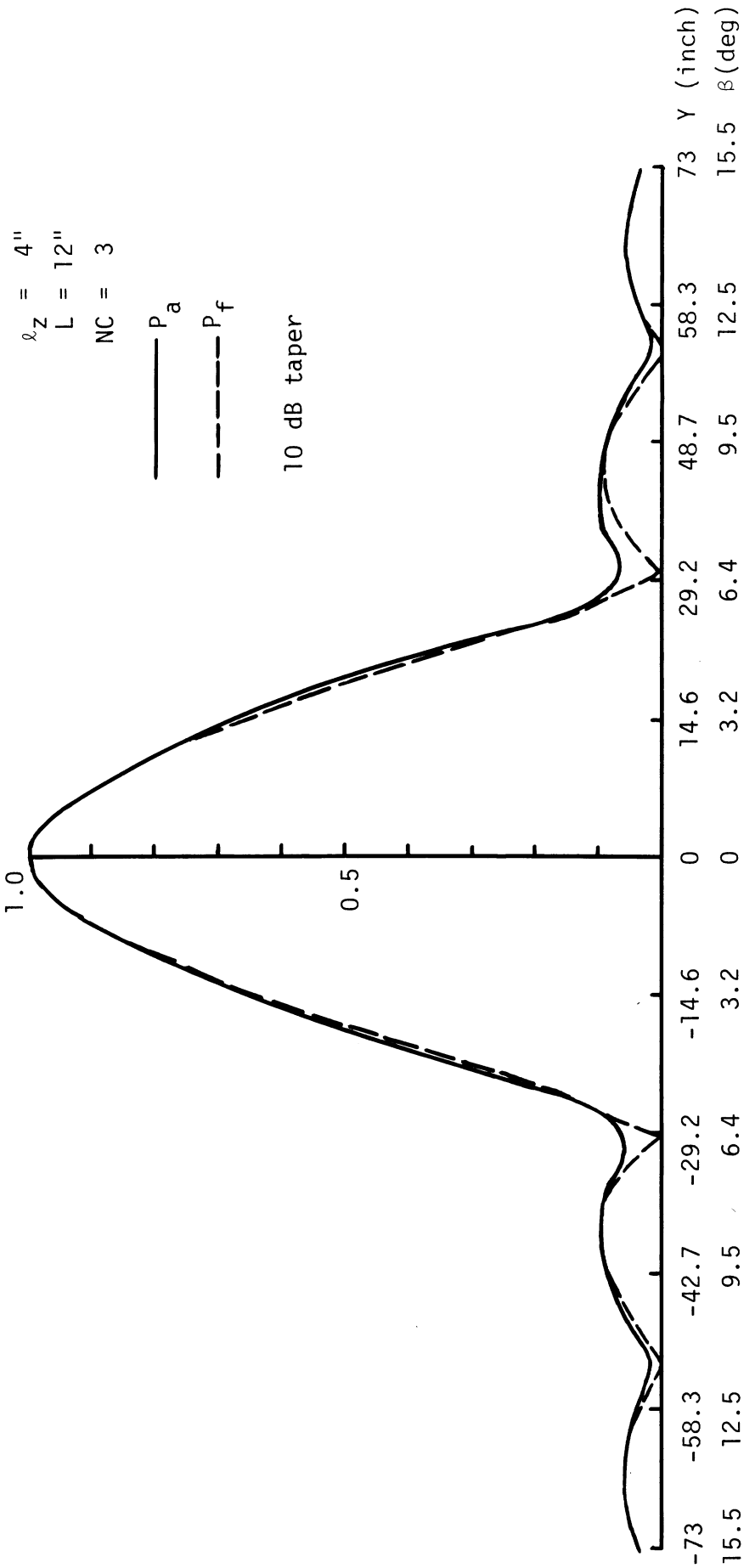

Figure PA-3: Far field pattern on E-plane (z = 30", x = 260").

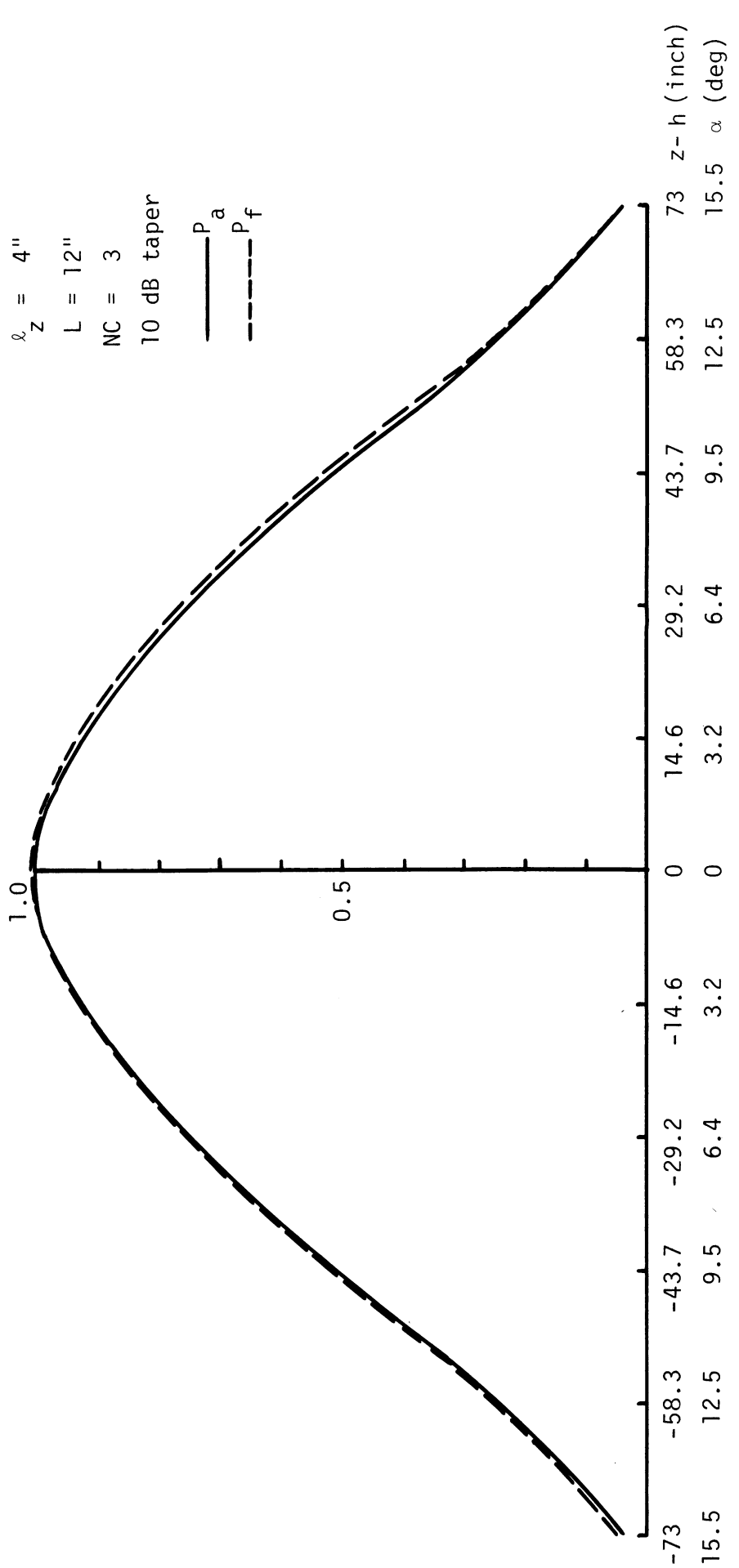

Figure PA-4: Far field patterns on H-plane (Y = 0, x = 260").

Figures PA-5 and PA-6 compare the near field patterns of Antenna-I (3) and Antenna-I (5) on the x_0 = 28.54" - plane. Note the close agreement. Figures PA-7 and PA-8 represent the near field patterns of Antenna-II (5) and Antenna-II (7) on the x_0 = 401" - plane. Again the agreement is excellent.

Figures PA-9 and PA-10 represent the far field pattern of Antenna-II. The far field patterns of Antenna-II (5), Antenna-II (7) and the pattern described by equation (28) agree so closely that we represented the far field patterns of these three by one of these only.

We note that the near field pattern of Antenna-II is quite uniform, but its strength is about 4/10 of the maximum far field pattern strength.

Based on these numerical results, we are led to the following observations for the near field pattern:

(a) For a given antenna aperture, the near field pattern is more uniform than the far field pattern both in the E- and H-plane;

(b) the near field pattern strength is weaker than that of the far field pattern;

(c) the greater the ratio L/ℓ_z of the antenna aperture, the more enhanced the effects of (a) and (b).

The observation of the weak pattern strength in the near field leads us to suspect that it is probably difficult to detect a relatively small scattering object in the near zone. Since enhanced amplitude taper does not

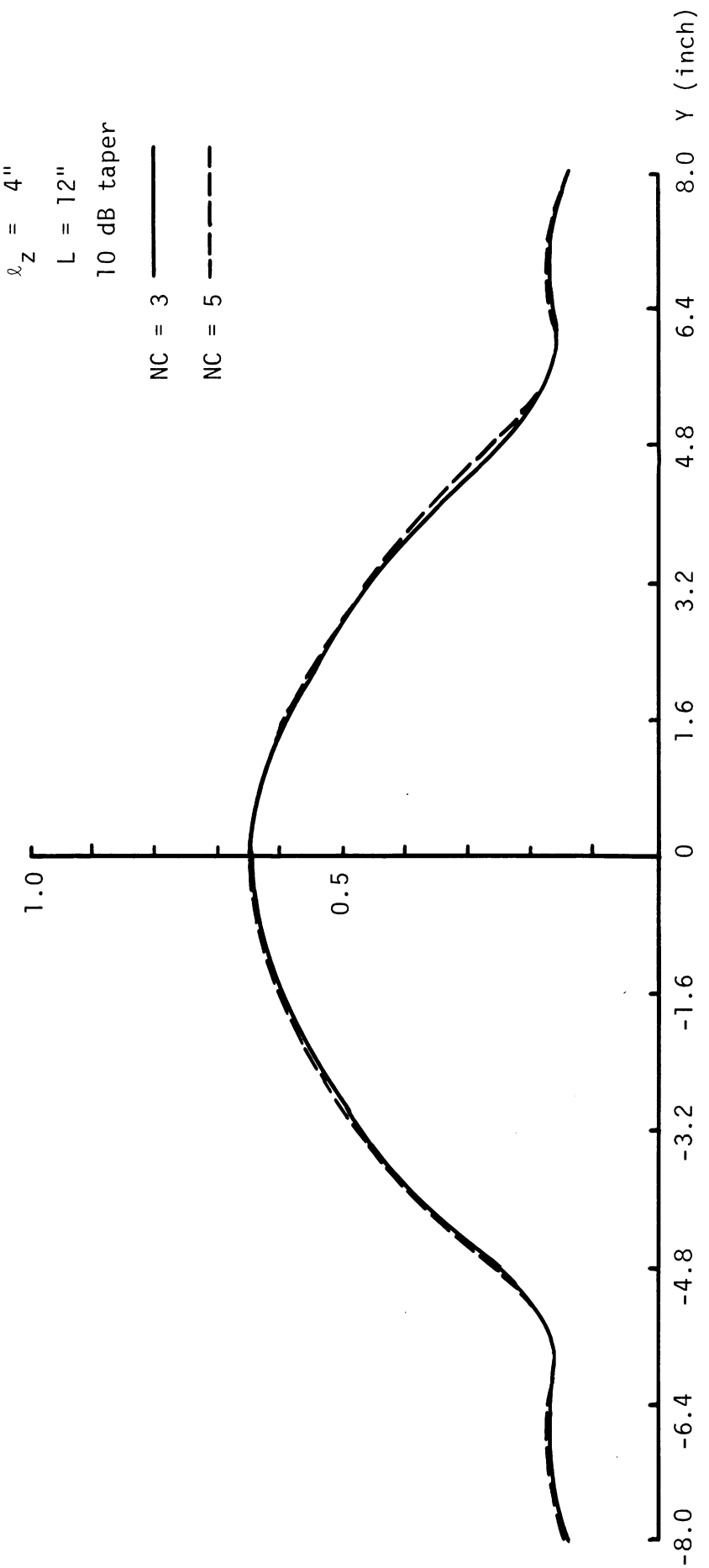

Figure PA-5: Effect of cell sizes on near field patterns on E-plane (z = 30", x = 28.54").

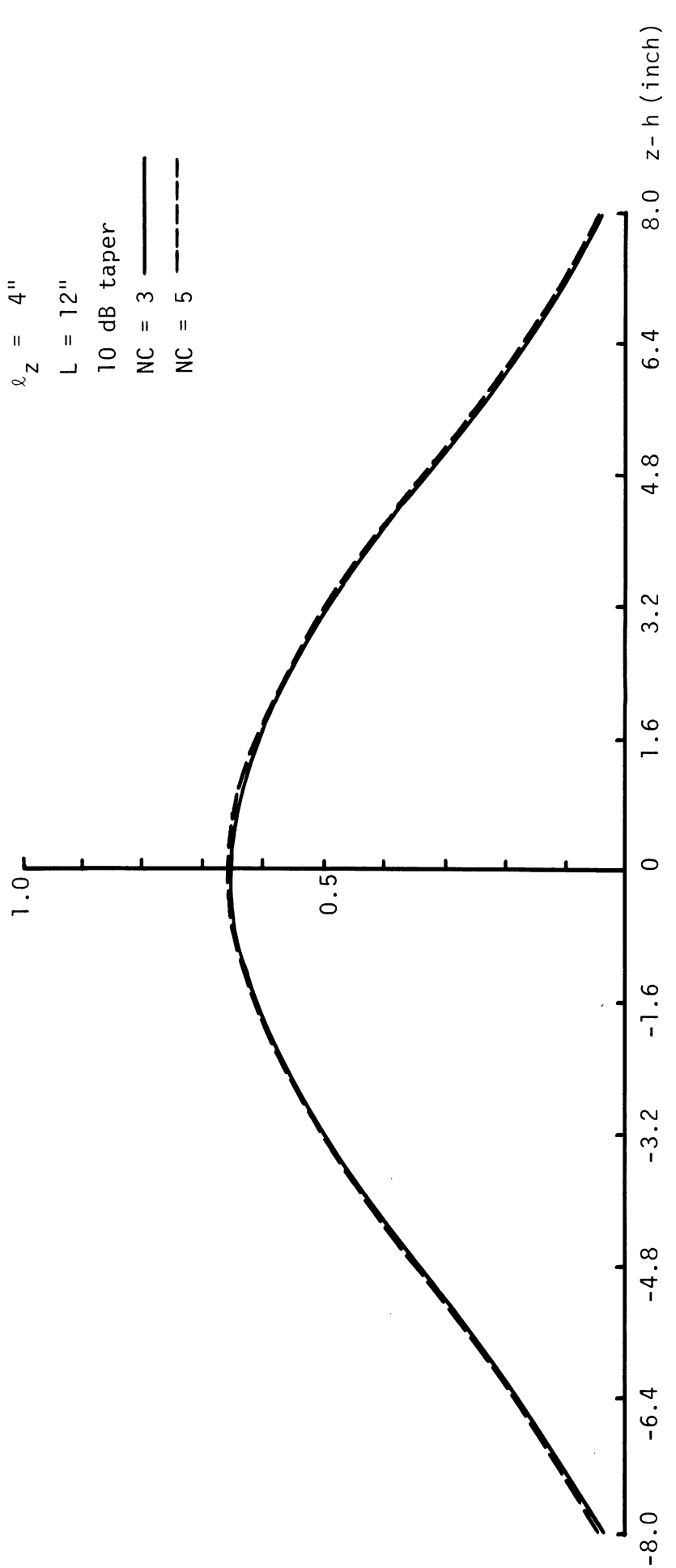

Figure PA-6: Effect of cell sizes on near field patterns on H-plane (z = 30", Y = 0).

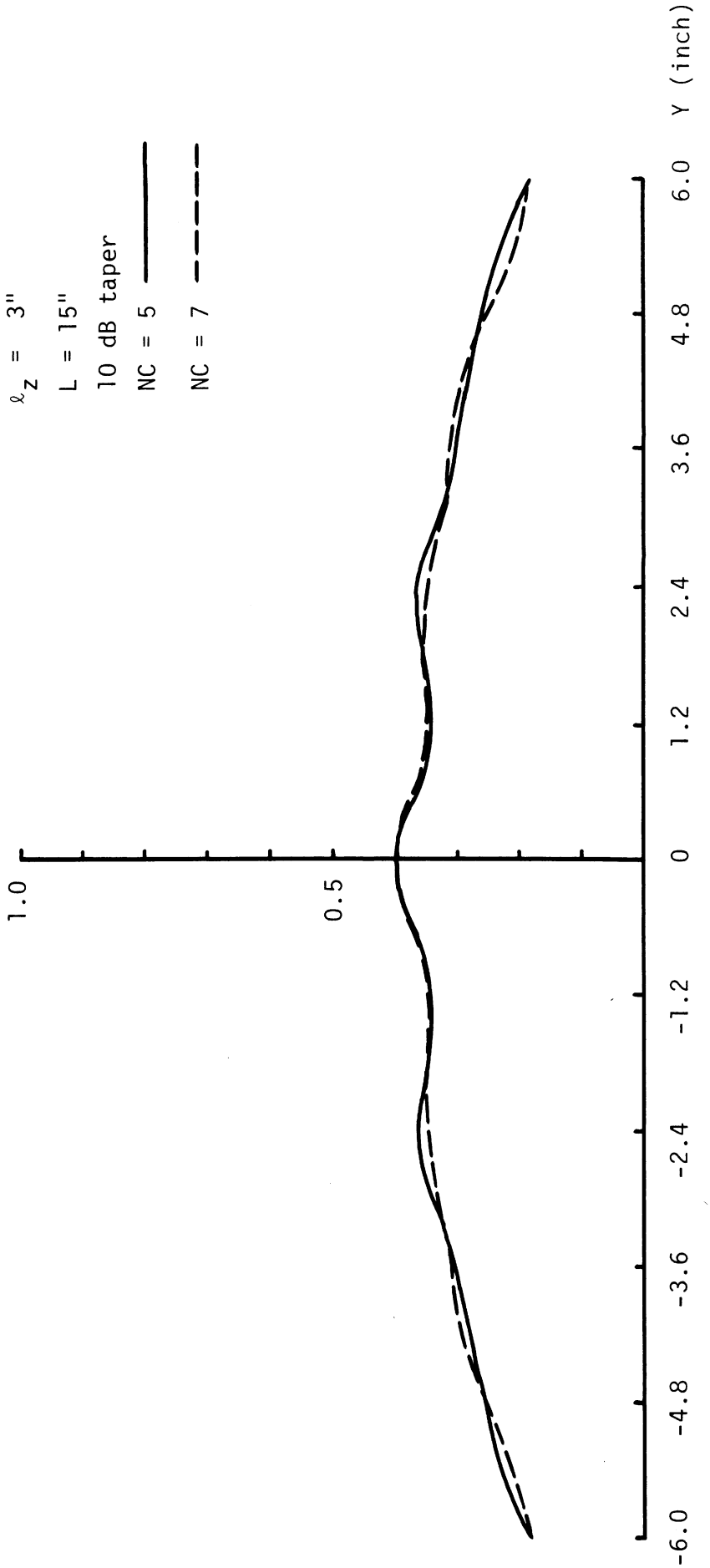

Figure PA-7: Effect of cell sizes on near field patternsn on E-plane (z = 30", x = 16.05").

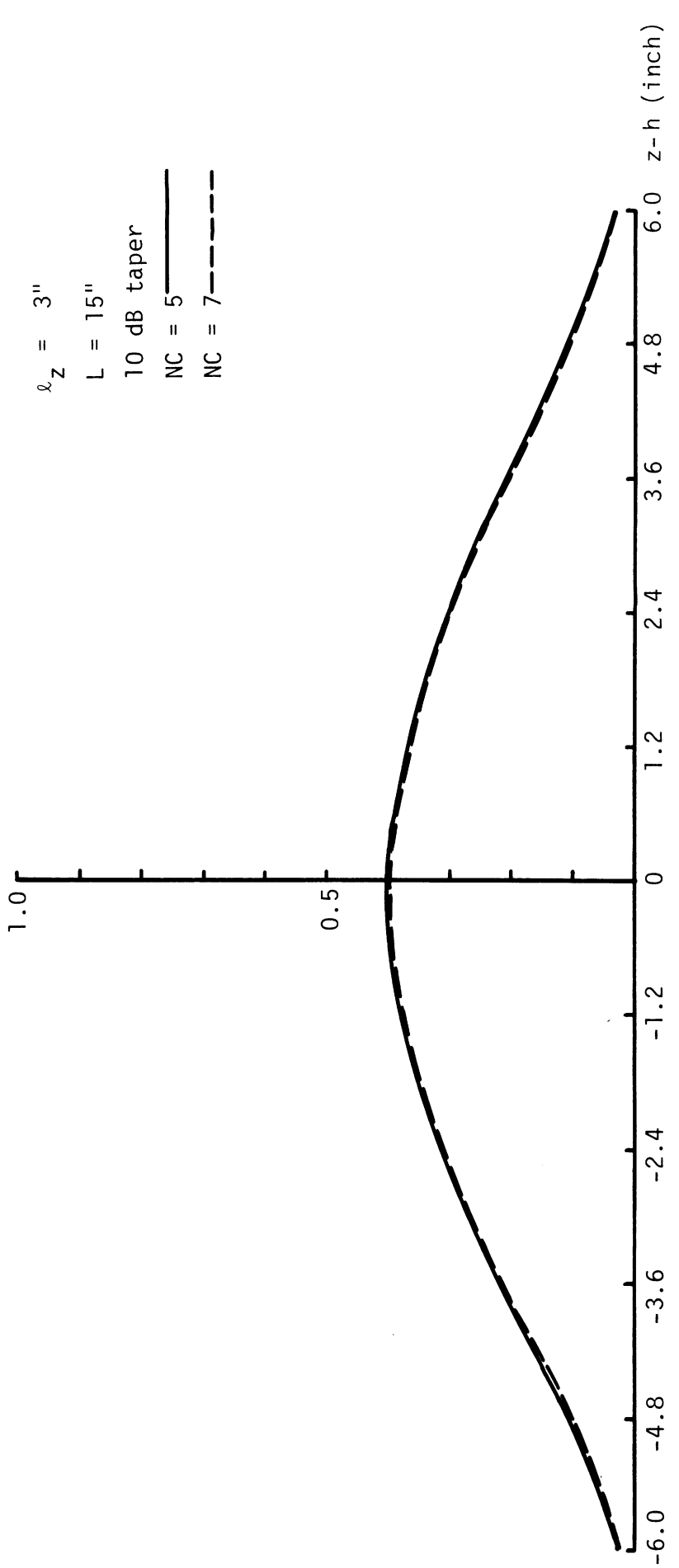

Figure PA-8: Effect of cell sizes on near field patterns on H-plane (z = 30", Y = 0).

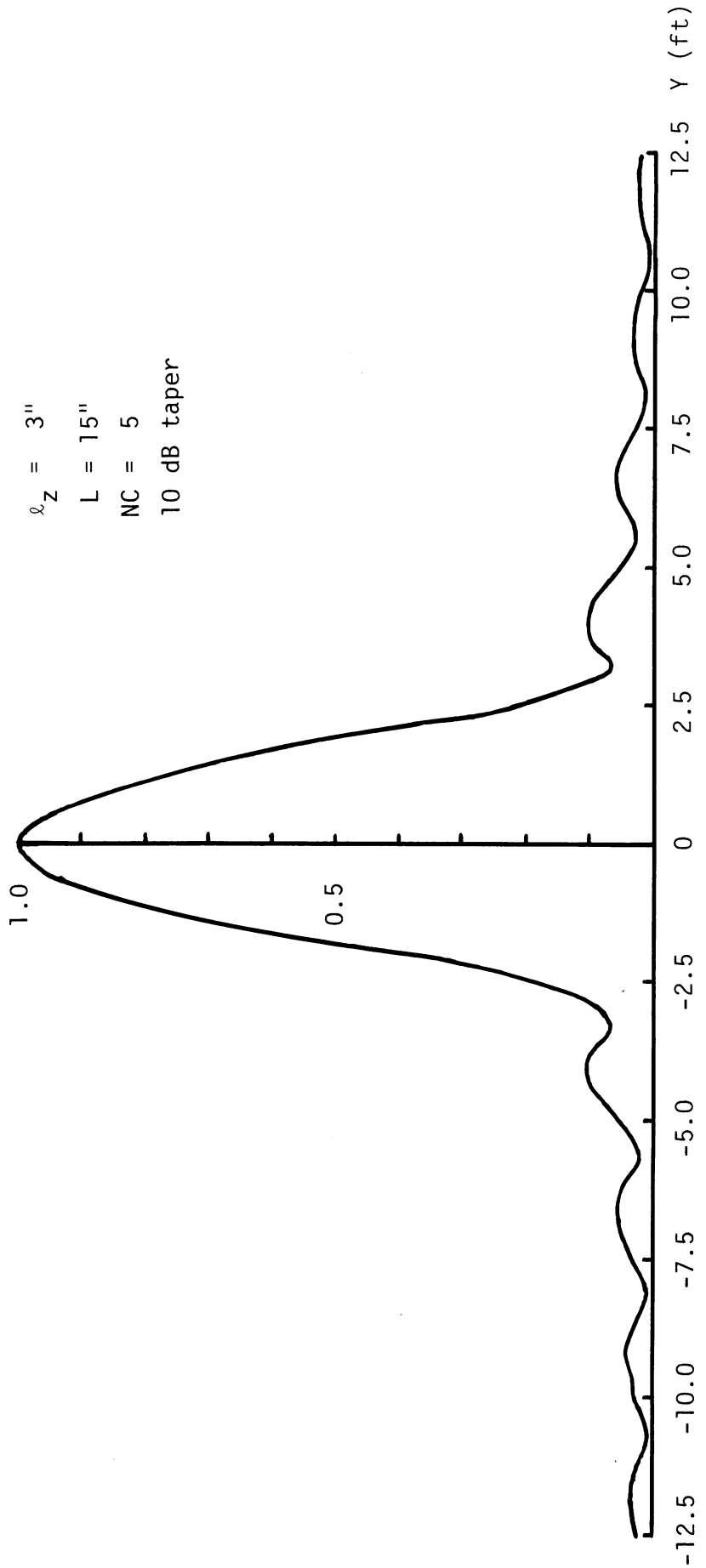

Figure PA-9: Far field pattern on E-plane (z = 30", x = 401").

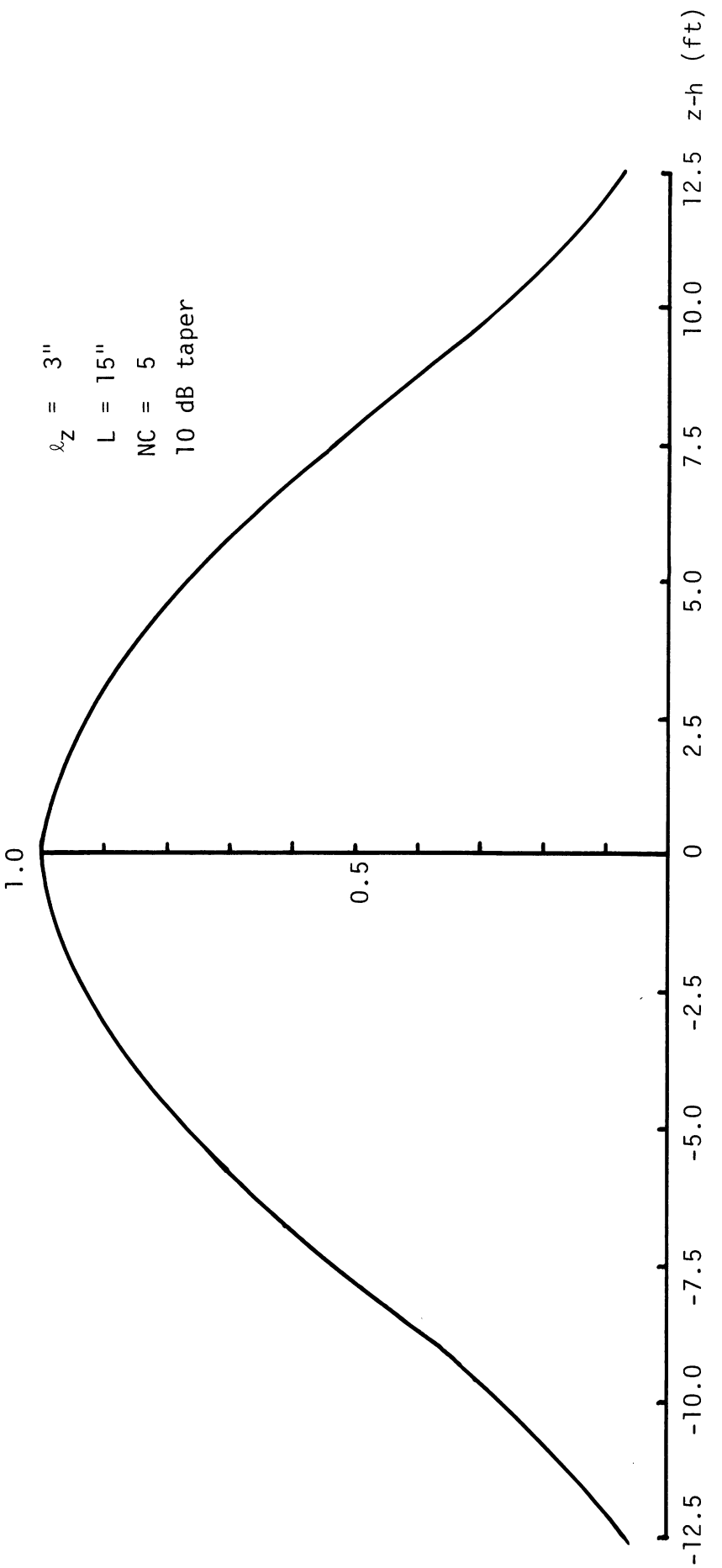

Figure PA-10: Far field pattern on H-plane (Y = 0, x = 401")/

increase the pattern strength significantly, an increased taper would not overcome this possible difficulty in detecting a small object in the near zone.

6.2 Normalized Fields

In Section 5 we derived the normalized electric field (modulus square) sensed by the receiving antenna, as given by equation (66). We present in this subsection some numerical results of equation (66) for a set of d, a, b, a_1, a_2, x_0 and z_0. Because of the choice of ℓ_z in both Antenna-I and Antenna-II, we set $a_1 = 0$ throughout.

We have chosen a metallic rectangular plate as the scattering object to simulate the average man. This simulation is perhaps adequate in the far zone. It is uncertain, however, how valid the simulation is in the near zone. Heuristically, it seems that the simulation would probably have some merit even in the near zone for a man in the upright posture. However, to simulate a crawling man flat on the ground in the near zone by a thin rectangular plate would not be adequate.

In Figures E-1 through E-20, the reflector dimension is 6" by 30", simulating a man in the standing posture looking in the direction perpendicular to the boresight plane; in Figures E-21 through E-27, the dimension and the orientation of the rectangular plate is taken so as to simulate approximately a man in a crouched and crawling posutre on the ground.

Figures E-1 through E-4 represent the variation of the normalized field with Antenna-I (3). The reflector (a = 6", b = 30": a standing man) is placed

in the region 2.5 ft $\leq x_0 \leq$ 50 ft., 0 $\leq y_0 \leq$ 5 ft., the antenna range d = 100 ft. Figures E-5 through E-10 represent the similar situation with Antenna-II (5) in the region 1.5 ft $\leq x_0 \leq$ 50 ft., 0 $\leq y_0 \leq$ 5 ft., d = 100 ft.

In these figures, a similar pattern of field variation at the receiving antenna is seen. Namely, a strong scattering (or blocking) of the wave occurs when the reflector center is directly in the boresight plane; as the plate is moved away from the boresight plane along the normal to the boresight plane, the maximum field is sensed by the receiving antenna when the plate center is about 1.5" away from the boresight plane, probably indicating a constructive phase interference of the scattered waves. Based on these results, one may conclude that, as a man in upright standing posture walks through anywhere in the boresight plane, the antenna system is likely to detect him.

Figures E-11 through E-18 are presented to show the effects of cell aperture sizes for Antenna-I and Antenna-II. All in all, the general agreement of the field variations are reasonably good, exhibiting similar variation patterns, but the null and peak in the field becomes sharper as the cell number increases, as one expects. In principle, the field variation based on more numerous cells (hence smaller cell apertures) of a given antenna aperture is expected to yield a more reliable result.

Figures E-19 and E-20 represent the field variations with Antenna-II (5) for the antenna range d = 300 ft. Compared with the corresponding case for d = 100 ft., there is no significant difference in field variation pattern.

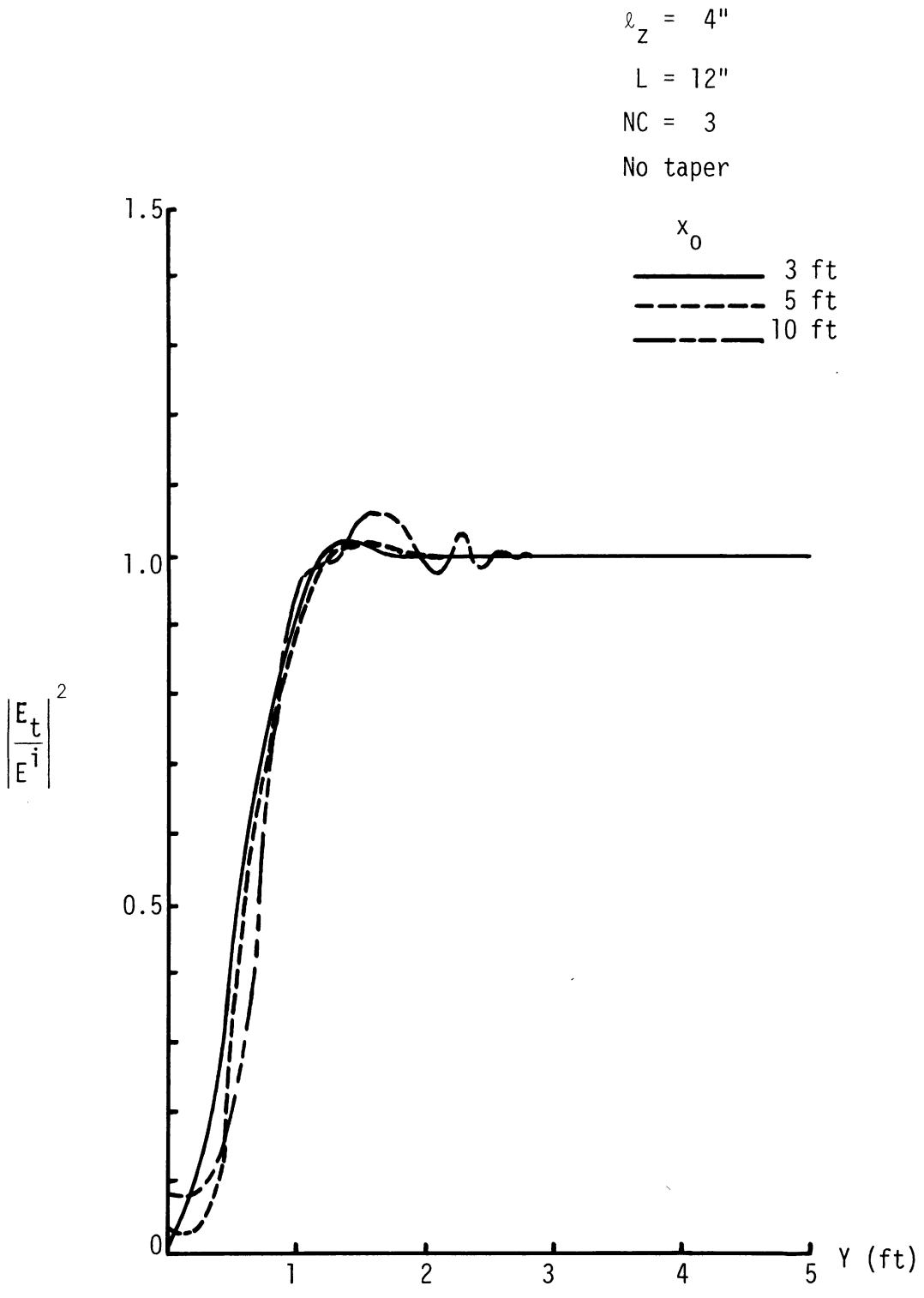

Figure E-1: Field variations on z = 30"-plane, a = 6", b = 30", h = 30", d = 100 ft.

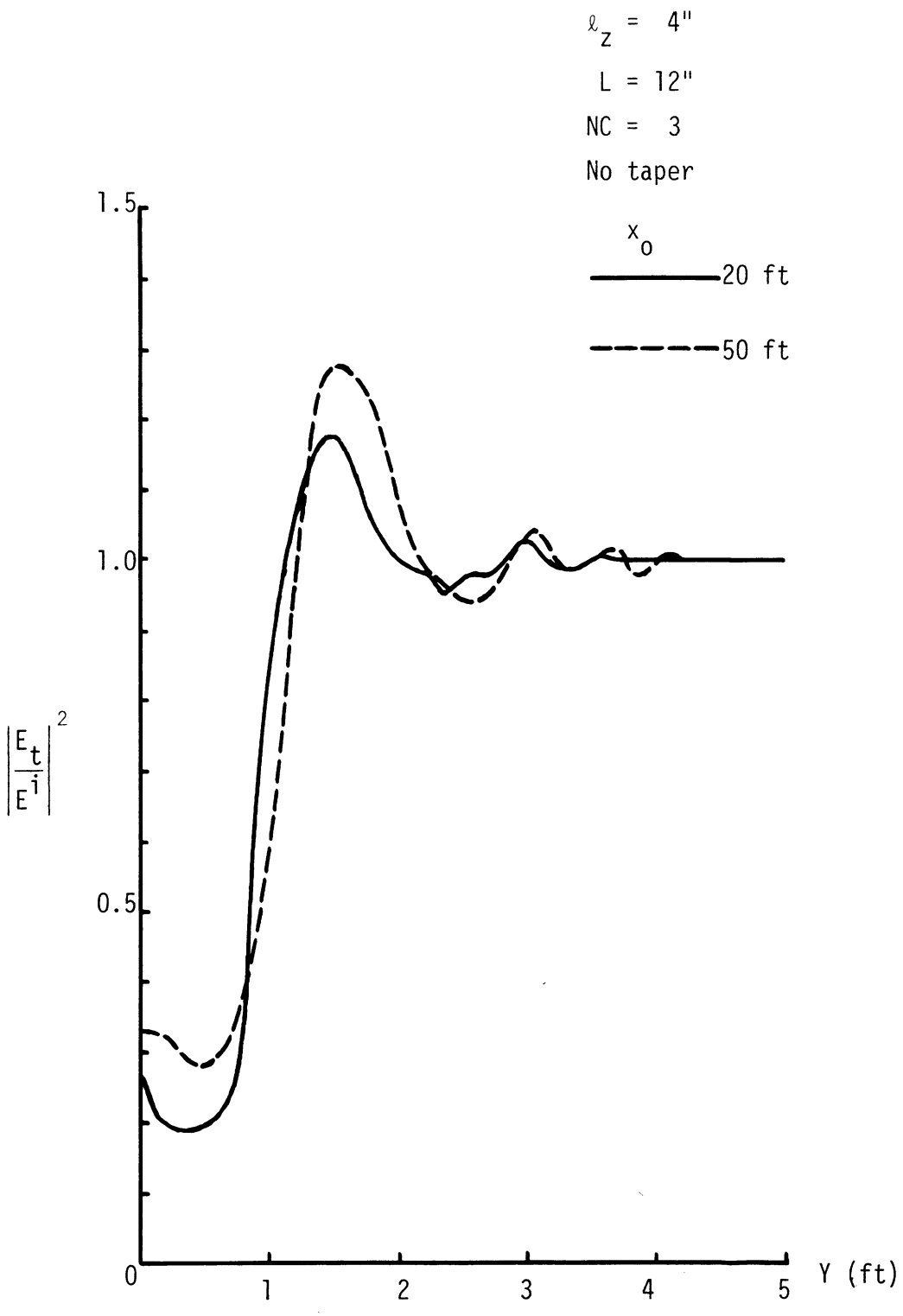

Figure E-2: Field variations on z = 30"-plane, a = 6", b = 30", h = 30", d = 100 ft.

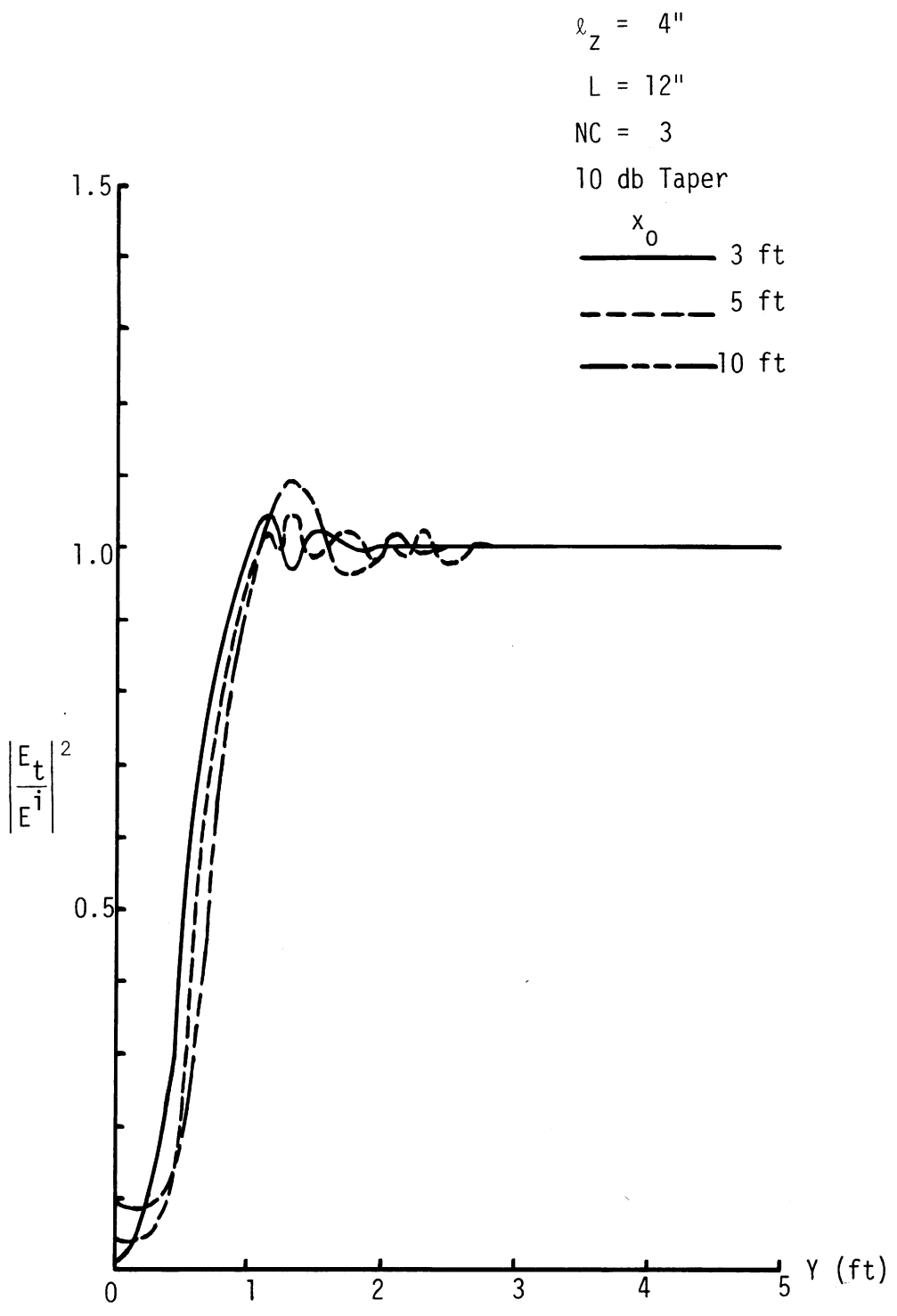

Figure E-3: Field variations on z = 30"-plane, a = 6", b = 30", h = 30", d = 100 ft.

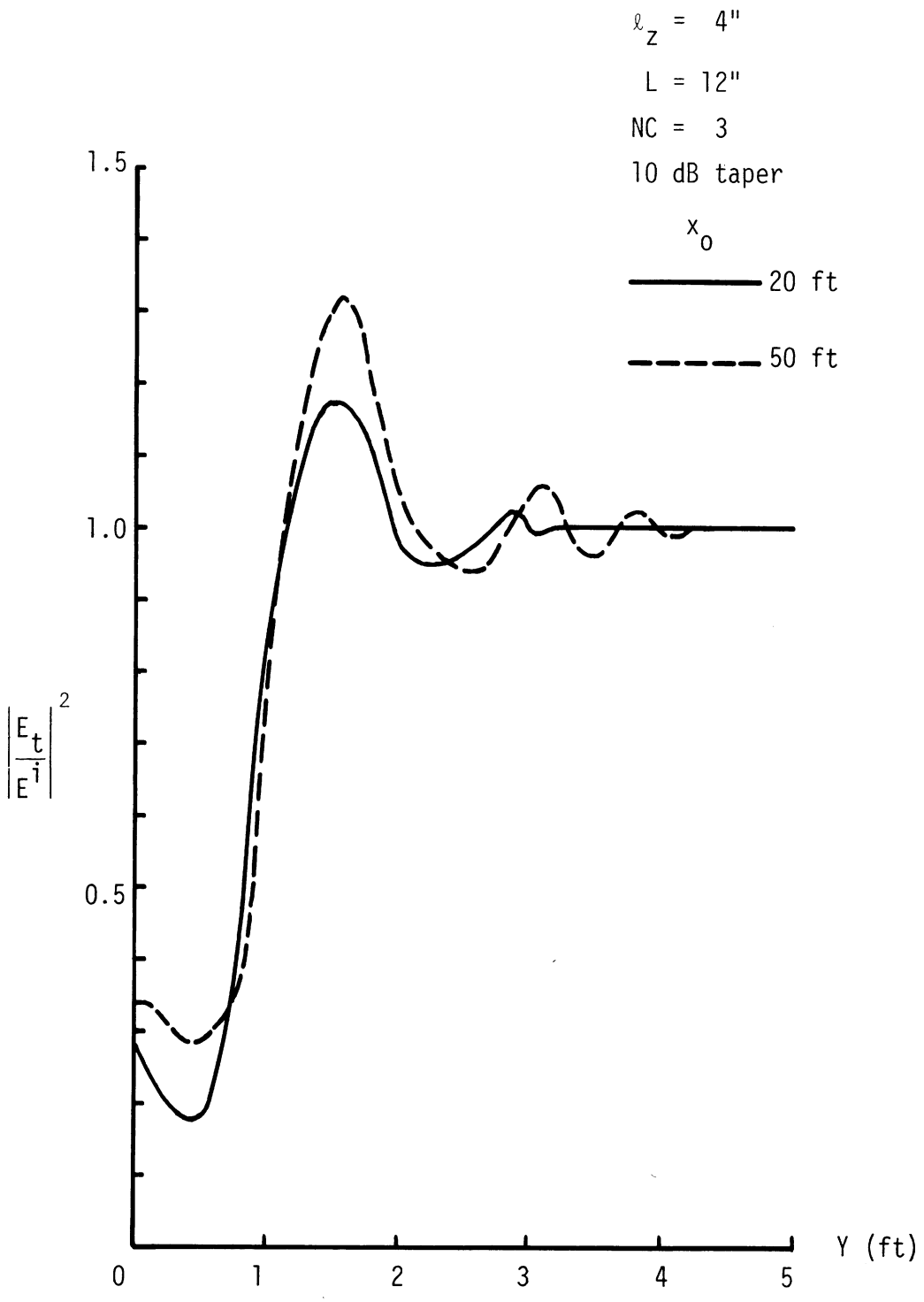

Figure E-4: Field variations on z = 30"-plane, a = 6", b = 30", h = 30", d = 100 ft.

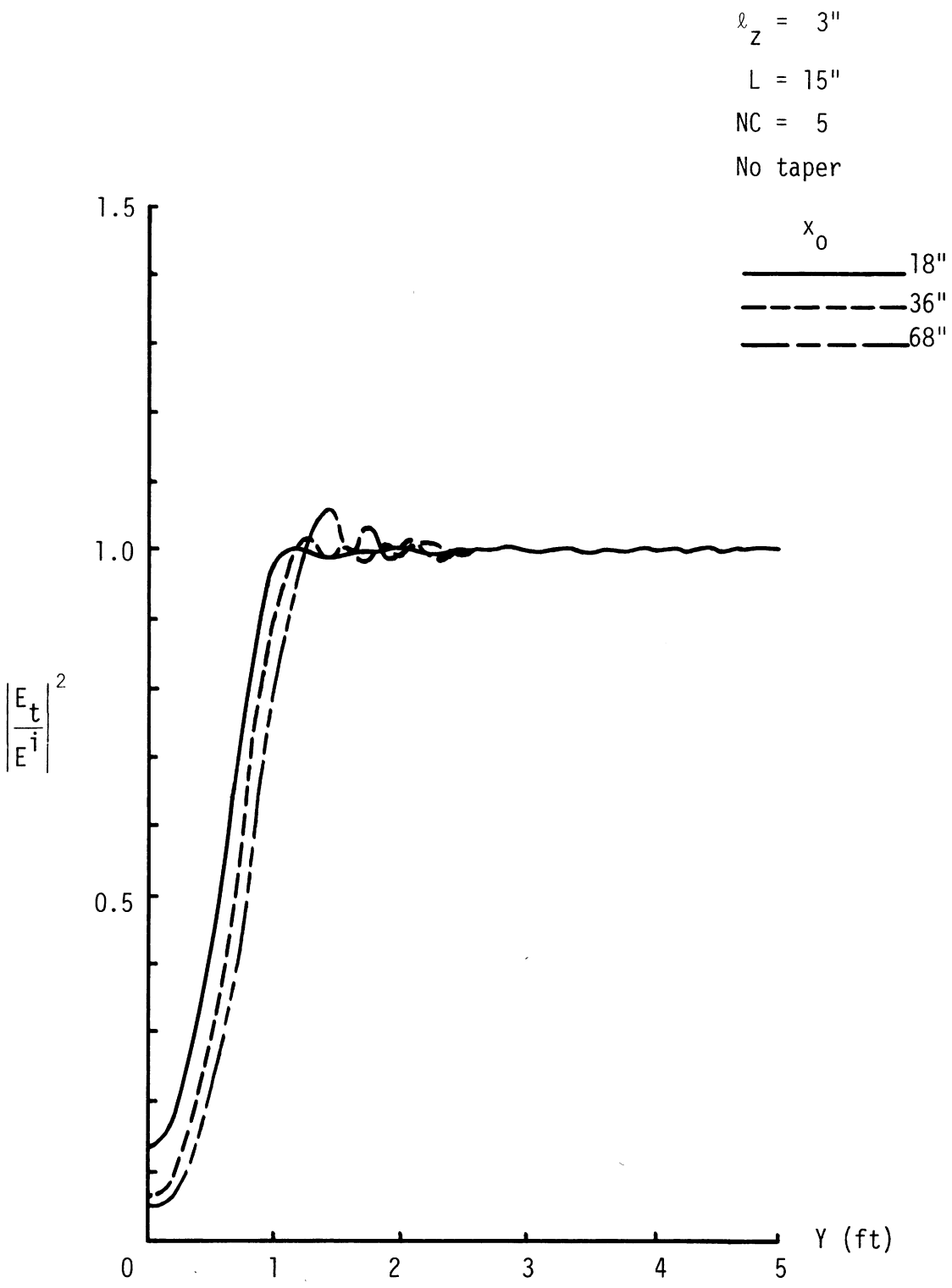

Figure E-5: Field variations on z = 30"-plane, a = 6", b = 30", h = 30", d = 100 ft.

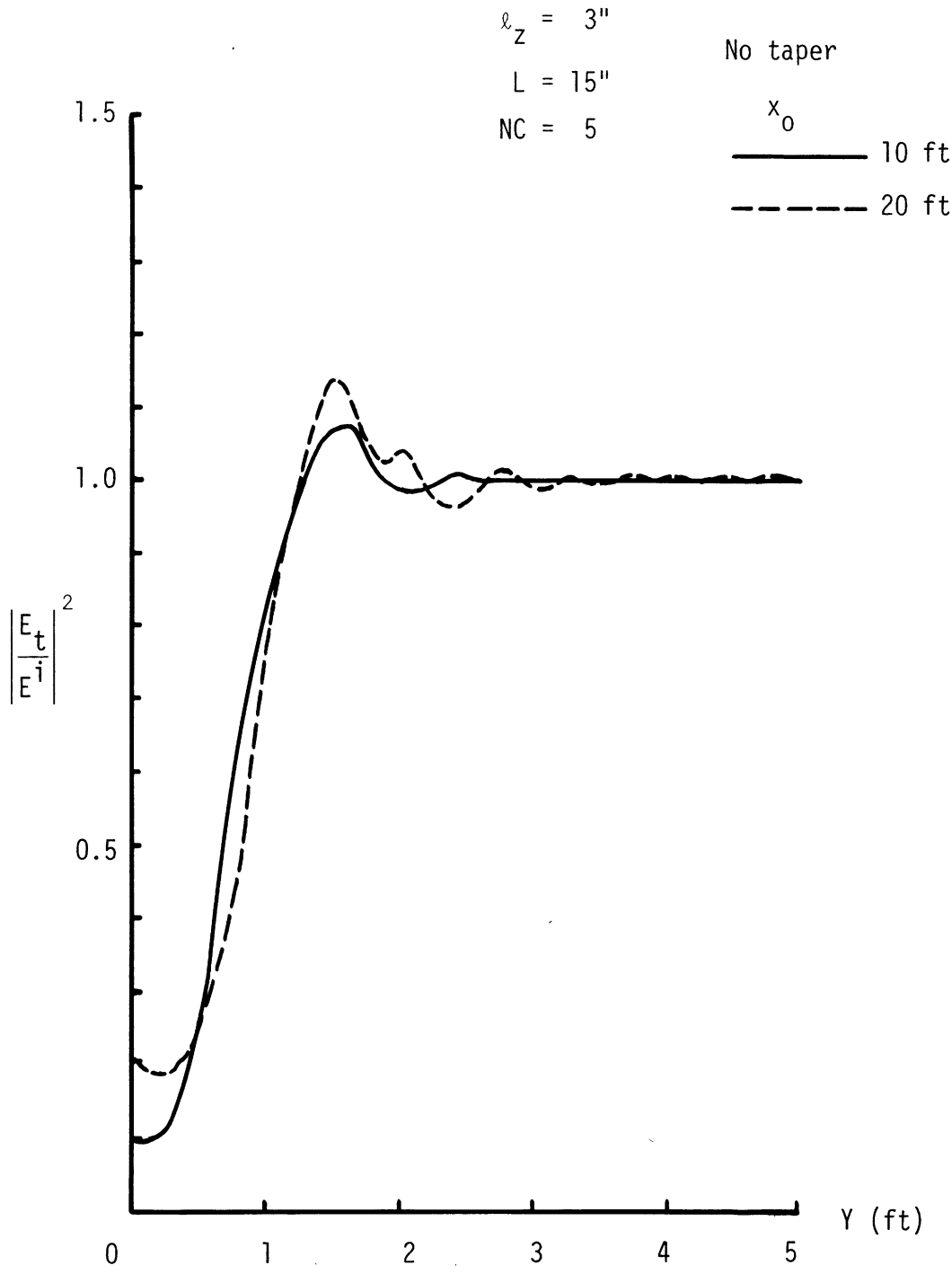

Figure E-6: Field variations on z = 30"-plane, a = 6", b = 30", h = 30", d = 100 ft.

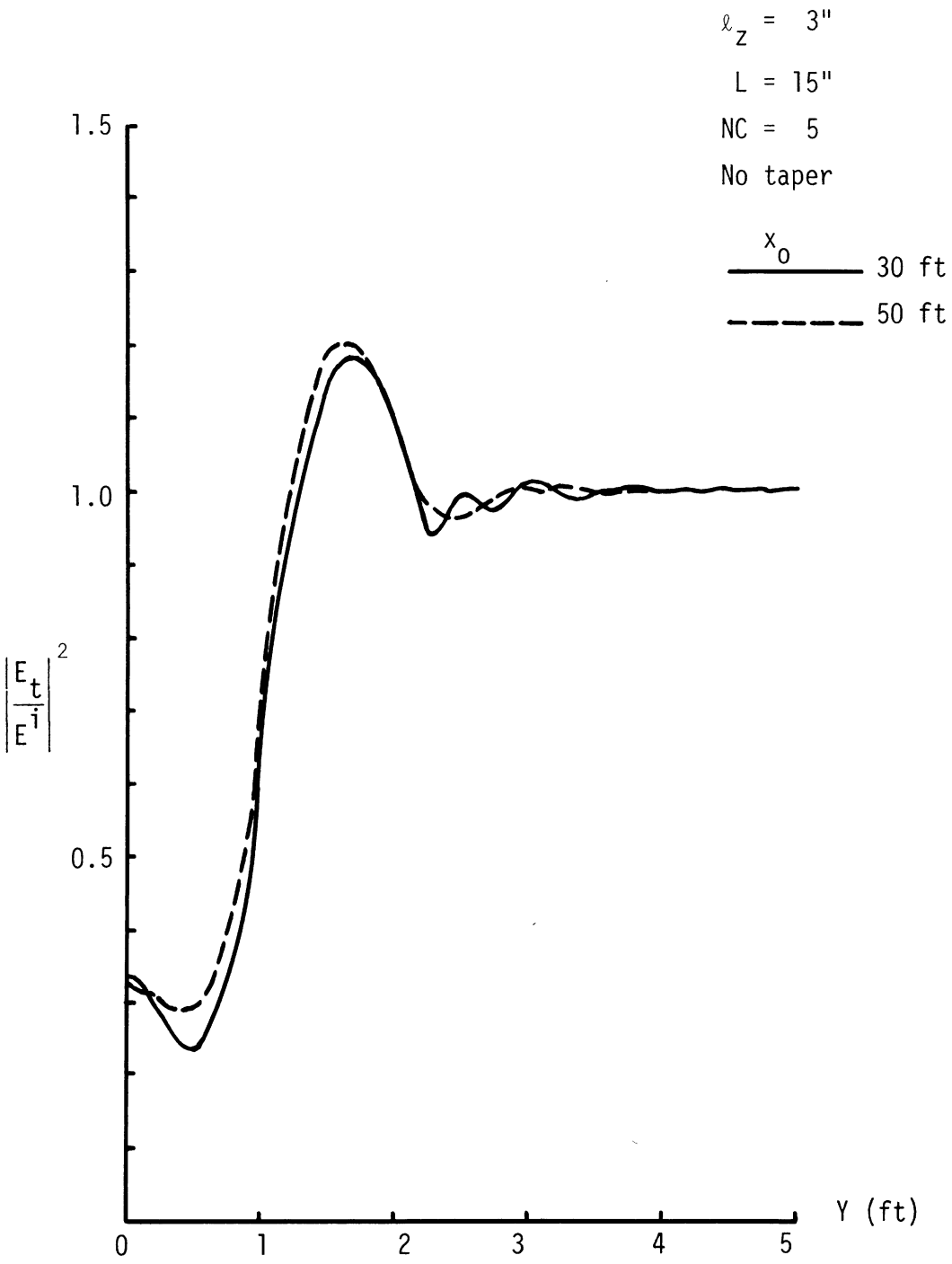

Figure E-7: Field variations on z = 30"-plane, a = 6", b = 30", h = 30", d = 100 ft.

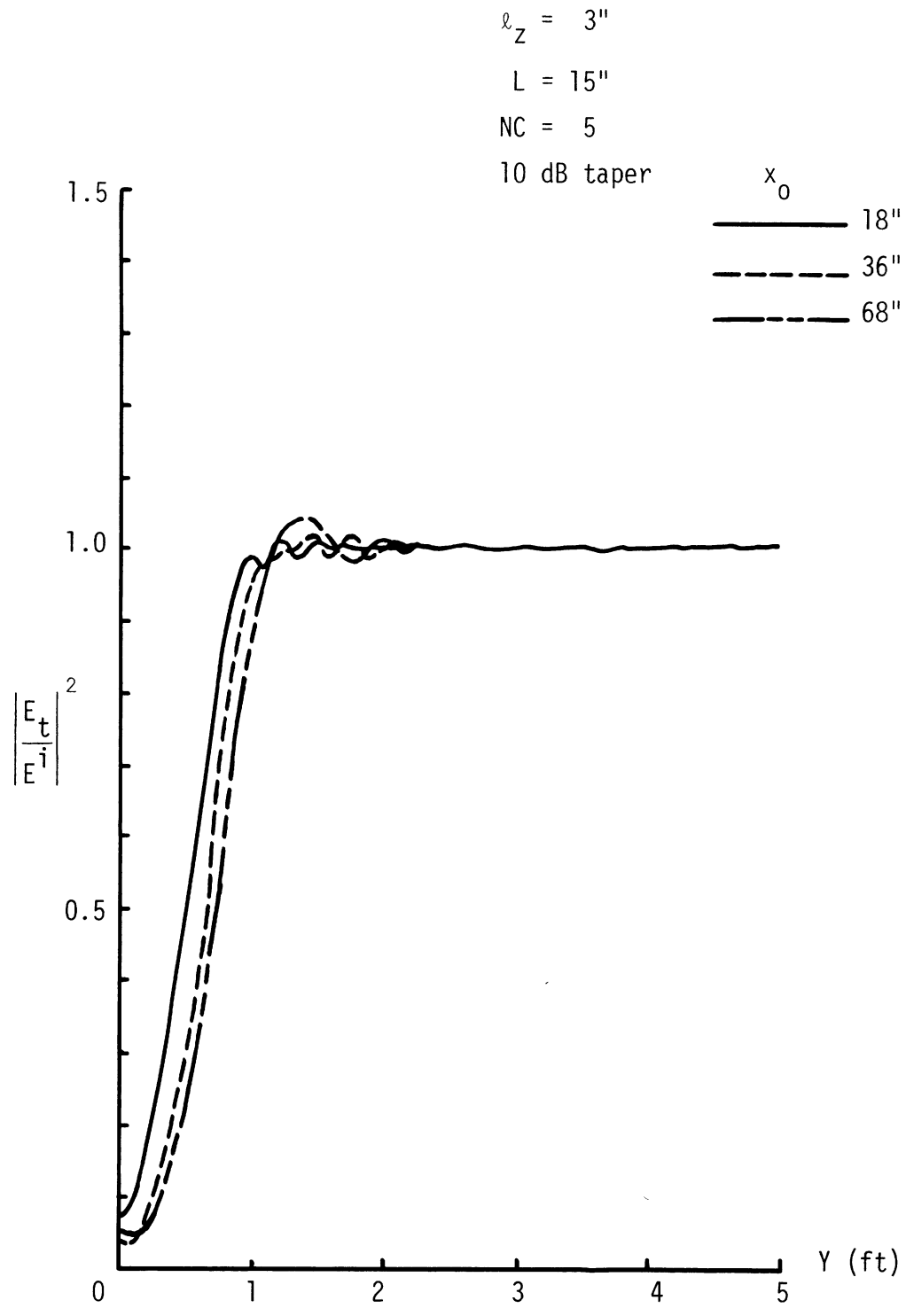

Figure E-8: Field variations on z = 30"-plane, a = 6", b = 30", h = 30", d = 100 ft.

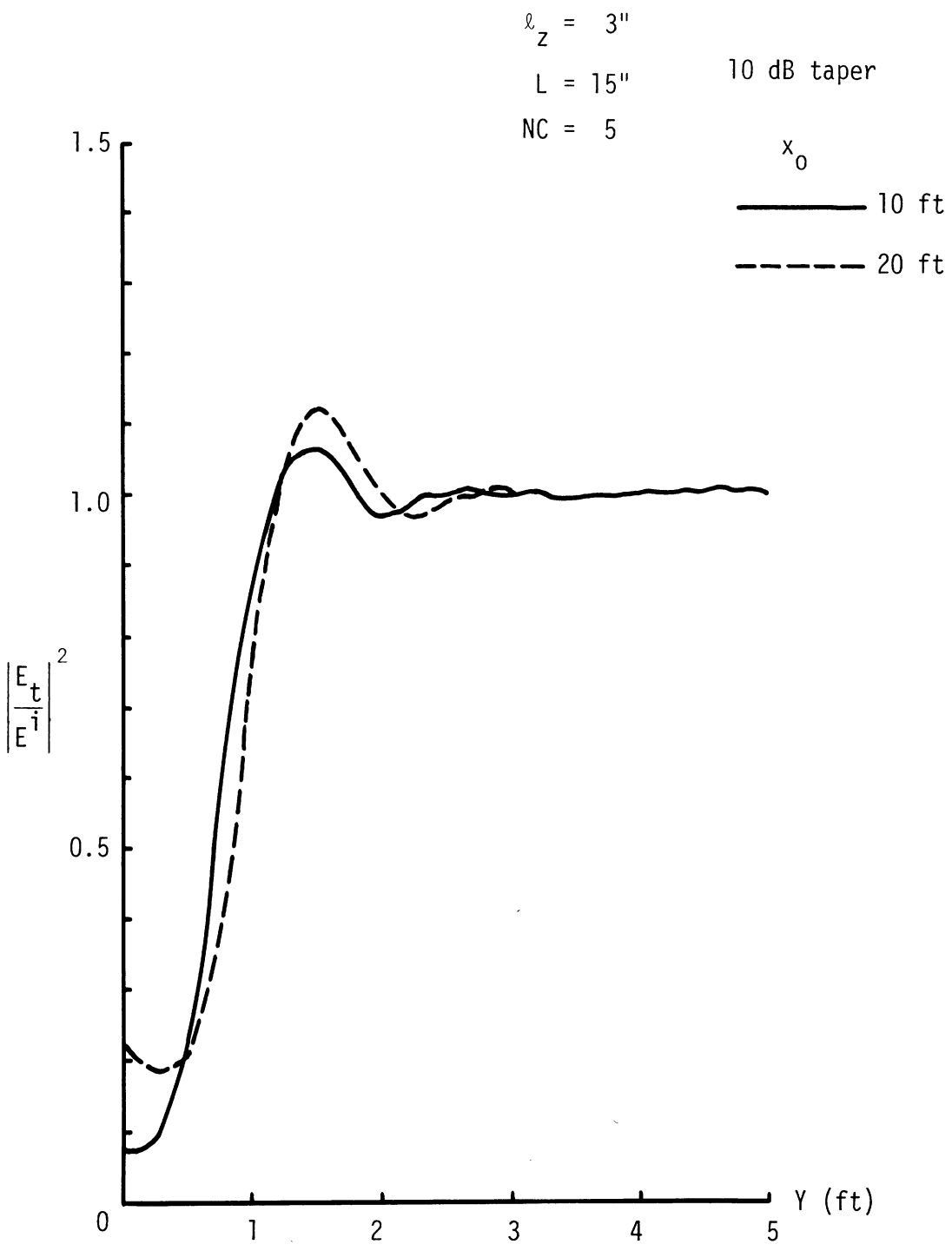

Figure E-9: Field variations on z = 30"-plane, a = 6", b = 30", h = 30", d = 100 ft.

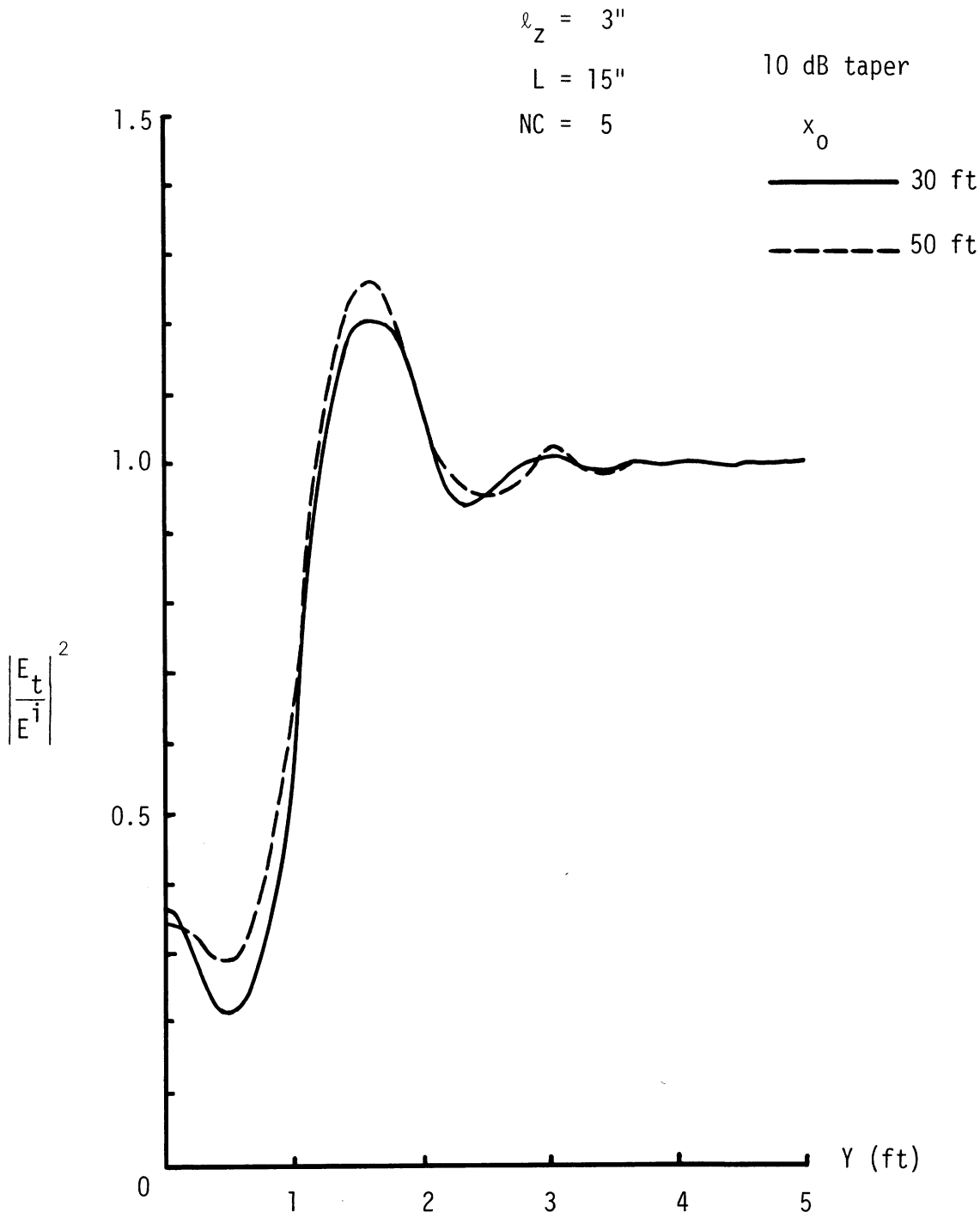

Figure E-10: Field variations on z = 30"-plane, a = 6", b = 30", h = 30", d = 100 ft.

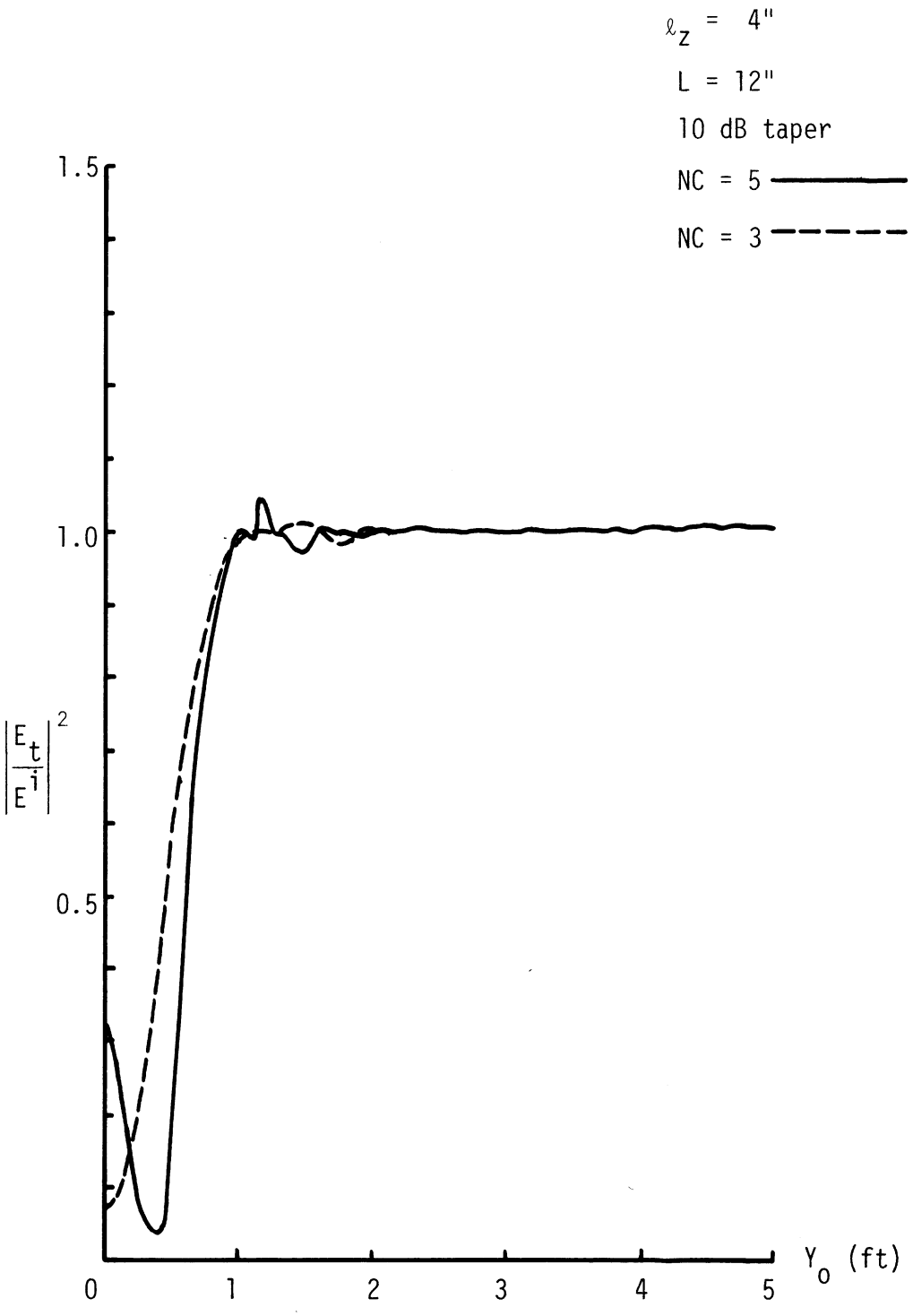

Figure E-11: Effect of cell sizes on the field variations on z = 30"-plane, x_o = 28.54", a = 6", b = 30", h = 30", d = 100^oft.

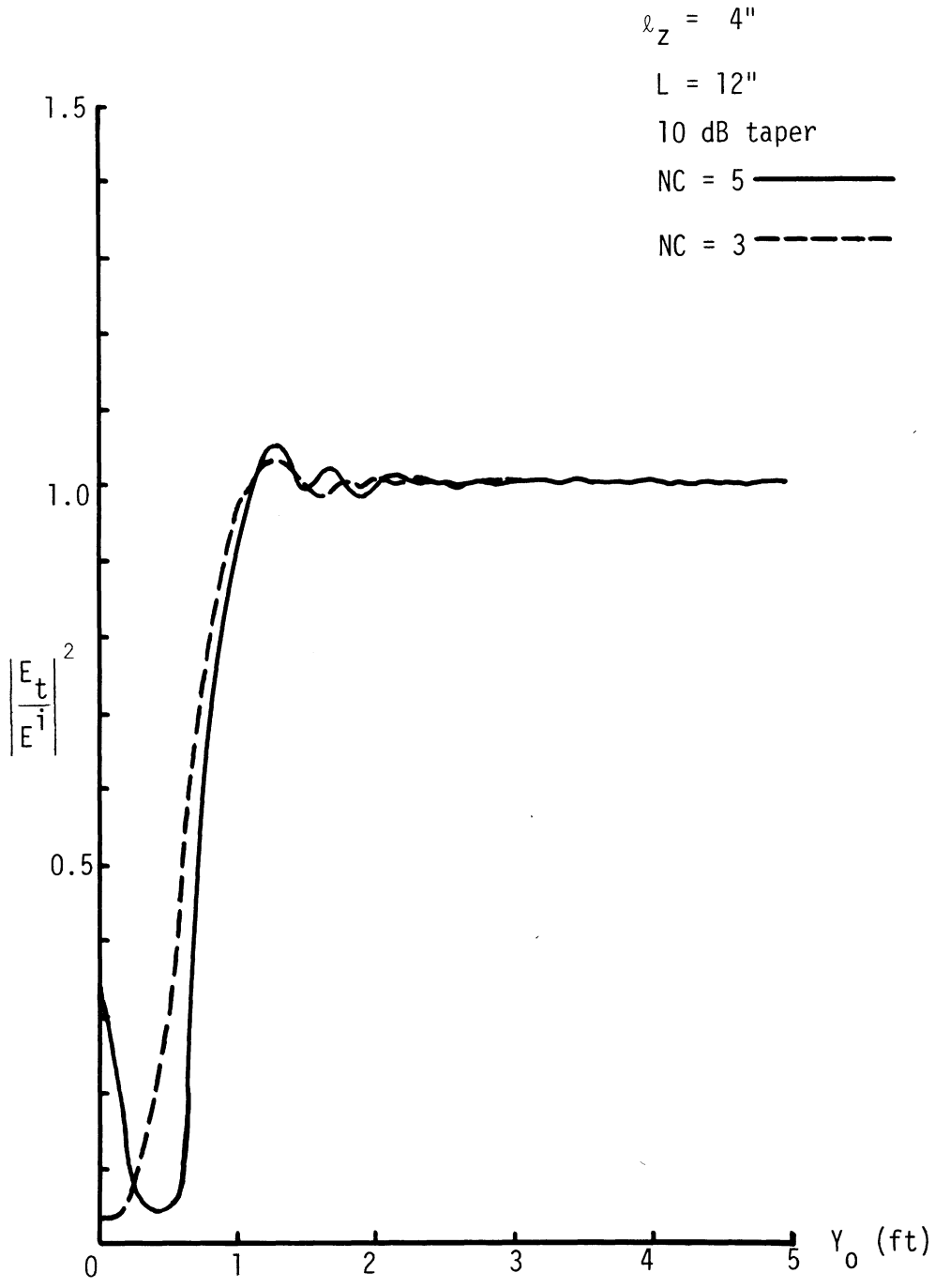

Figure E-12: Effect of cell sizes on field variations on z = 30"-plane, x_o = 36", a = 6", b = 30", h = 30", d = 100 ft.

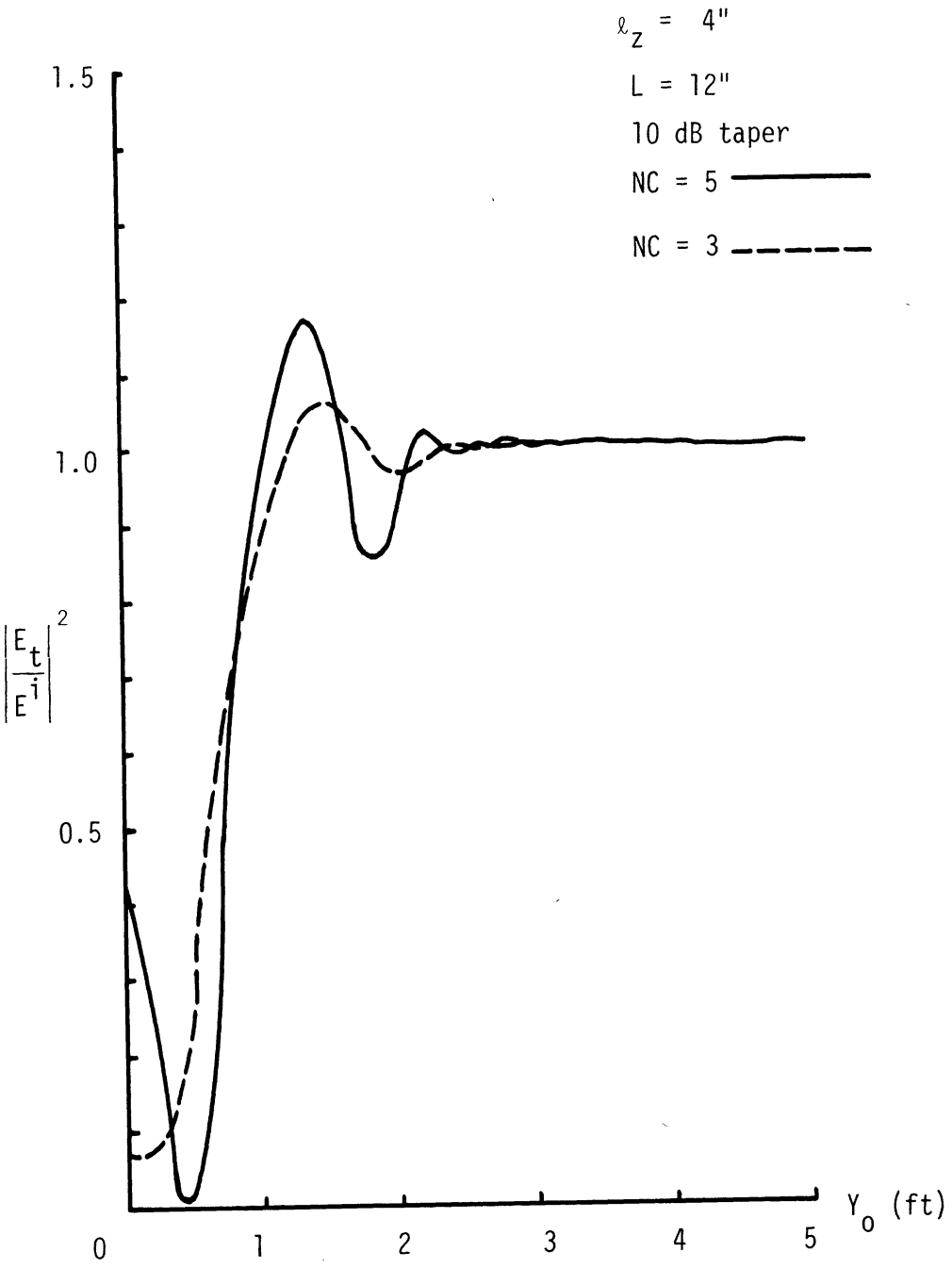

Figure E-13: Effect of cell sizes on field variations on z = 30"-plane, x_o = 10 ft, a = 6", b = 30", h = 30", d = 100 ft.

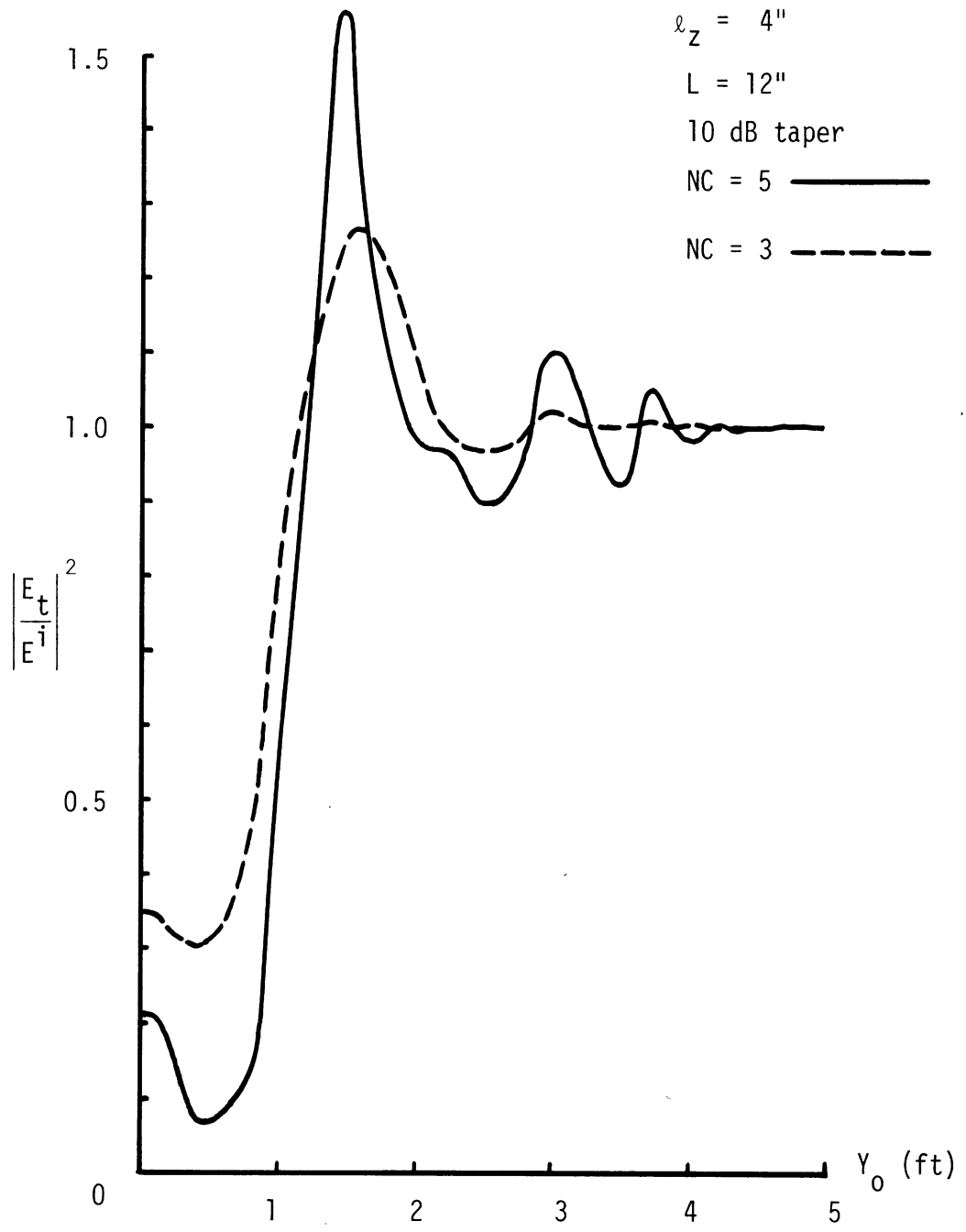

Figure E-14: Effect of cell sizes on field variations on z = 30"-plane, x_o = 50 ft, a = 6", b = 30", h = 30", d = 100 ft.

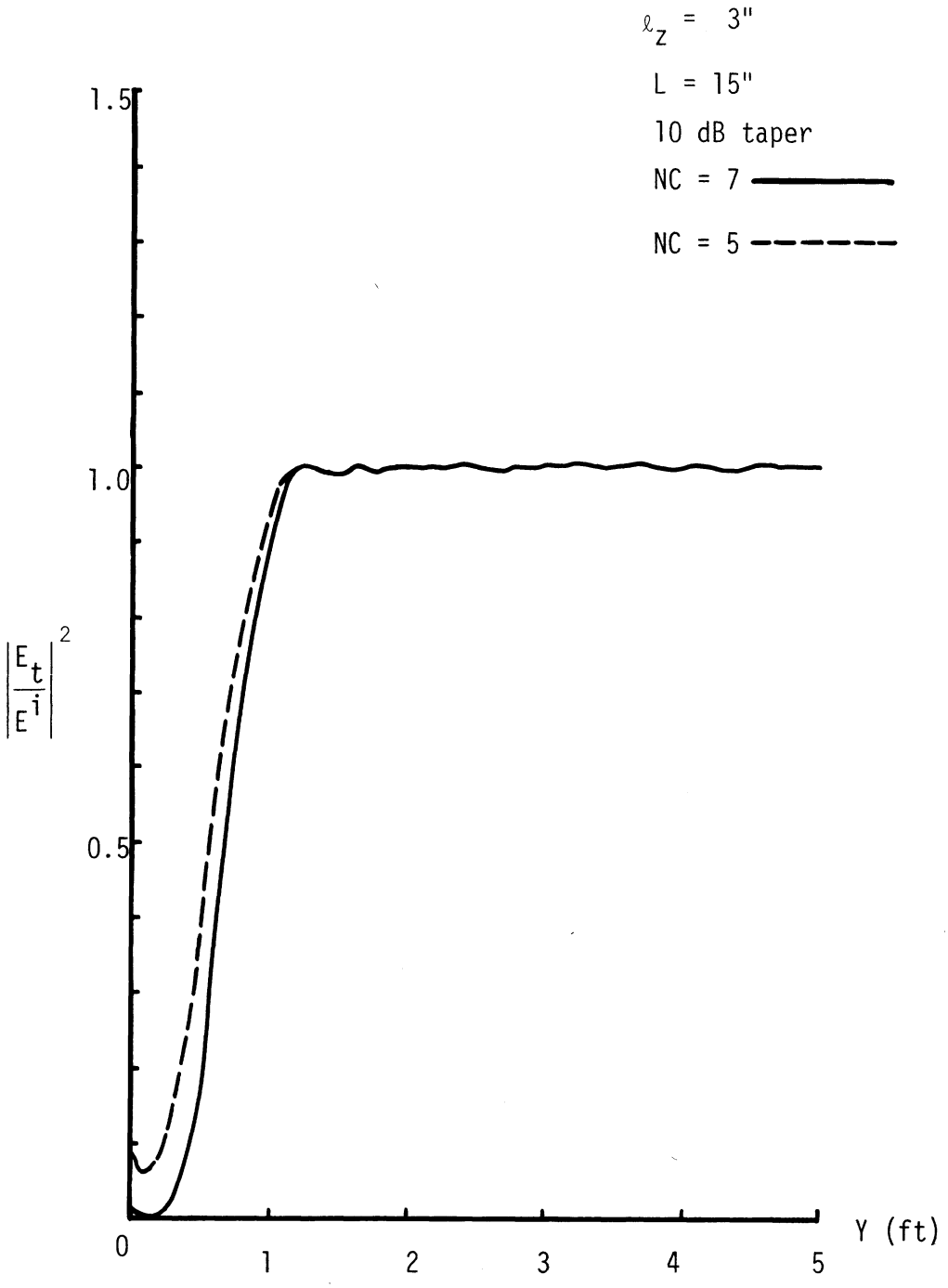

Figure E-15: Effect of cell sizes on field variations on z = 30"-plane, x_o = 18", a = 6", b = 30", h = 30", d = 100 ft.

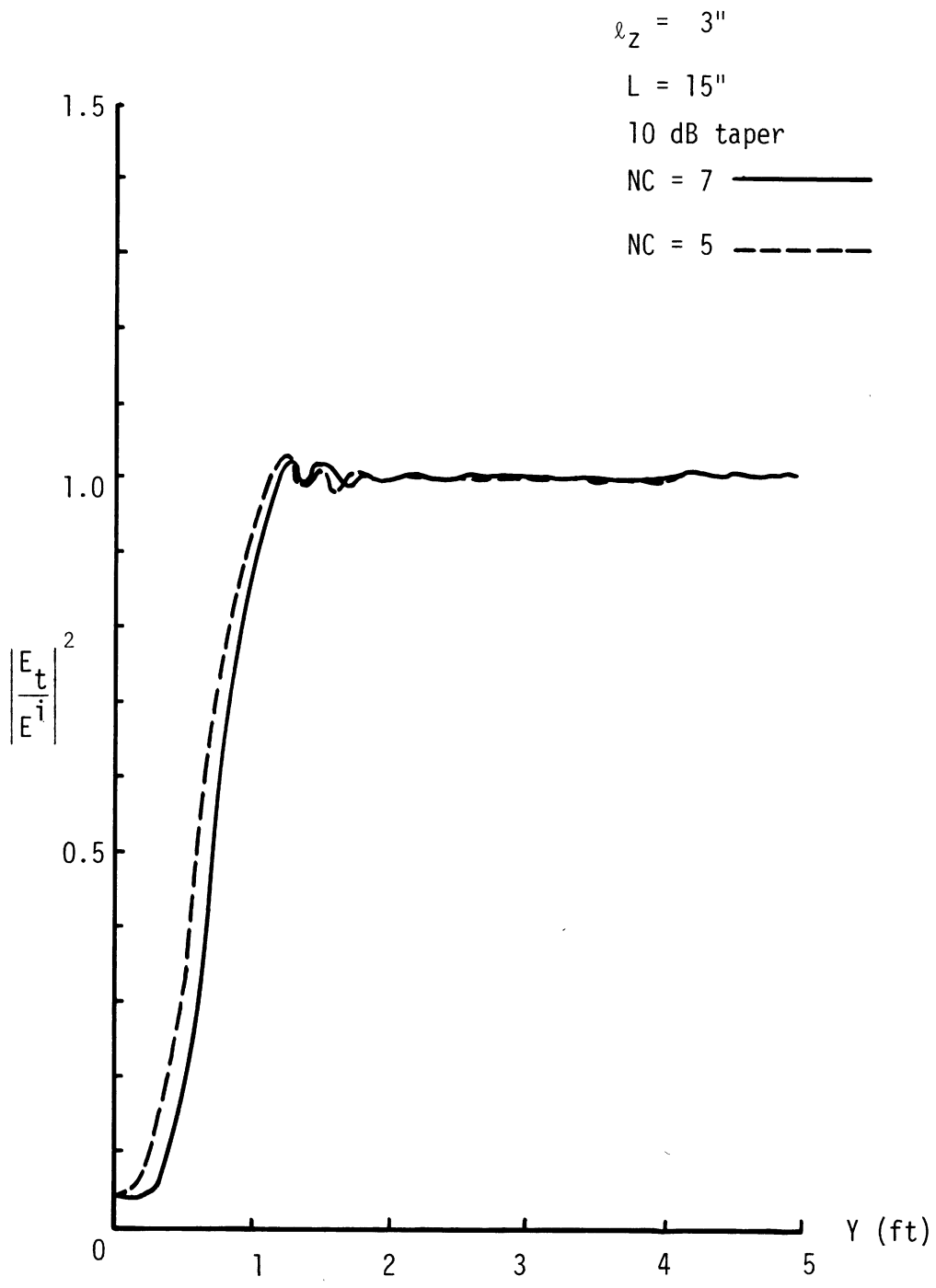

Figure E-16: Effect of cell sizes on field variations on z = 30"-plane, x_o = 36", a = 6", b = 30", h = 30", d = 100 ft.

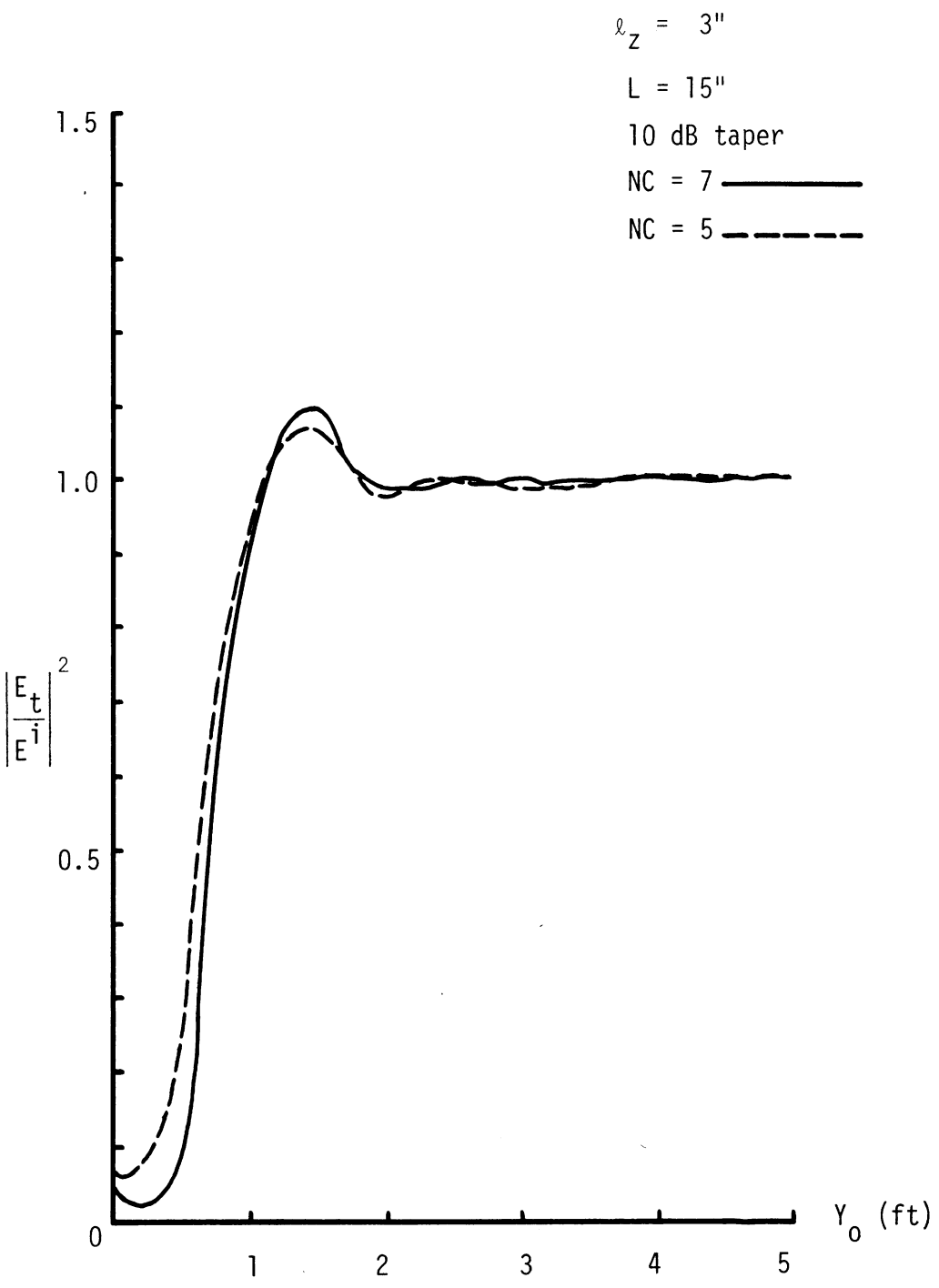

Figure E-17: Effect of cell sizes on field variations on z = 30"-plane, x_o = 10 ft, a = 6", b = 30", h = 30", d = 100 ft.

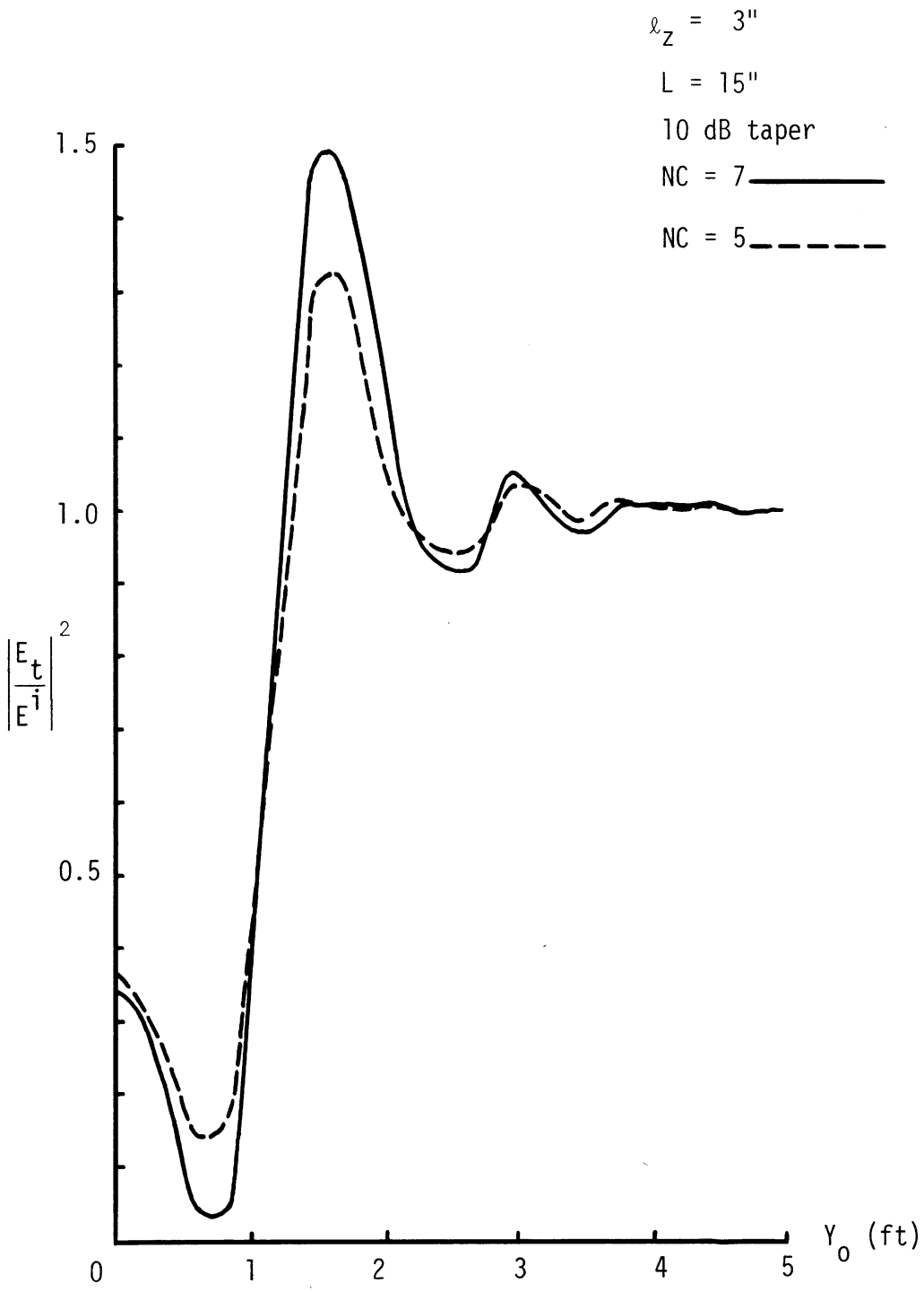

Figure E-18: Effect of cell sizes on field variations on z = 30"-plane, x_o = 50 ft, a = 6", b = 30", h = 30", d = 100 ft.

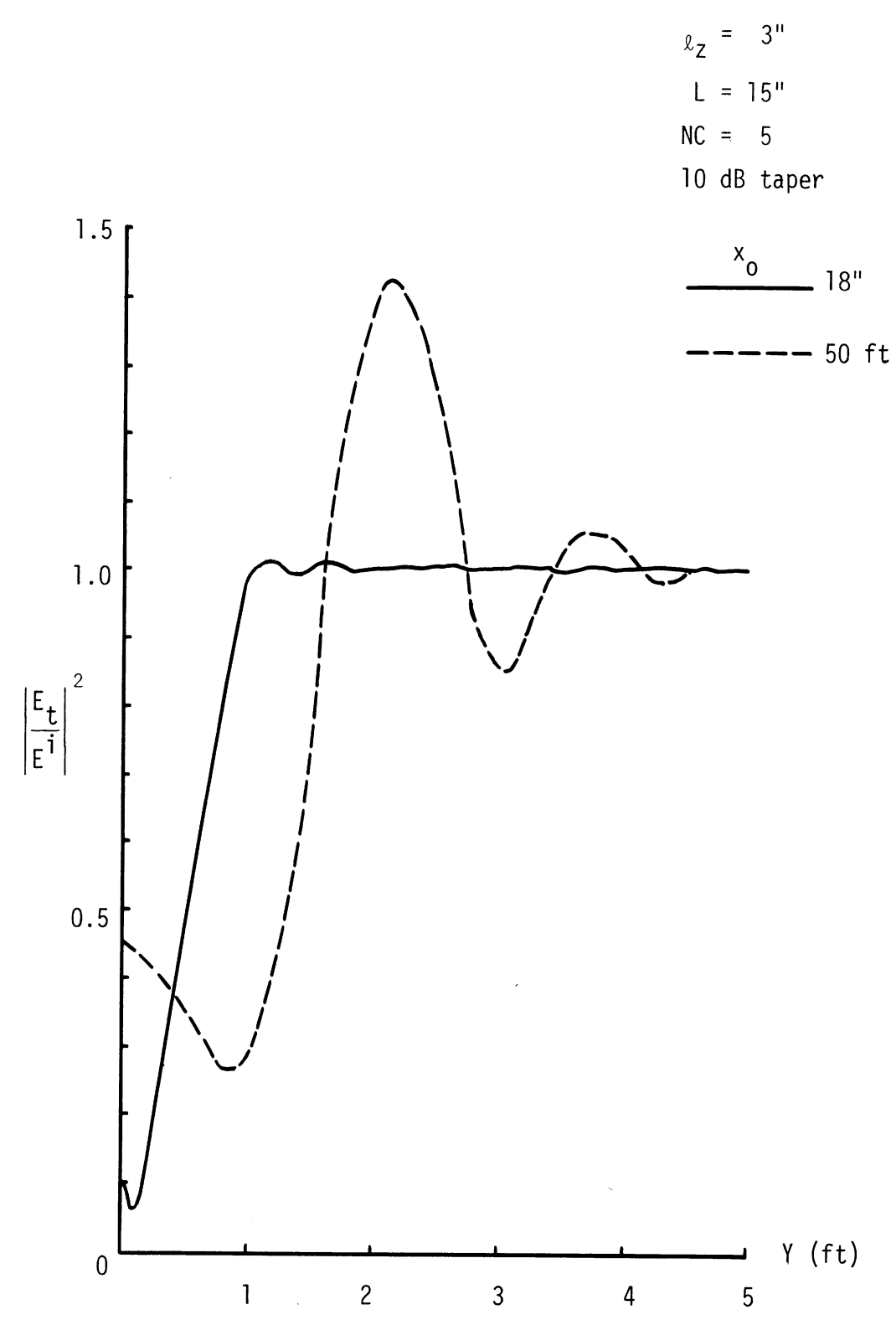

Figure E-19: Field variations on z = 30"-plane, a = 6", b = 30", h = 30", d = 300 ft.

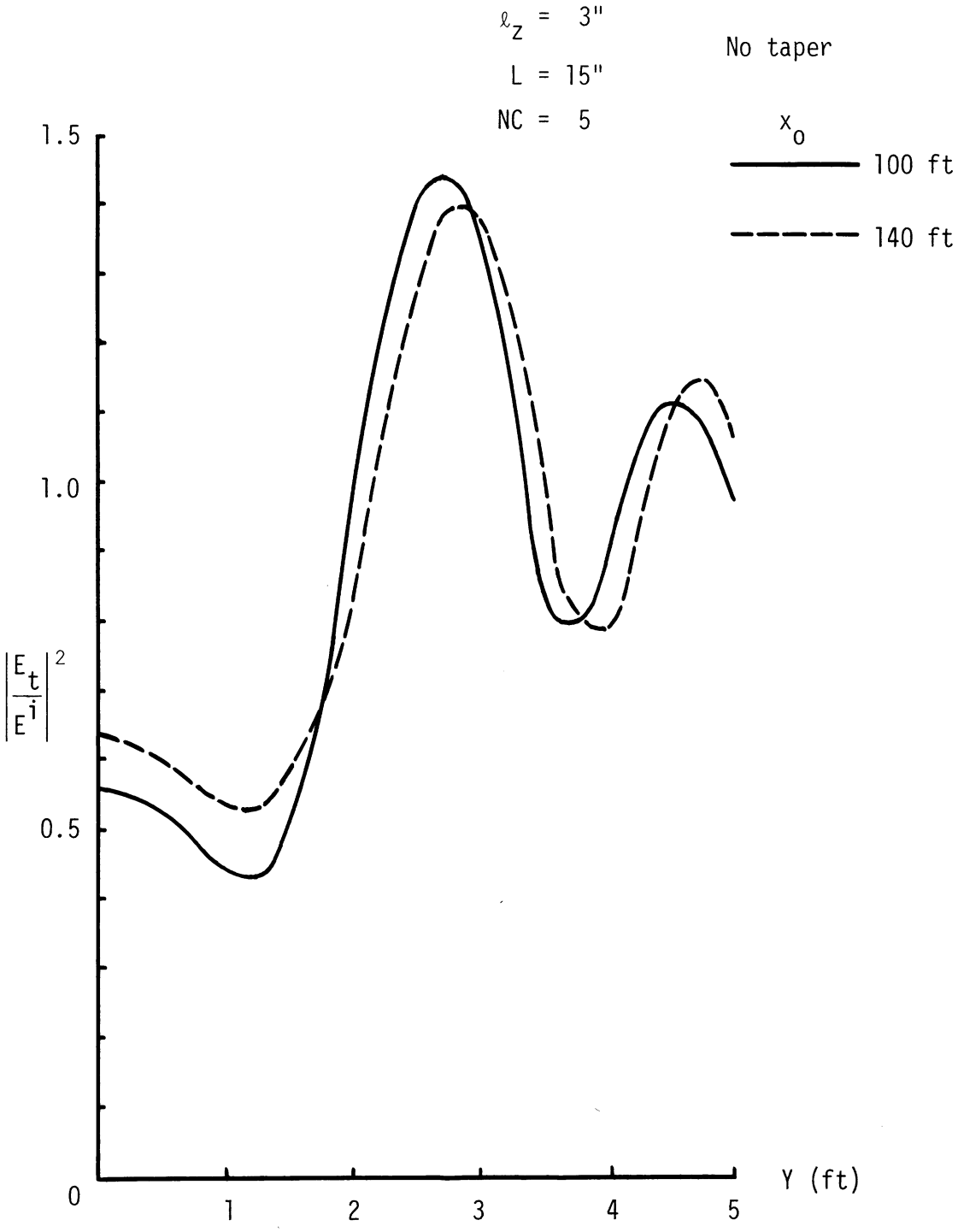

Figure E-20: Field variations on z = 30"-plane, a = 6", b = 30", h = 30", d = 300 ft.

Up to this point, we have considered the effect of a man in upright standing posture walking through the boresight plane. Our theoretical results have shown that the man's presence would be detected, regardless of the position along the line parallel to the boresight line.

In Figures E-21 through E-24, we attempt to simulate a man in various crouching positions by adjusting the height of the rectangular plate. As previously remakred at the beginning of this section, a simulation of a man in a crouched, or crawling posture on the ground by a thin rectangular plate may not be adequate in the near zone. Therefore, the numerical results presented here for the above situation (in the near zone) should be taken with allowance.

It is seen in Figures E-21 through E-24 that, as an average man moves through the boresight plane in crouched postures to heights of 30" and 40" above the ground (remember that the antenna height is fixed at 30" above the ground), the pattern of field variations does not differ much from that for a man in the standing posture. However, for a man crouched to the height of 10" above the ground, the pattern of field variations at the receiving antenna exhibits a marked difference, significant field being sensed when the man is in the boresight plane. At any rate, the presence of a man crouched as low as 10" above the ground could be detected by our antenna system.*

In Figures E-25 through E-27, we simulate a man crawling flat on the ground by a thin plate. Again, such a man could be detected.

* The detectability here is dependent on the calibration.

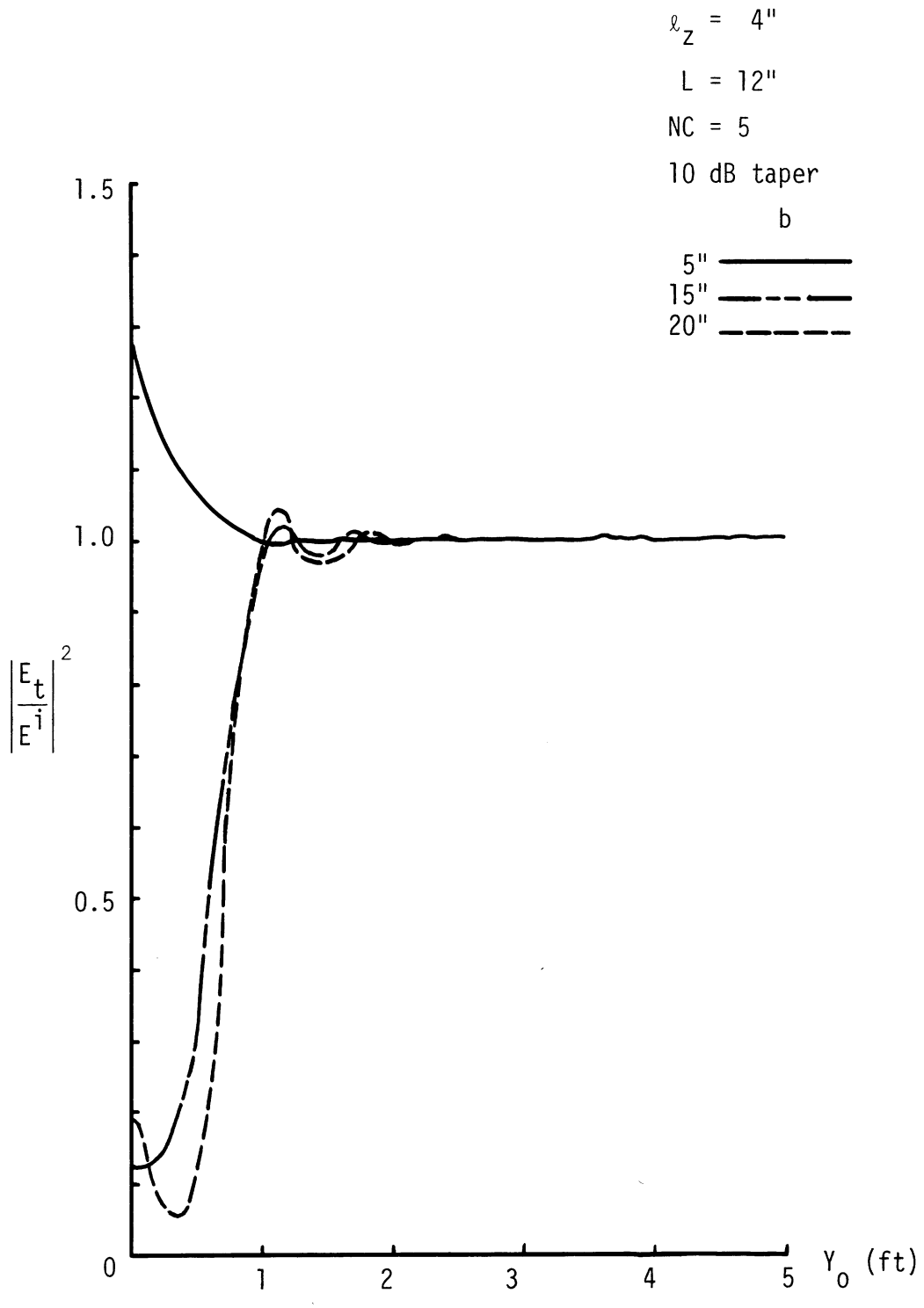

Figure E-21: Field variations on z = 30"-plane, x_o = 28.54", for different scattering object heights; a = 6", h = 30", d = 100 ft.

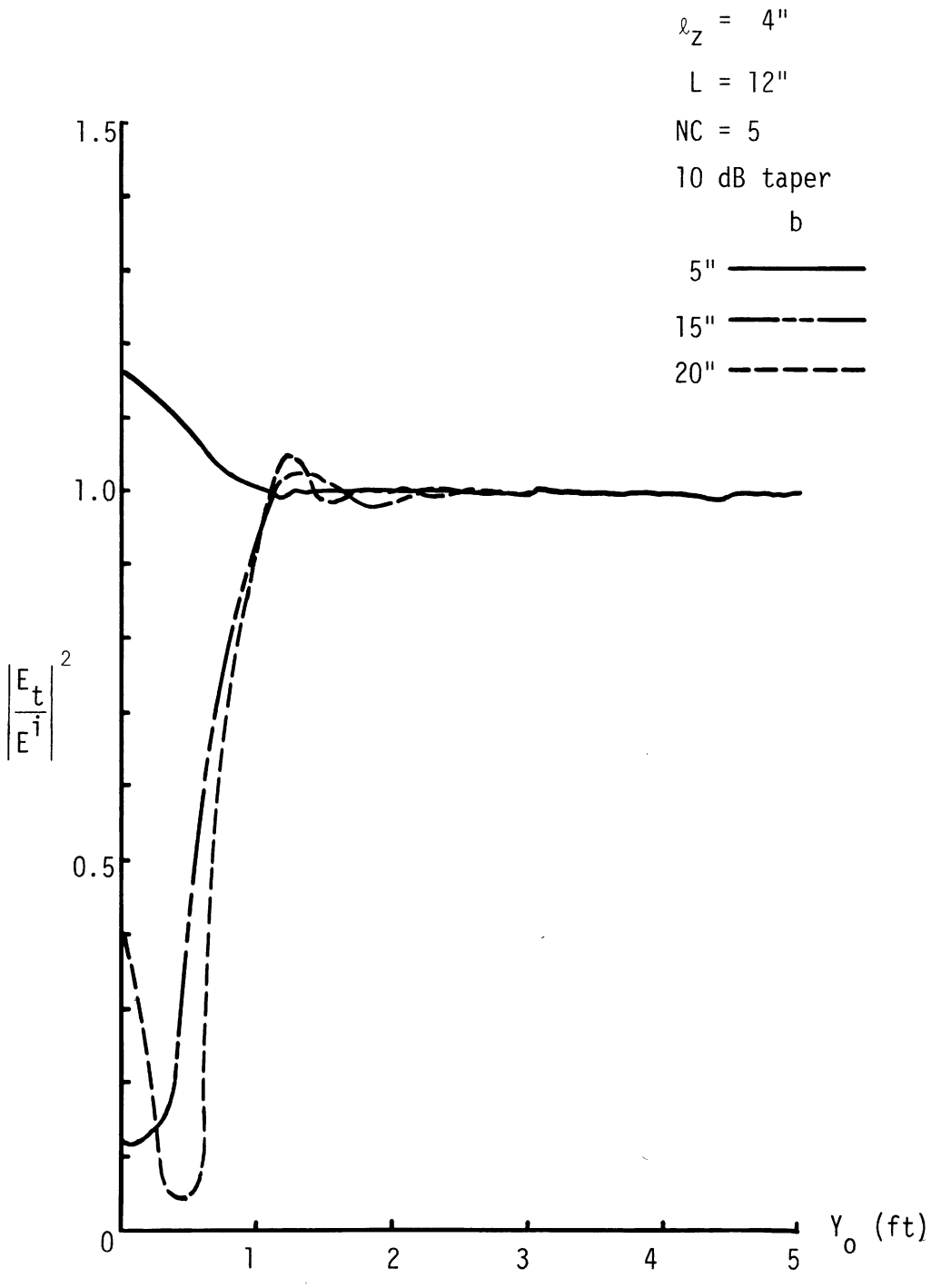

Figure E-22: Field variations on z = 30"-plane, x_o = 36" for different scattering object heights; a = 6", h = 30", d = 100 ft.

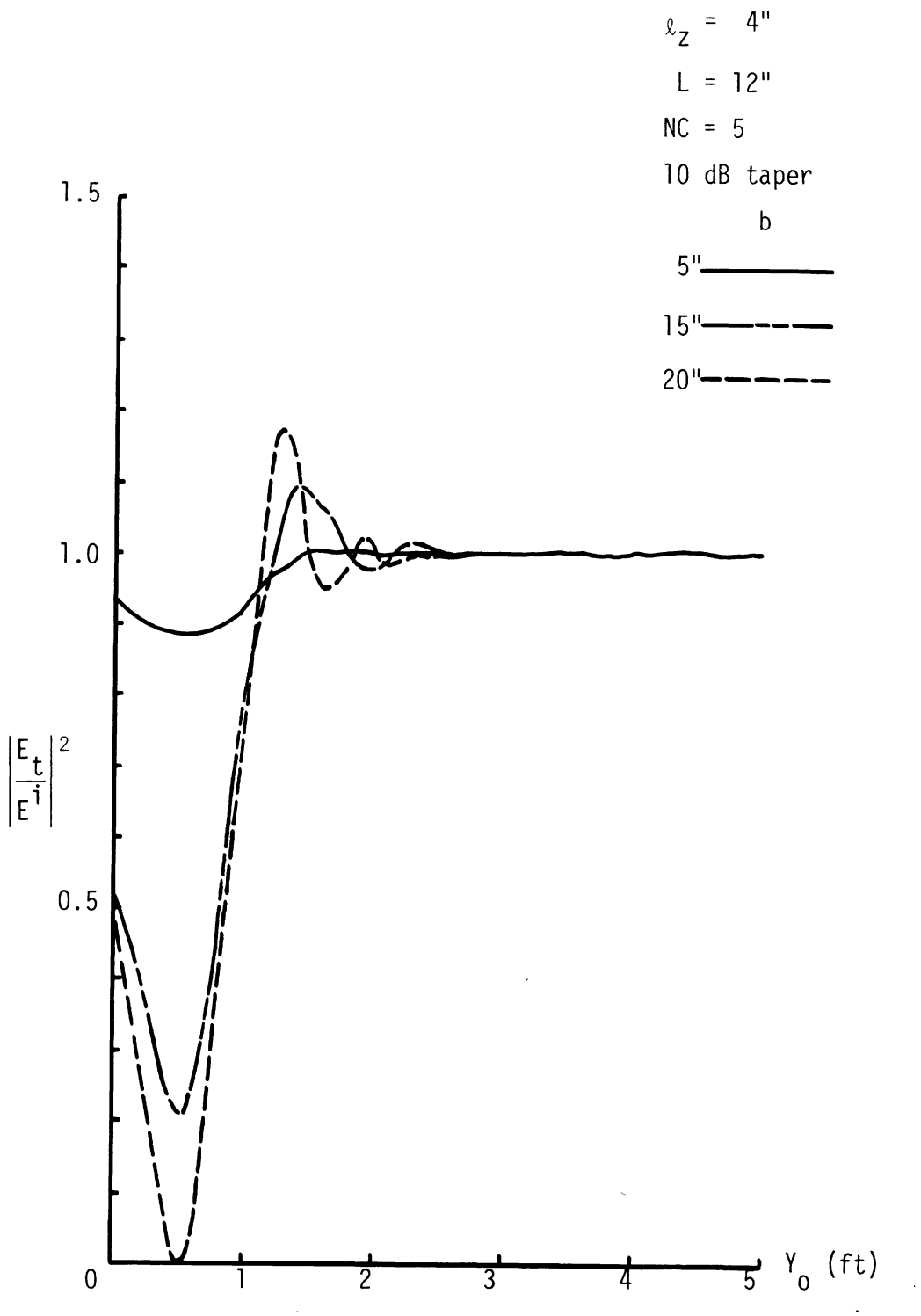

Figure E-23: Field variations on z = 30"-plane, x_o = 10 ft, for different scattering object heights; a = 6", h = 30", d = 100 ft.

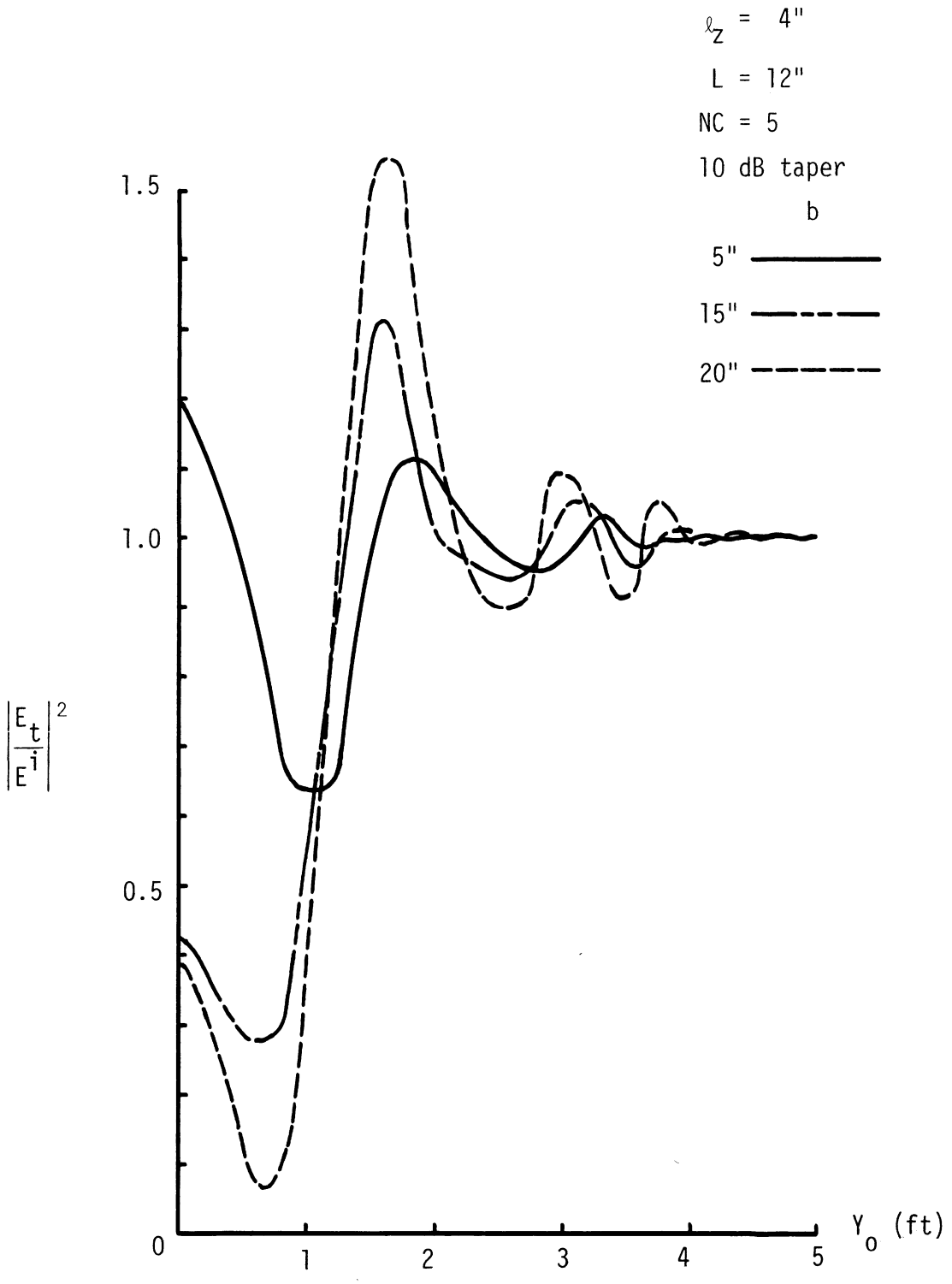

Figure E-24: Field variations on z = 30"-plane, x_o = 50 ft, for different scattering object heights; a = 6", h = 30", d = 100 ft.

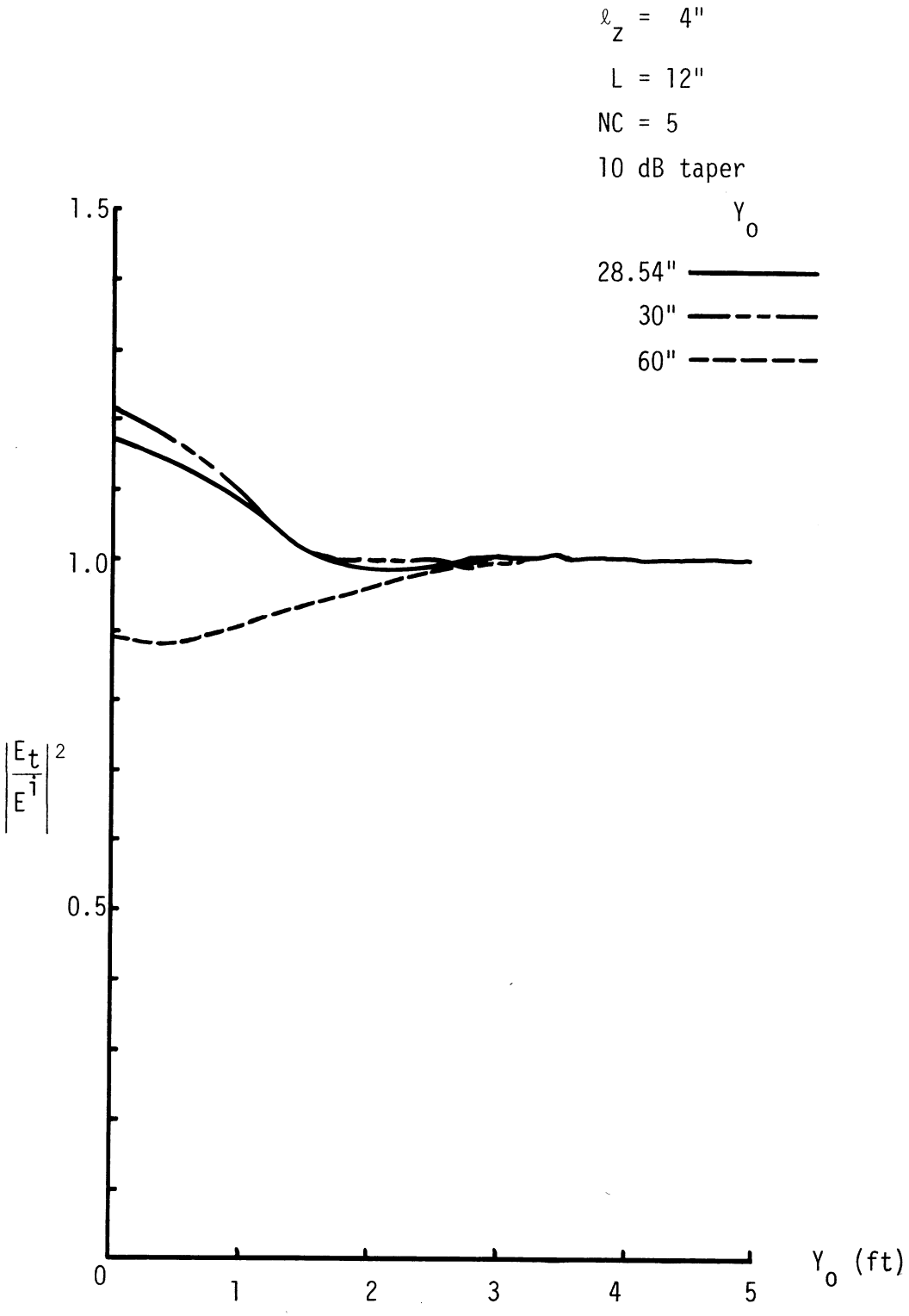

Figure E-25: Field variations for a = 30", b = 6" (a crawling man), h = 30", d = 100 ft.

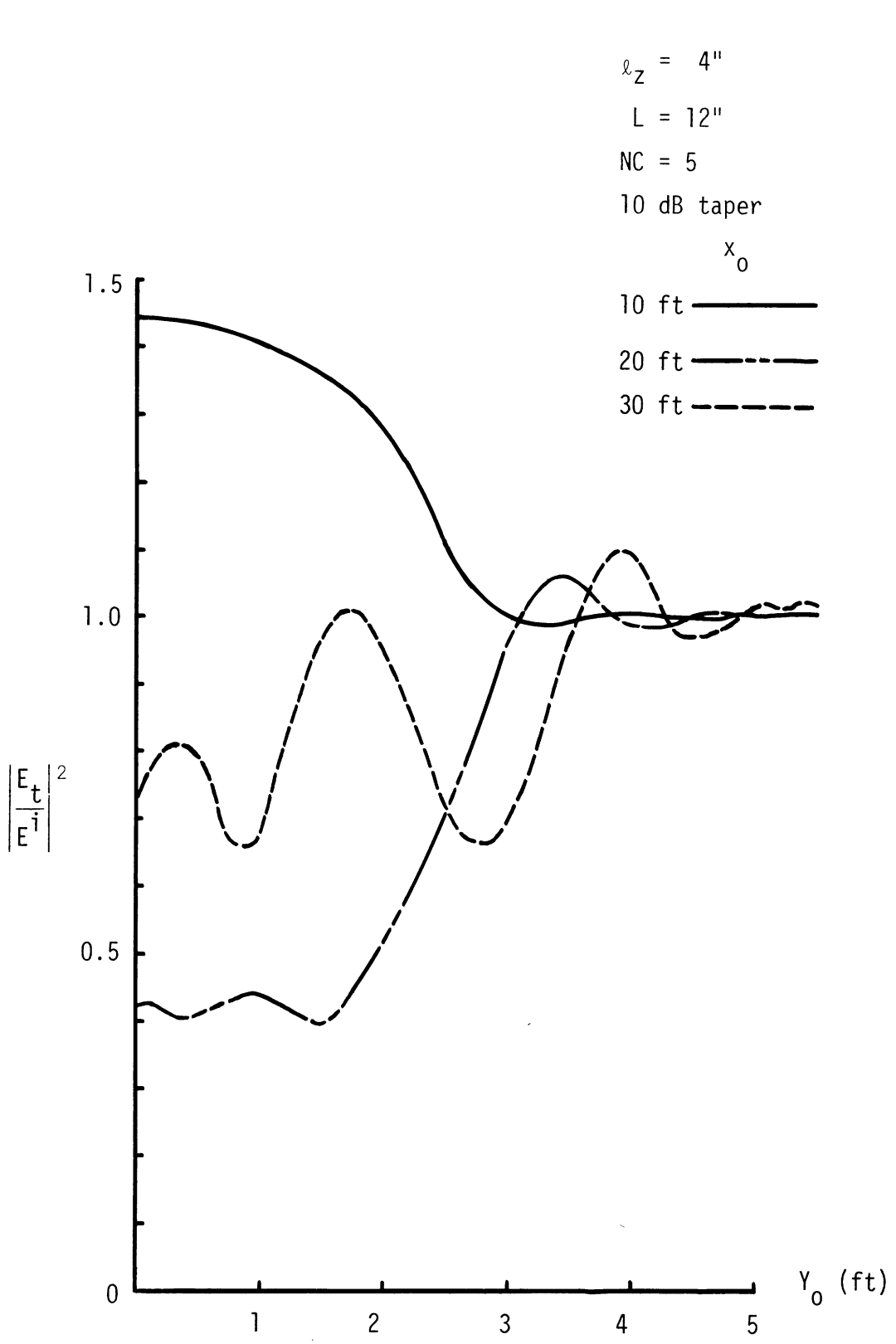

Figure E-26: Field variation for a = 30", b = 6" (a crawling man), h = 30", d = 100 ft.

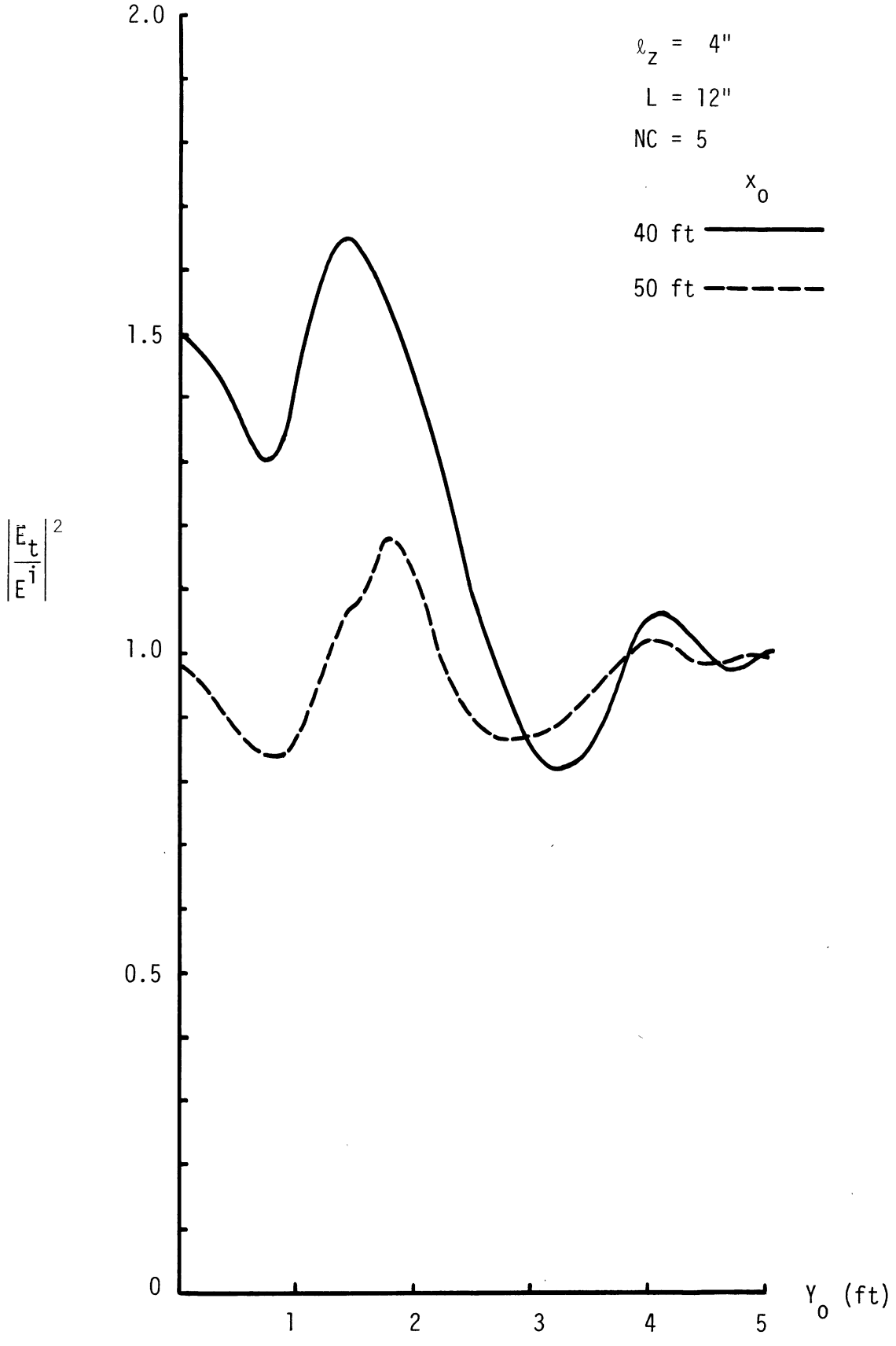

Figure E-27: Field variations for a = 30", b = 6" (a crawling man), h = 30", d = 100 ft.

7. CONCLUSION

We have carried out a theoretical scattering analysis for the purpose of determining qualitatively the detectability of a human intruder as the intruder moves through the boresight plane of our antenna system.

The key assumptions made in the analysis are: (i) an intruder can be simulated by a thin metallic rectangular plate of appropriate dimensions; (ii) the field pattern of our antenna varies over the illuminated side of the rectangular plate (i.e. the intruder) in such a way that the pattern at the center of the plate is an adequate representative pattern of the patterns over the entire illuminated area of the plate; (iii) the ground is level and smooth devoid of significant roughness or random variation of surface.

Based on these assumptions, we have computed the normalized field (to be more precise, the modulus square of the normalized field) sensed by the receiving antenna with the one transmitter/one receiver antenna system. Our numerical results indicate that an average human intruder, when he moves through the boresight plane, can be detected, regardless of the point in the boresight plane.

As pointed out previously, however, our model of an average human intruder may not be an adequate one when the intruder crosses the boresight plane in the near zone, say, $0 \leq x_0 \lesssim 10$ ft., in a crowched, or crawling posture. Therefore, the numerical data for this case may not be reliable ones.

A possible improvement one could contemplate would be adjoining a supplementary antenna system to our antenna system in such a way that illumination in the near zone can be enhanced. It seems that such a scheme would make the detection of a small scattering object in the near zone easier.

Another area of possible improvement over the present analysis would be a more realistic simulation of a crawling man in the near zone, in the form of a rectangular box. Such analysis can be done with some modifications to the present analysis.

APPENDIX 1. PROGRAM LIST

The program list presented here is for computation of the normalized field (equation (66)). The user needs to specify the following input data:

W : wavelength

D : antenna range

AH : antenna height

AL : Y-dimension of antenna aperture

ALZ : Z-dimension of antenna aperture.

Then, the program prints out the antenna far zone distance (in inches). The user needs then to process to specify the rest of the input data:

NC : number of cell apertures into which the antenna aperture is to be divided.

The program prints out the cell far zone distance in inches. The user then should remember that the smallest XO should not be smaller than the cell far zone distance.

AZO : amplitude aperture taper (in dB) across the Z-dimension of the aperture. If ALZ is chosen to be sufficiently small, the user may set AZO = 0.

AYO : amplitude aperture taper (in dB) across the Y-dimension of the aperture. If 10 dB taper is desired, the user writes AYO = 10., etc.

A : reflector Y-dimension (half)

B : reflector Z-dimension (half)

XO : reflector x-coordinate

ZO : reflector center Z-coordinate

DYO : step size with which to move the reflector in the Y-direction. The program reaches 5 ft. in y_o, regardless of the step size the user specifies.

Then, the program prints out first the undisturbed field (equation (46)) and proceeds to print out

XO YO ZO ENOM EPHASE .

In the IBM 360/168 at the University of Michigan Computing Center, the typical CPU time for the program for normalized field for 20 points of YO is around 0.289 seconds.

For the user's convenience, we list the variable names in the program and the corresponding notations in the text.

AL = L	NC = 2N + 1
ALZ = ℓ_z	ANOM = ℓ/L
ALY = ℓ_y	(XO, YO, ZO) = (x_o, y_o, z_o)
AZ = a_1	R21 = $(\overset{xo}{R}_2)_1$
AY = a_2	R22 = $(\overset{xo}{R}_2)_2$
AH = h	DEL = $\hat{\delta}$
D = d	PO = $P_I^i/\ell L/P_{Mf}$

PIO = $P_I / \ell L / P_{Mf}$

TED = E_t^i

Q = q

TIB1 = $I^{(1)}(b)$

TIB2 = $I^{(2)}(b)$

TIB3 = $I^{(3)}(b)$

TIB4 = $I^{(4)}(b)$

YNO = y_n^o $(= n\ell_y, \quad -N \leq n \leq N)$

EPN = ε_n , $\quad -N \leq n \leq N$

TIN = $I_n(a)$, $\quad -N \leq n \leq N$;

BZ1 = $\overline{Z}^{(1)}$

BZ2 = $\overline{Z}^{(2)}$

BY1 = $\overline{Y}^{(1)}$

BY2 = $\overline{Y}^{(2)}$;

PA1 = $\overline{M}_z^{(1)}$ $(\overline{\alpha}^{(1)})$

PA2 = $\overline{M}_z^{(2)}$ $(\overline{\alpha}^{(2)})$

PB1 = $\overline{M}_y^{(1)}$ $(\overline{\beta}^{(1)})$

PB2 = $\overline{M}_y^{(2)}$ $(\overline{\beta}^{(2)})$

TP1 = $P_{II}^{(1)}$ $(\overline{\alpha}^{(1)}, \overline{\beta}^{(1)}) \equiv \overline{M}_z^{(1)} \overline{M}_y^{(1)} / P_{Mf}$

TP2 = $P_{II}^{(2)}$ $(\overline{\alpha}^{(2)}, \overline{\beta}^{(2)}) \equiv \overline{M}_z^{(2)} \overline{M}_y^{(2)} / P_{Mf}$;

YMMO = $y_o - y_n^o$, $\quad -N \leq n \leq N$

RN1 = $(R_n^{vo})_1$,

RN2 = $(R_n^{vo})_2$;

$$AZ1 = Z_n^{(1)}, \qquad -N \leq n \leq N$$

$$AZ2 = Z_n^{(2)},$$

$$PAL1 = M_z^{(1)}\left(\alpha_n^{(1)}\right),$$

$$PAL2 = M_z^{(2)}\left(\alpha_n^{(2)}\right);$$

$$AY1 = Y_n^{(1)}, \qquad -N \leq n \leq N$$

$$AY2 = Y_n^{(2)},$$

$$TPBL = M_y^{(1)}\left(\beta_n^{(1)}\right),$$

$$TPBLL = M_y^{(2)}\left(\beta_n^{(2)}\right),$$

$$TSUM1 = \sum_{n=-N}^{N} P_I^{(1)}\, I_n(a)\, \frac{\ell}{L},$$

$$TSUM2 = \sum_{n=-N}^{N} P_I^{(2)}\, I_n(a)\, \frac{\ell}{L};$$

$$TSE1 = E_1^s,$$

$$TSE2 = E_2^s,$$

$$TSE3 = E_3^s,$$

$$TSE4 = E_4^s,$$

$$TSET = E_t^s \equiv \sum_{m=1}^{4} E_m^s,$$

$$TET = E_t^i + E_t^s = E_t$$

$$ENOM = \left|E_t/E_t^i\right|^2$$

EPHASE = $I_m\ (E_t/E_t^i)$;

TIB1 = $I^{(1)}(b)$,

TIB2 = $I^{(2)}(b)$,

TIB3 = $I^{(3)}(b)$,

TIB4 = $I^{(4)}(b)$.

SUBROUTINE FRES (ACI, SI, X) :

ACI = sgn (u) Real $[F(u^2)]$,

SI = sgn (u) $I_m\ [F(u^2)]$.

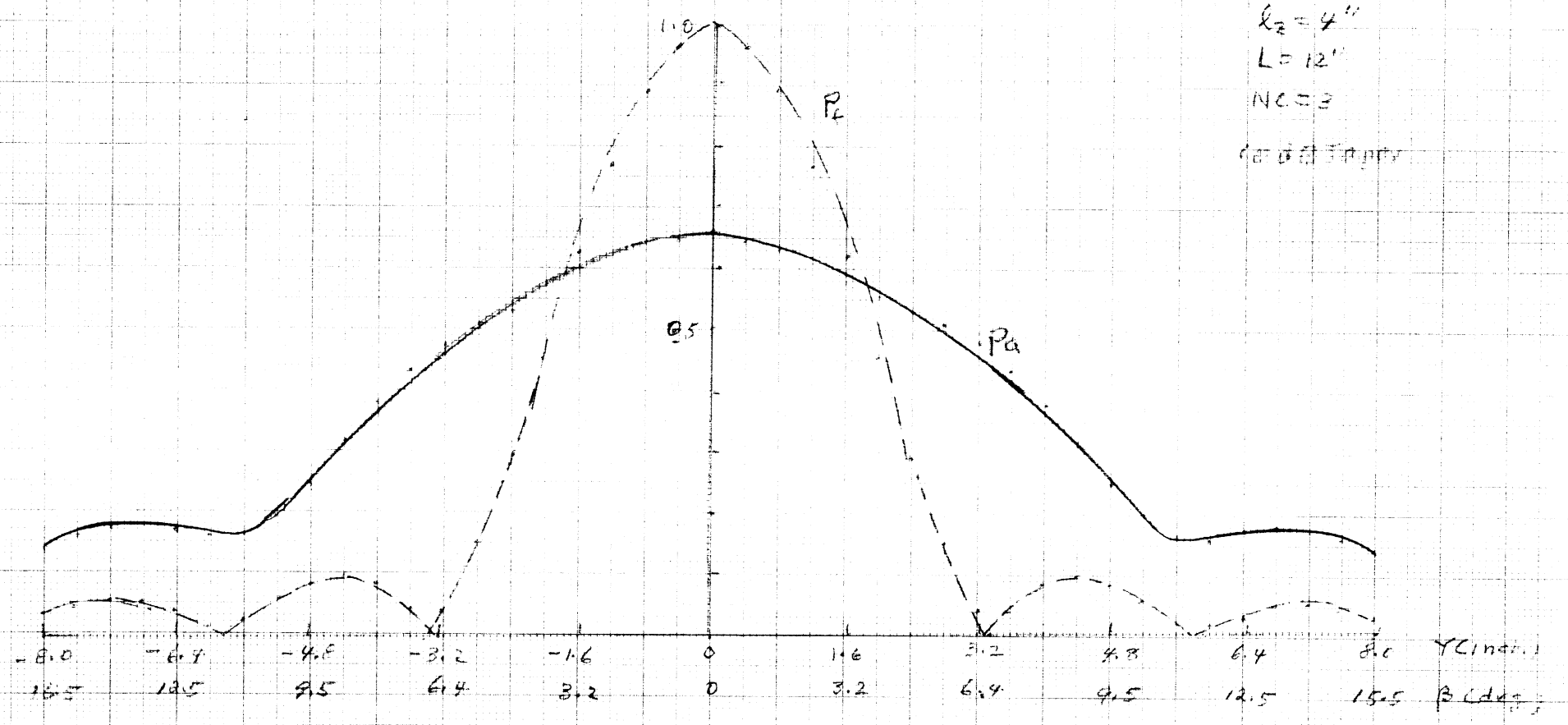

Fig PA-1 : Near field pattern on E-plane ($Z = 20''$ $X = 28.5\lambda''$)

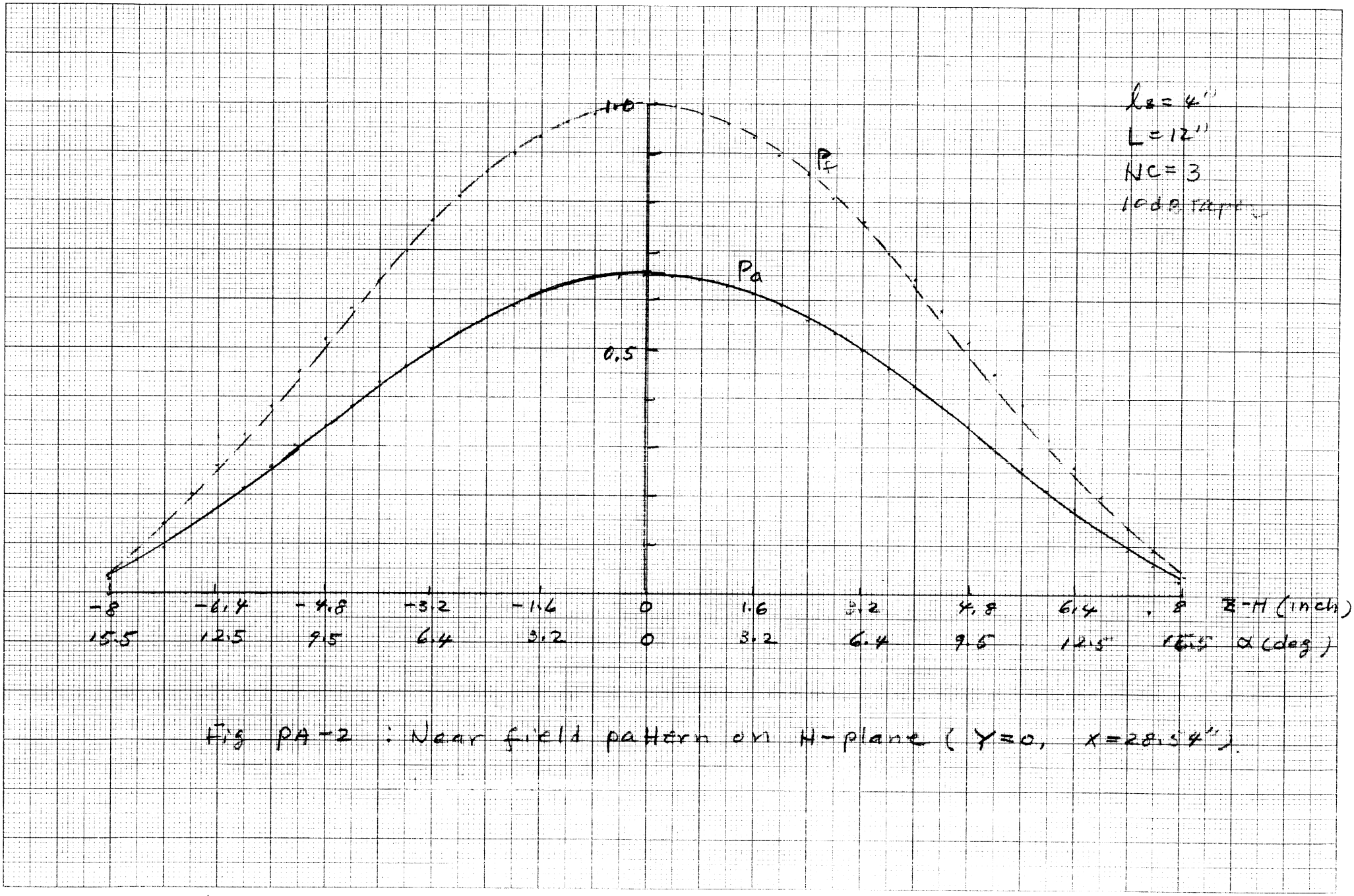

Fig PA-2 : Near field pattern on H-plane (Y=0, X=28.5 4'').

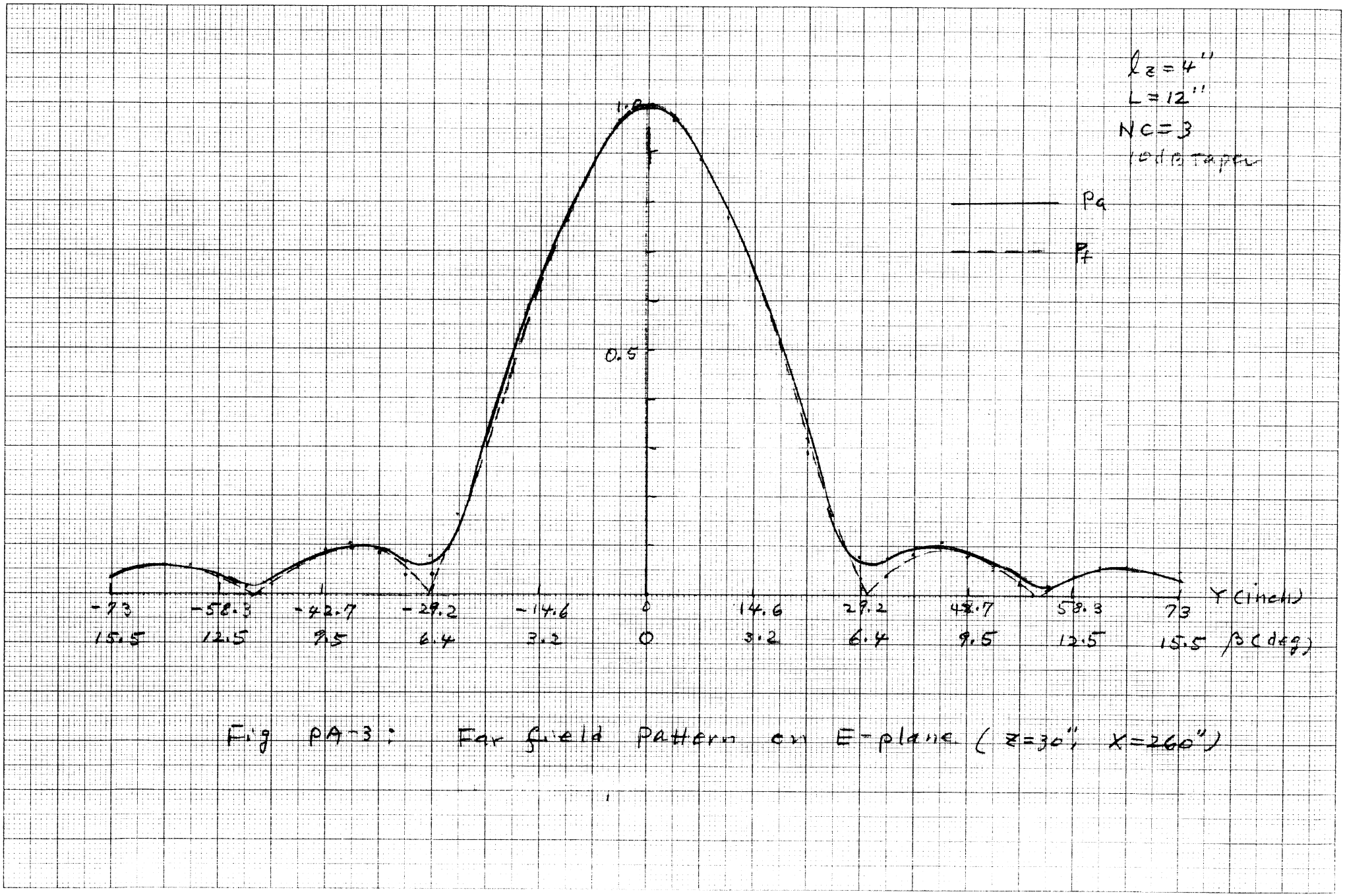

Fig PA-3 : Far field pattern on E-plane ($z = 30''$, $X = 260''$)

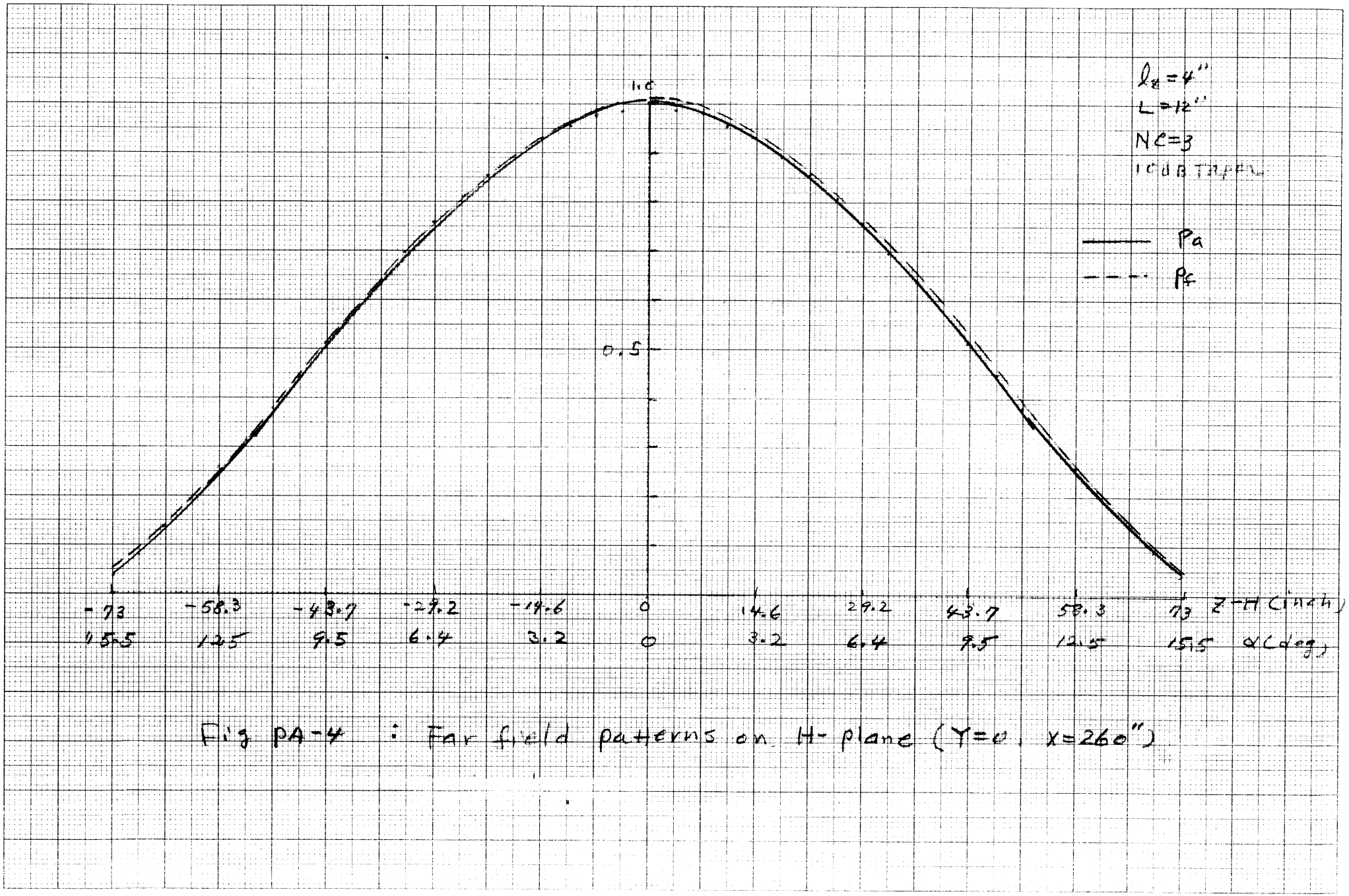

Fig PA-4 : Far field patterns on H-plane (Y=0, X=260")

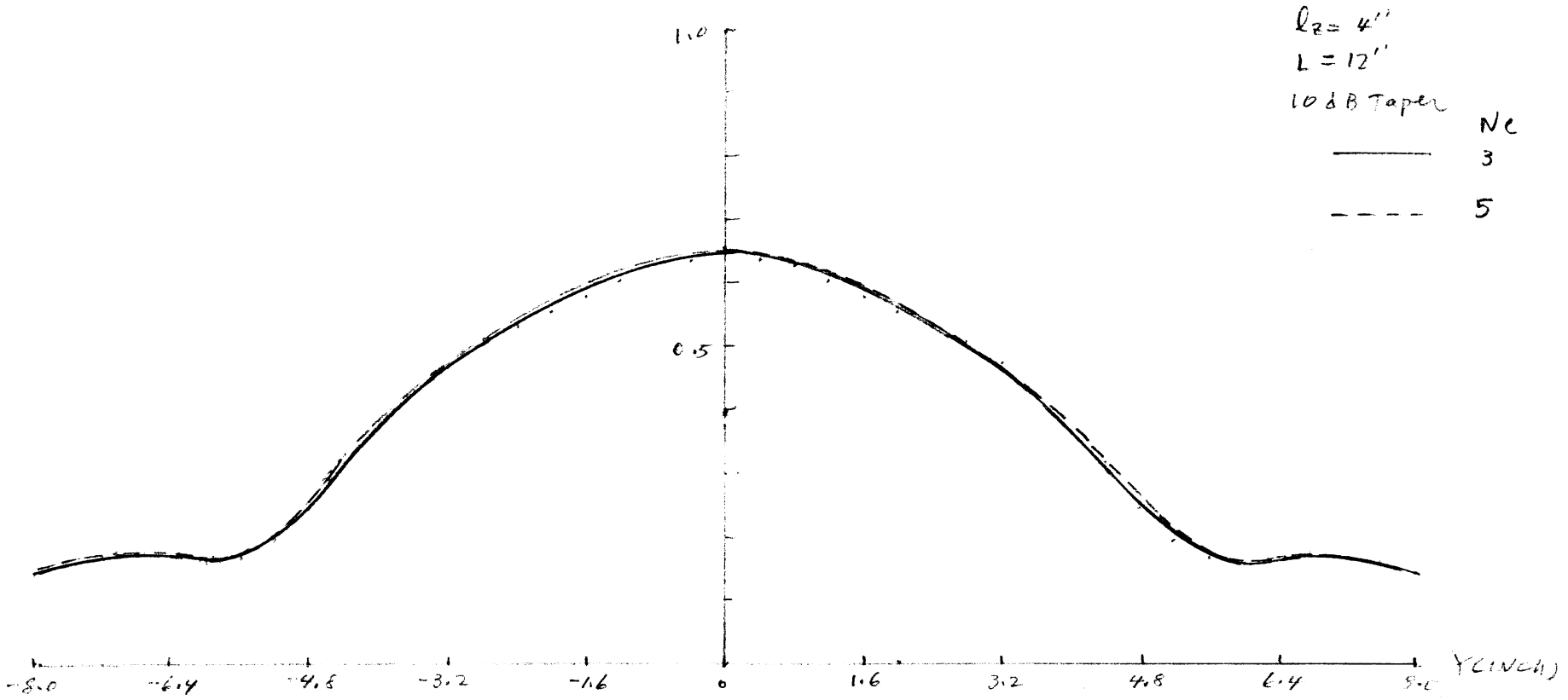

Fig PA-5 : Effect of cell sizes on near field patterns on E-plane (l_z = 30", X = 28.5")

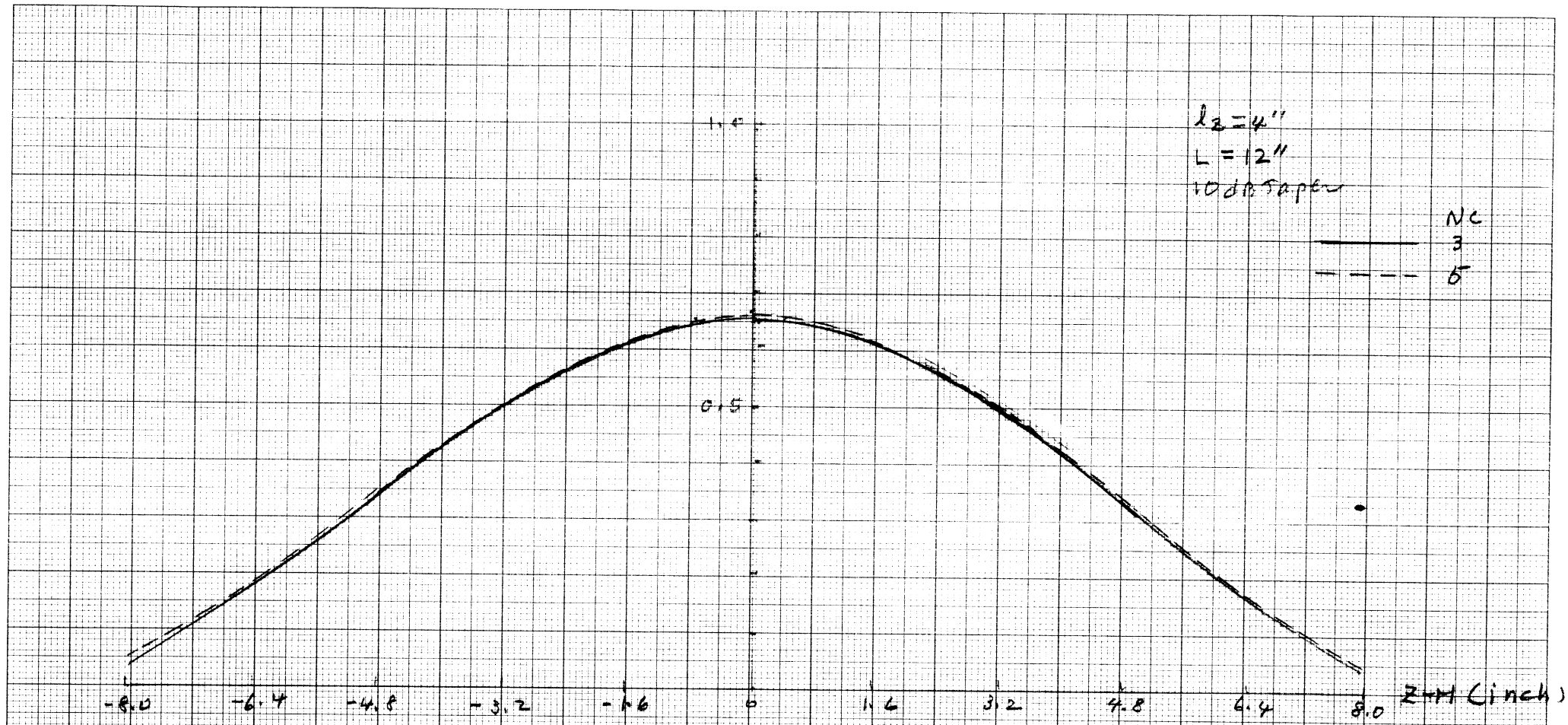

Fig PA-6 : Effect of cell sizes on near field patterns on H-plane ($Z = 0''$, $Y = 0$).

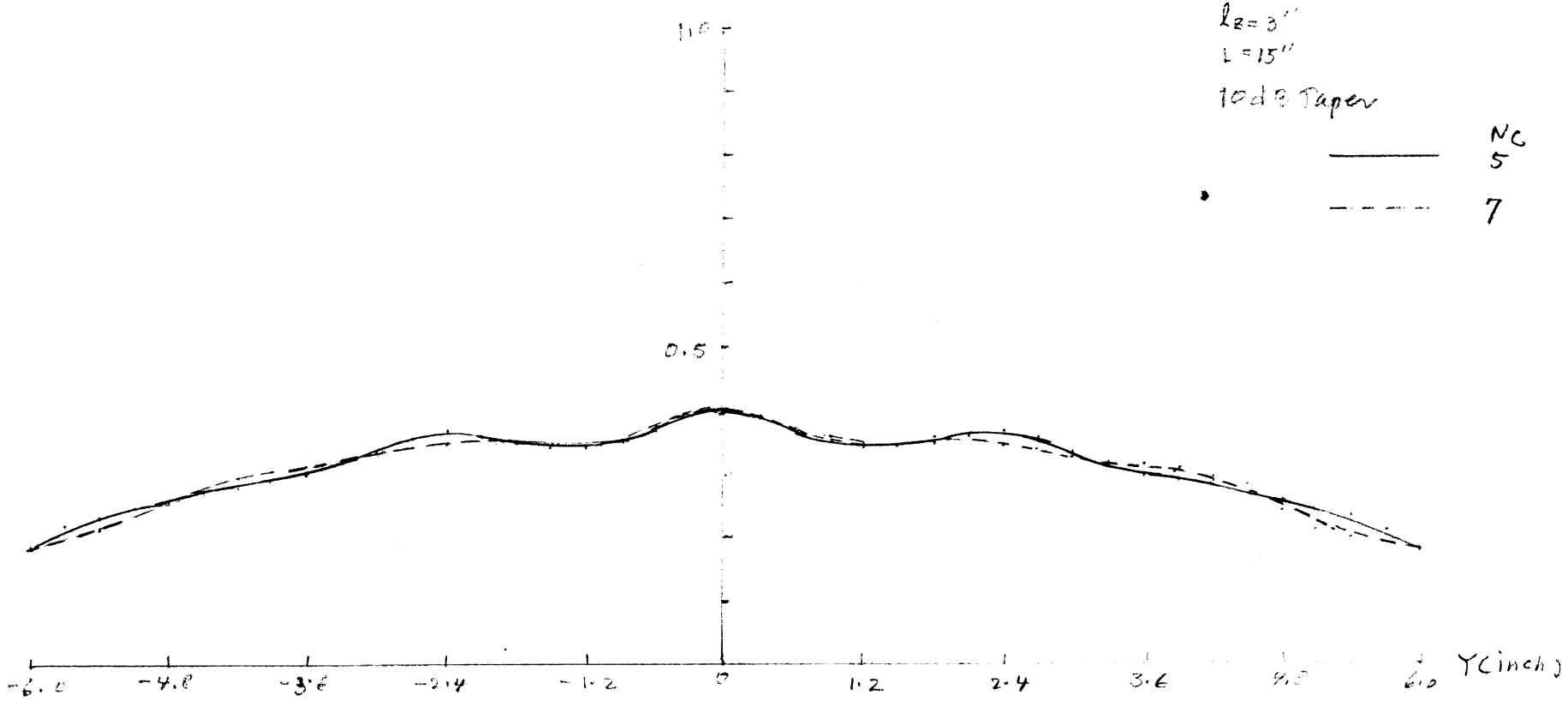

Fig PA-7 : Effect of cell sizes on near field patterns on E plane ($z = 30''$, $x = 16.05''$)

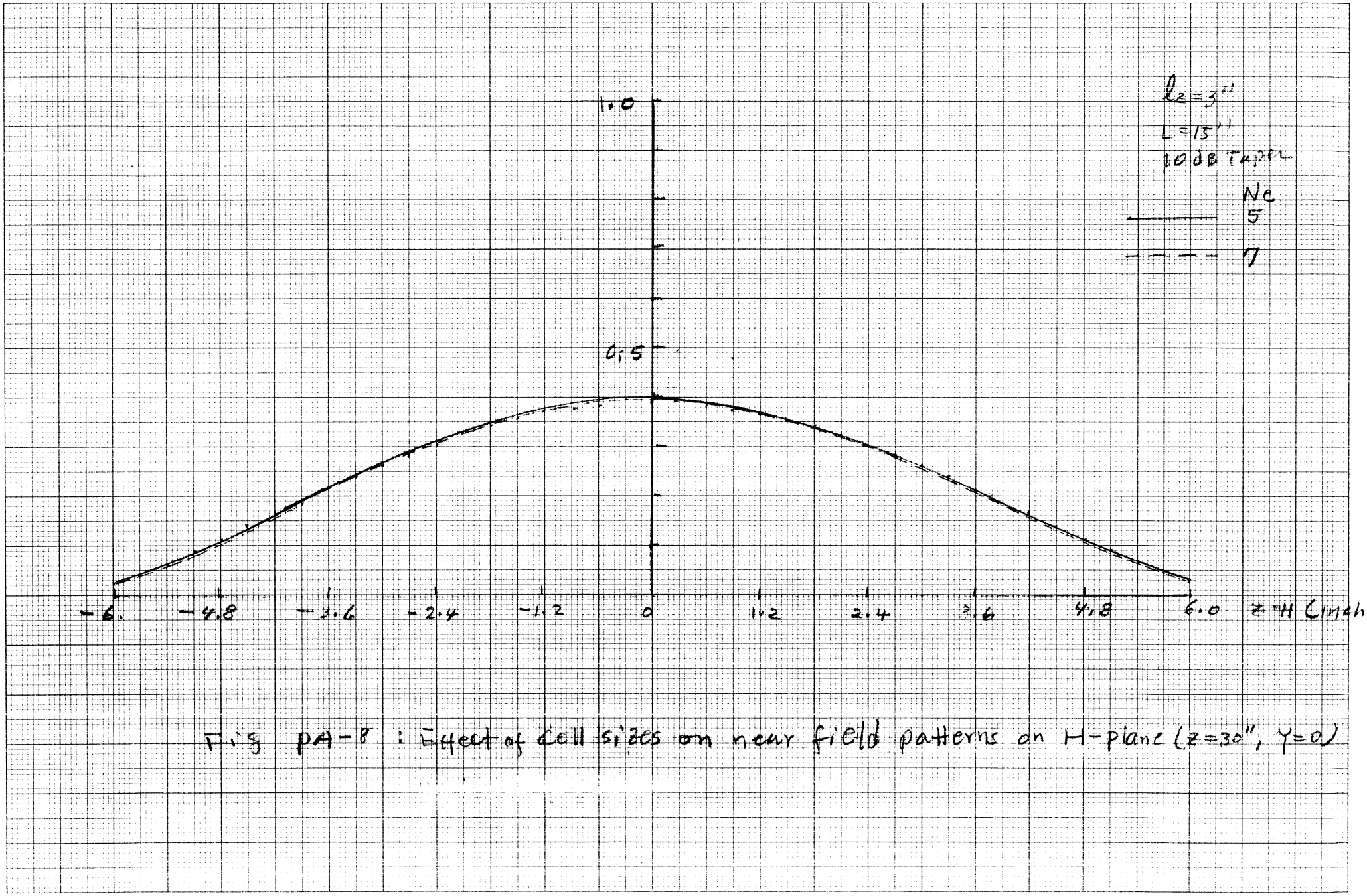

Fig pA-8 : Effect of cell sizes on near field patterns on H-plane (z=30", Y=0)

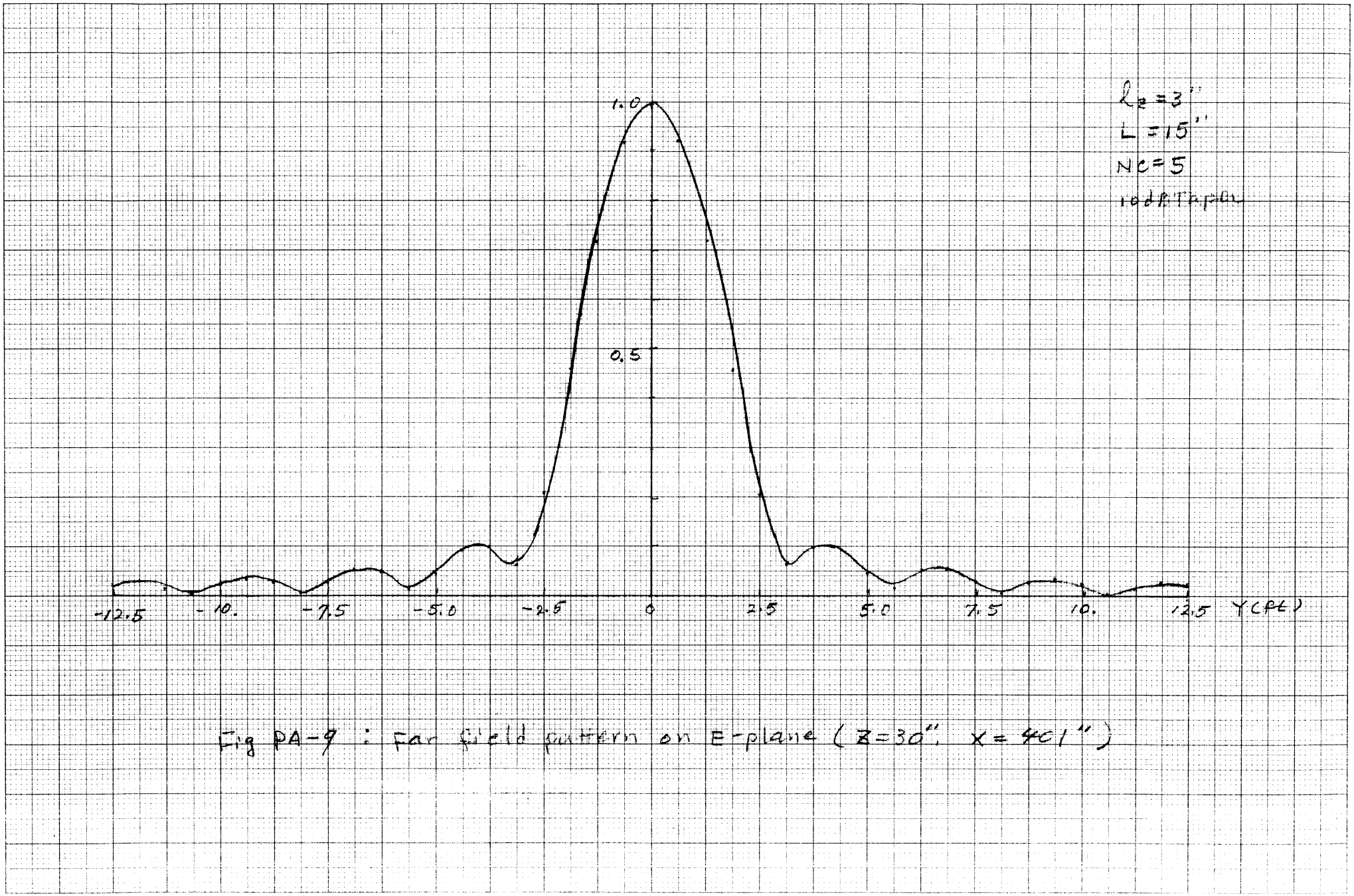

Fig PA-9 : Far field pattern on E-plane ($Z = 30''$, $X = 4C/1''$)

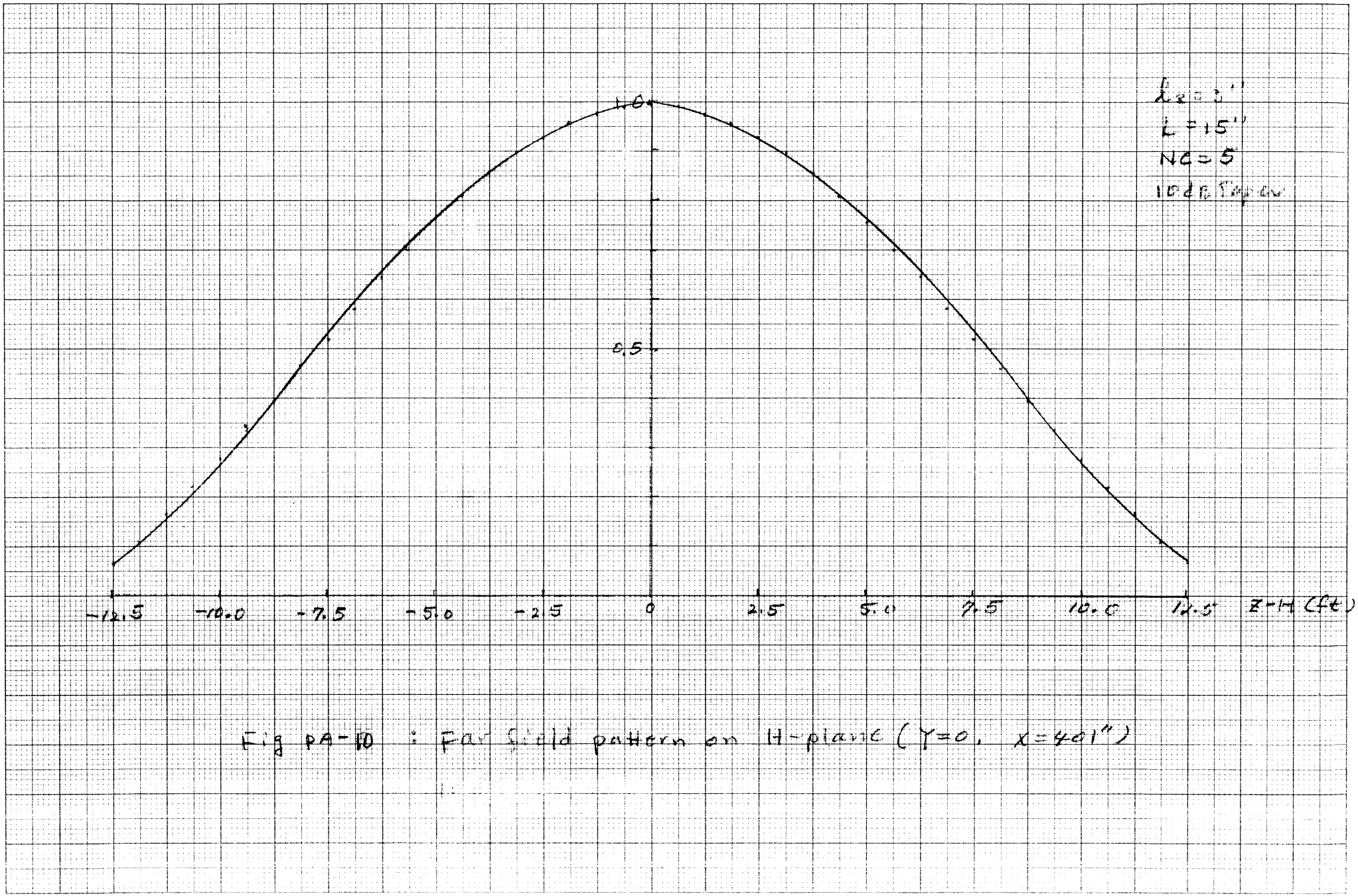

Fig PA-10 : Far field pattern on H-plane ($\gamma = 0$, $x = 401''$)

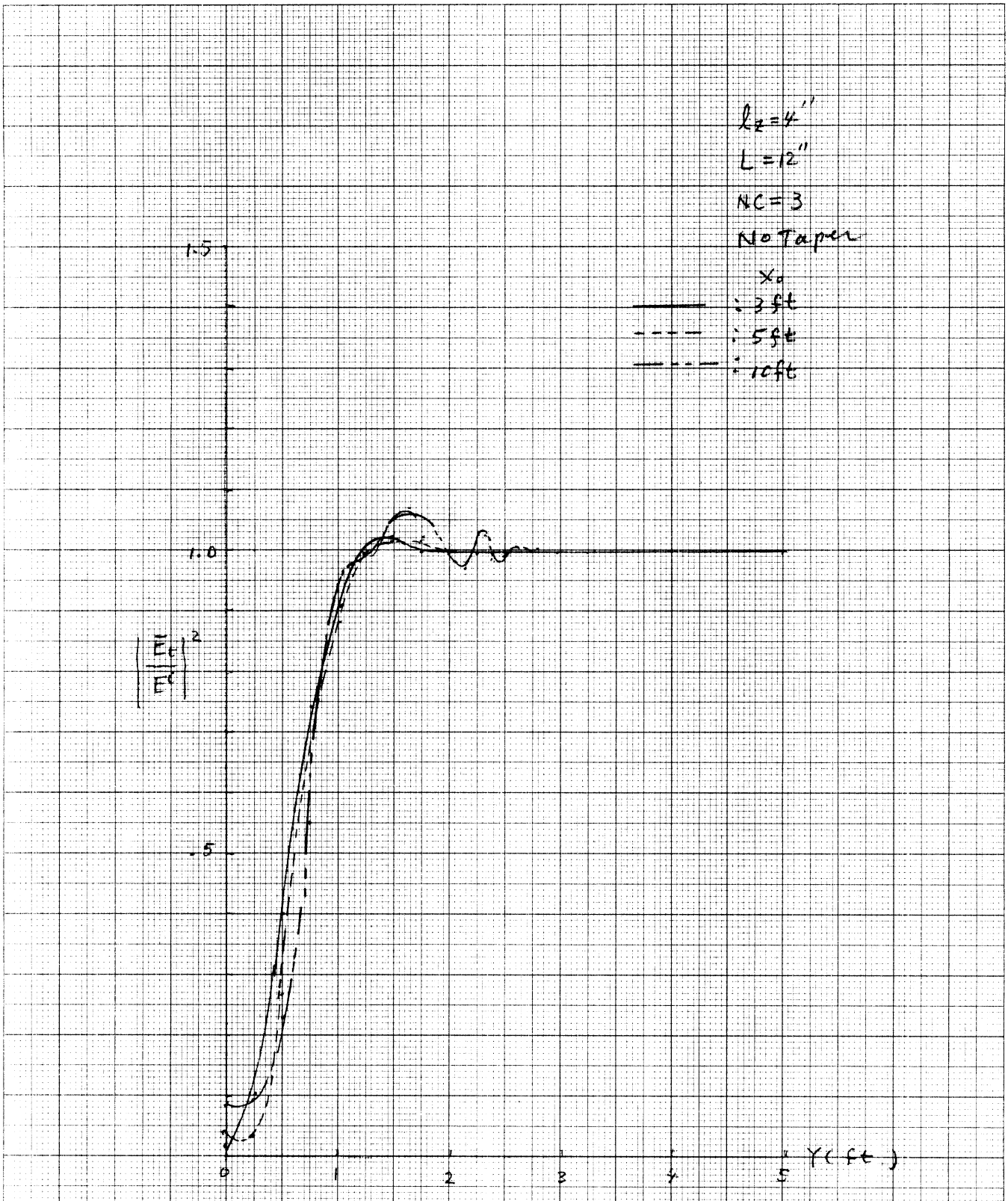

Fig E-1 : Field Variations on $z = 30''$-plane. $a = 6''$, $b = 30''$, $h = 30''$, $d = 100$ ft.

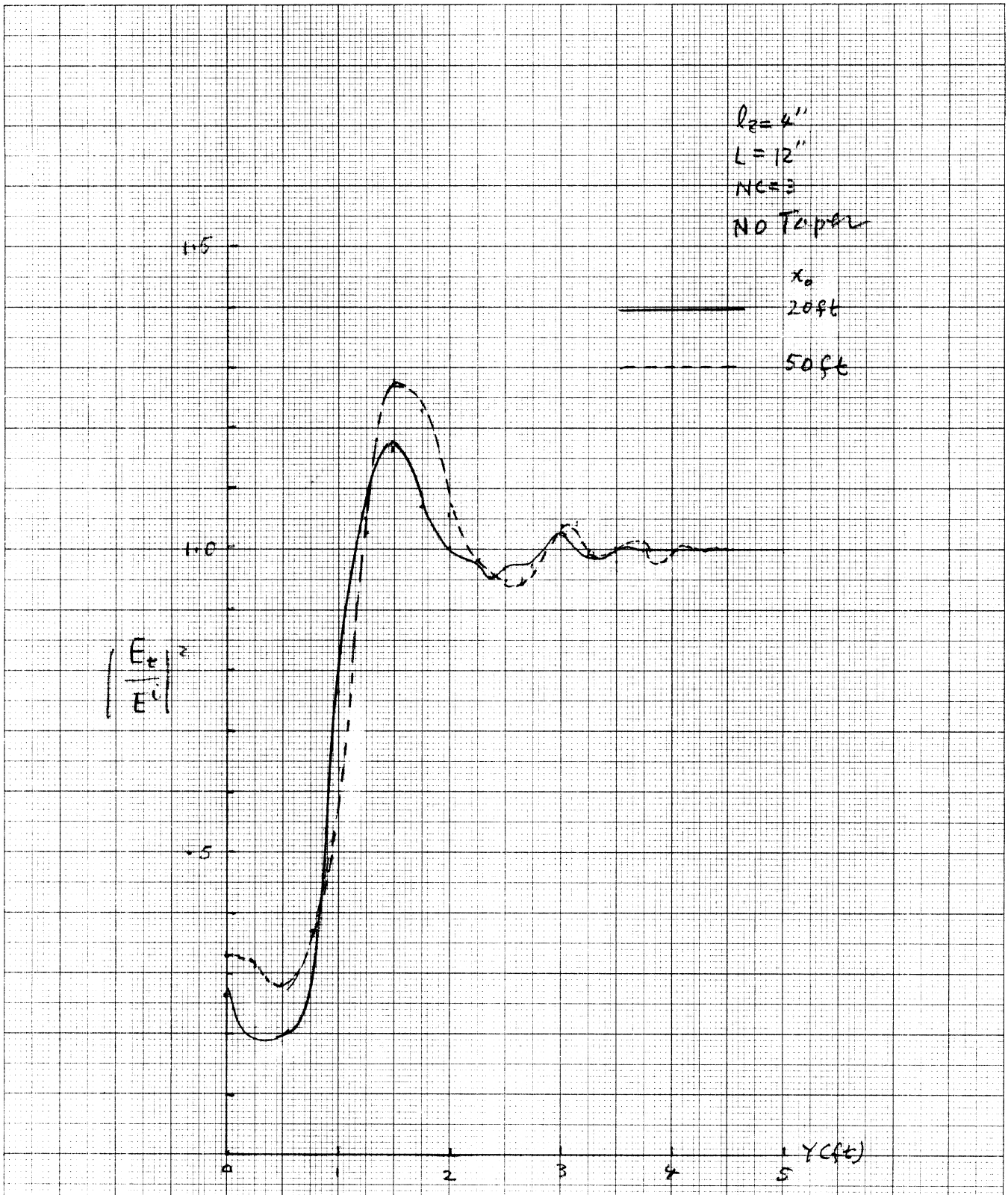

Fig E-2 : Field variations on $z = 30''$-plane. $a = 6''$, $b = 30''$, $h = 30''$, $d = 100$ ft.

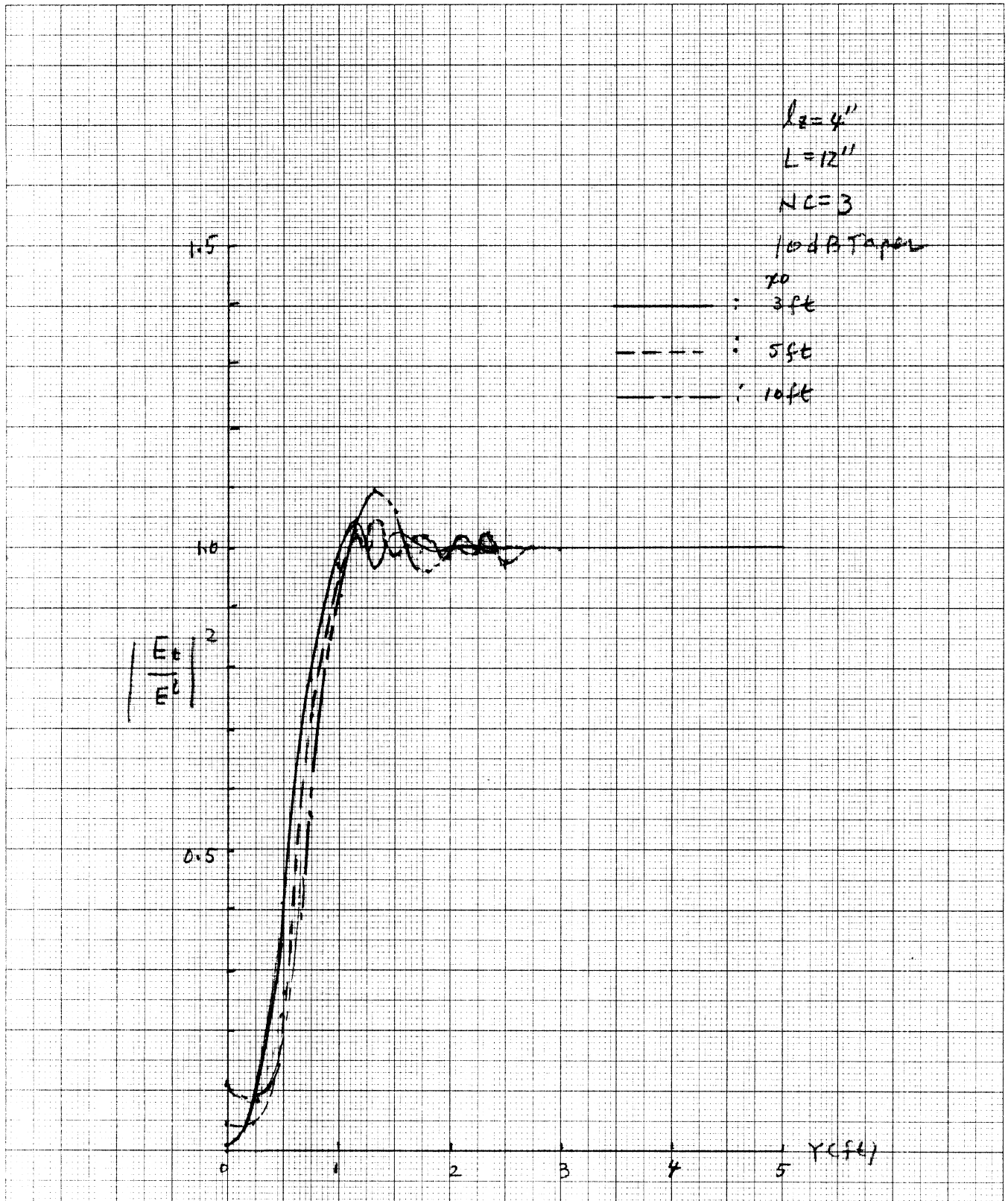

Fig E-3: Field variations on $z = 30''$-plane, $a = 6''$, $b = 30''$, $h = 30''$, $d = 100$ ft.

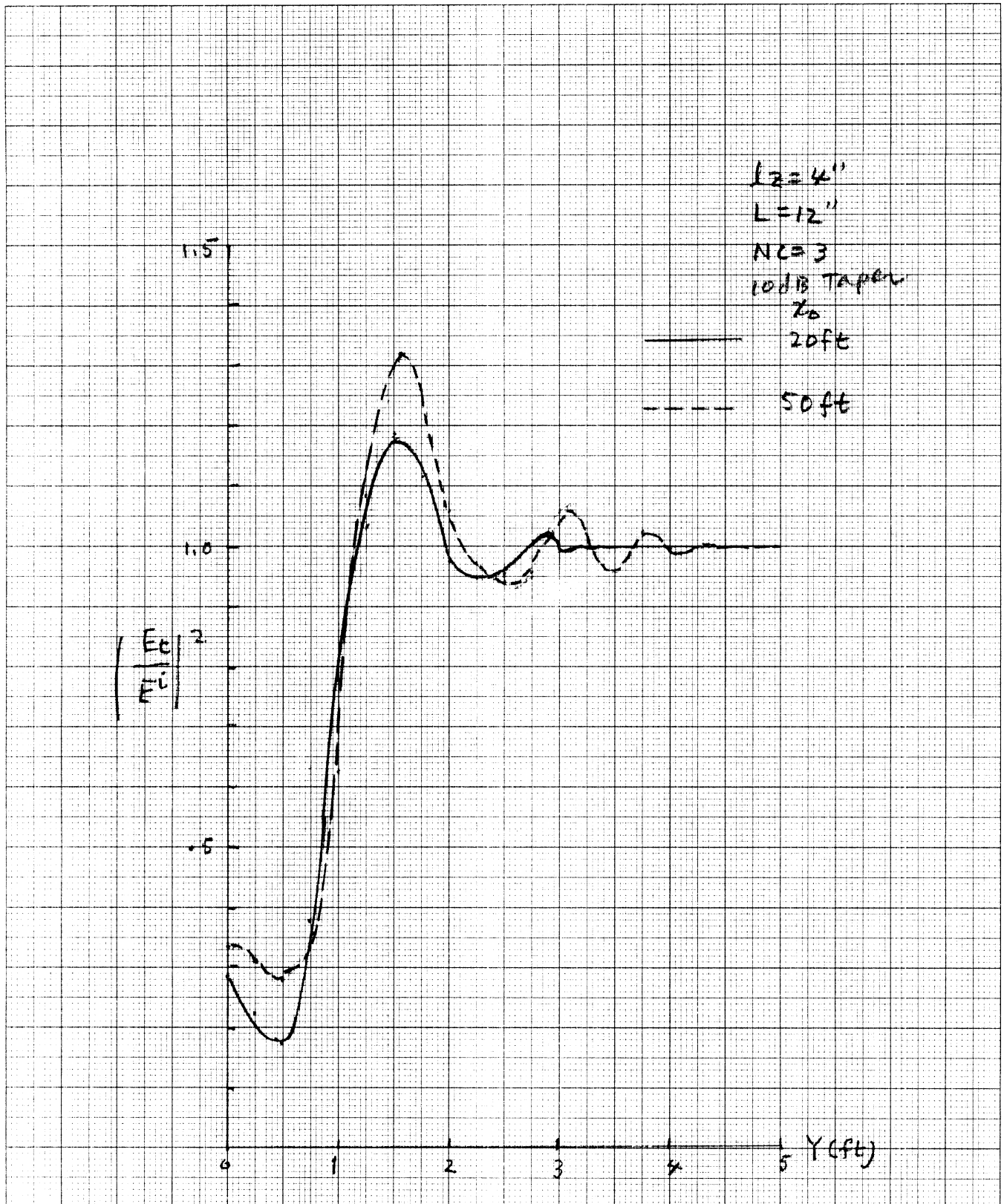

Fig E-4 : Field variations on z = 30" - plane, a = 6", b = 30", h = 30", d = 10ft.

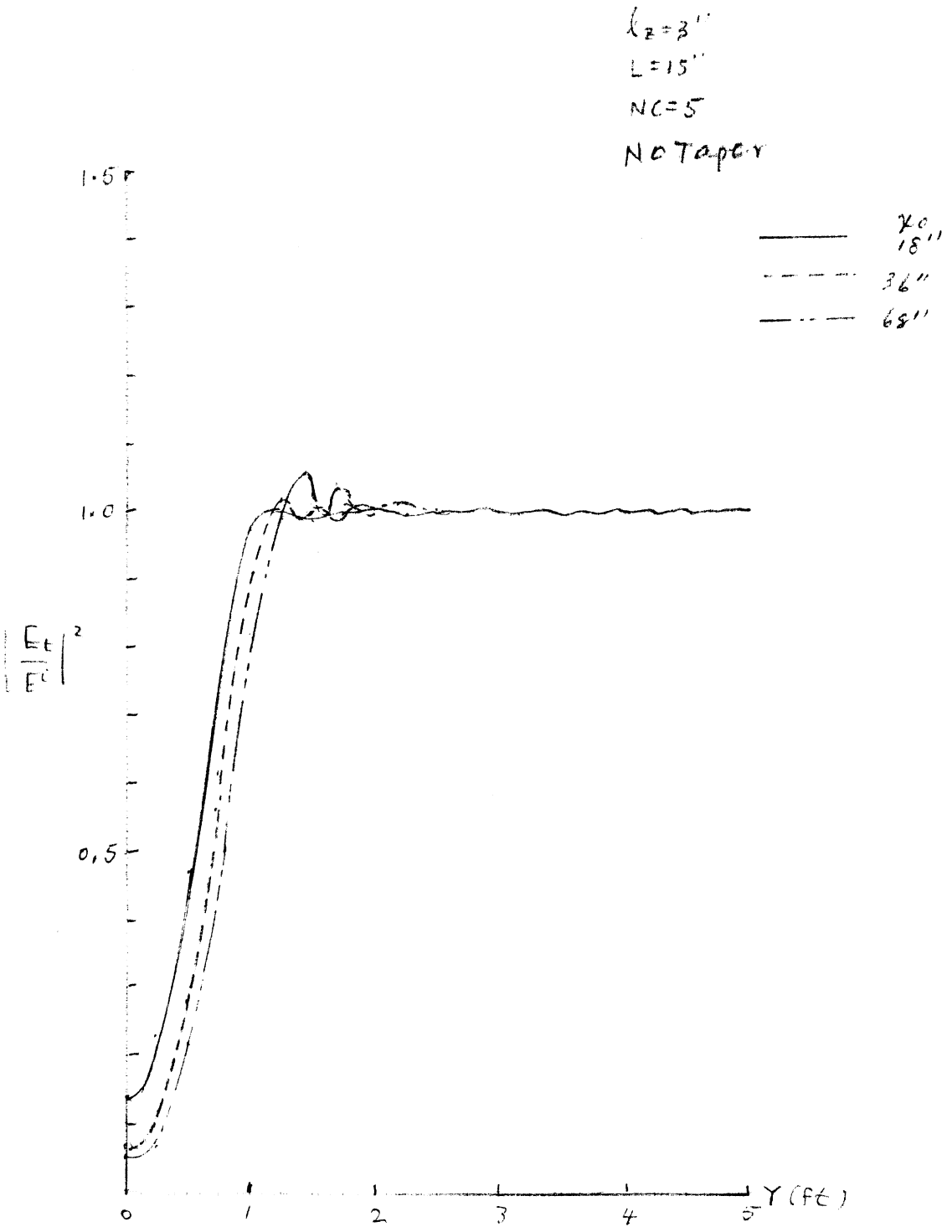

Fig E-5 Field variations on $z = 30''$-plane, $a = 6''$, $b = 30''$, $h = 30''$, $d = 100$ ft.

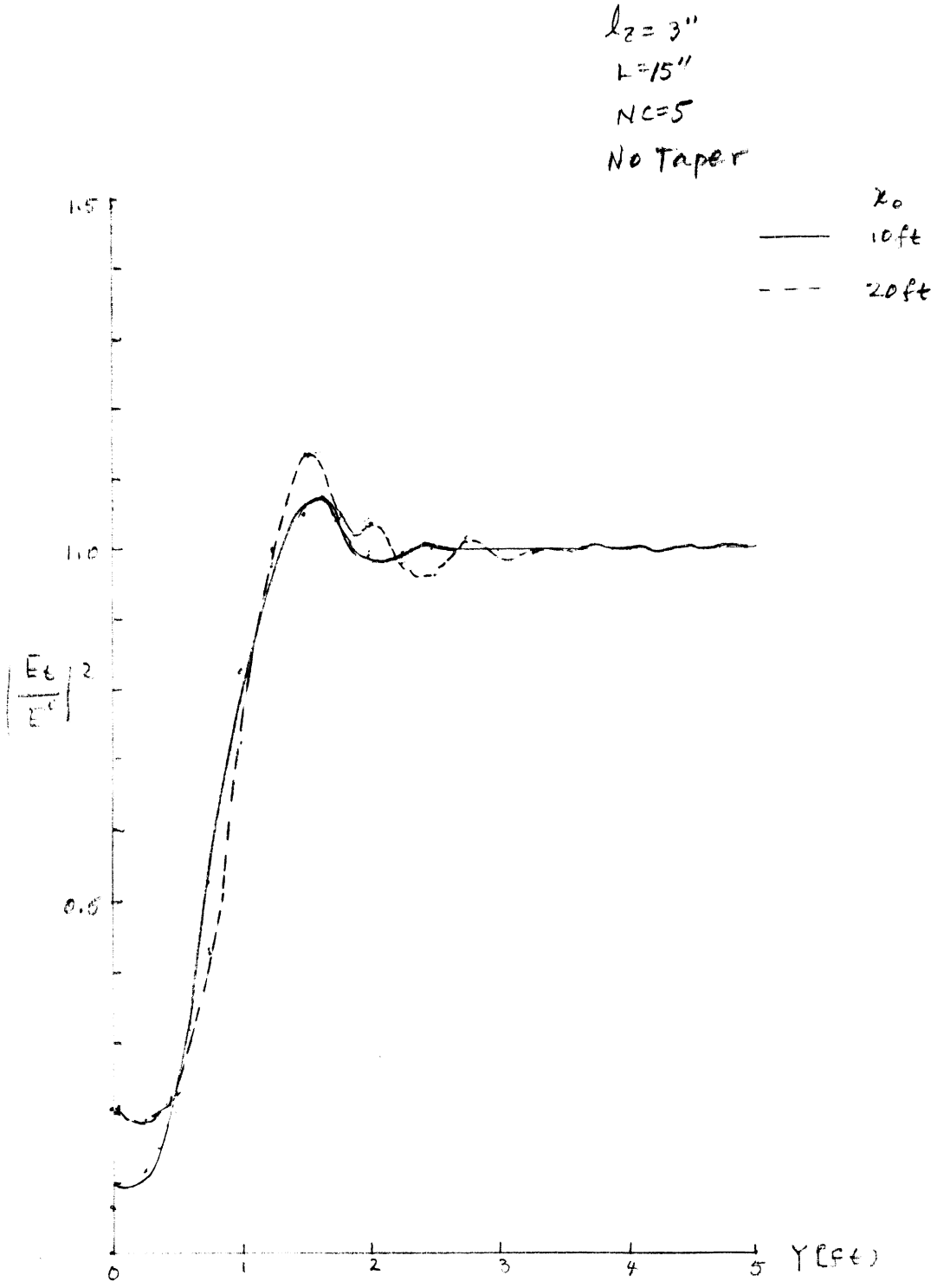

Fig E-6 : Field Variations on $z = 30''$-plane, $a = 6''$, $b = 30''$
$h = 30''$, $d = 10$ ft.

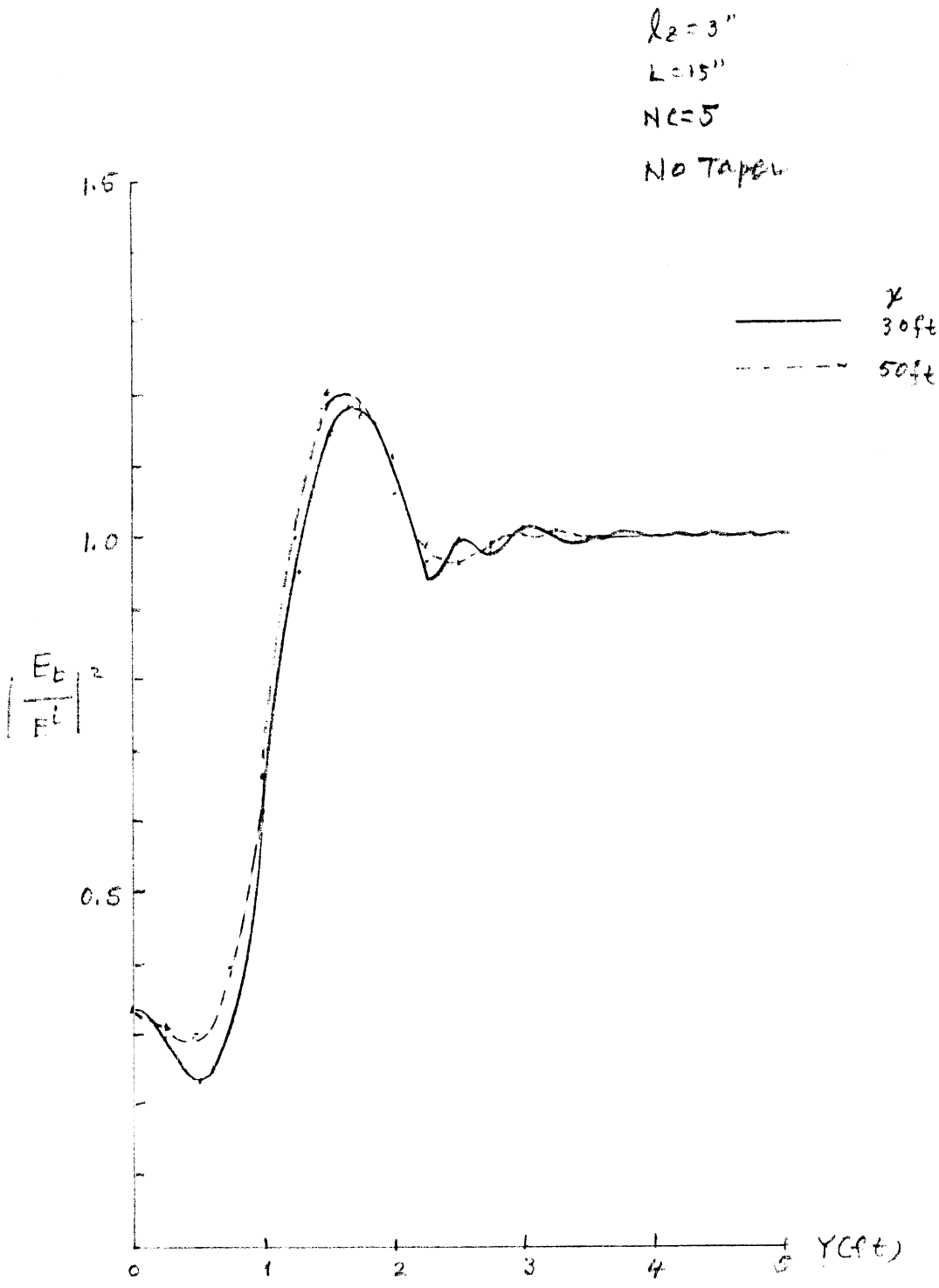

Fig E-7 : Field variations on $z = 30''$-plane. $a = 6''$, $b = 30''$ $h = 30''$, $d = 100ft$.

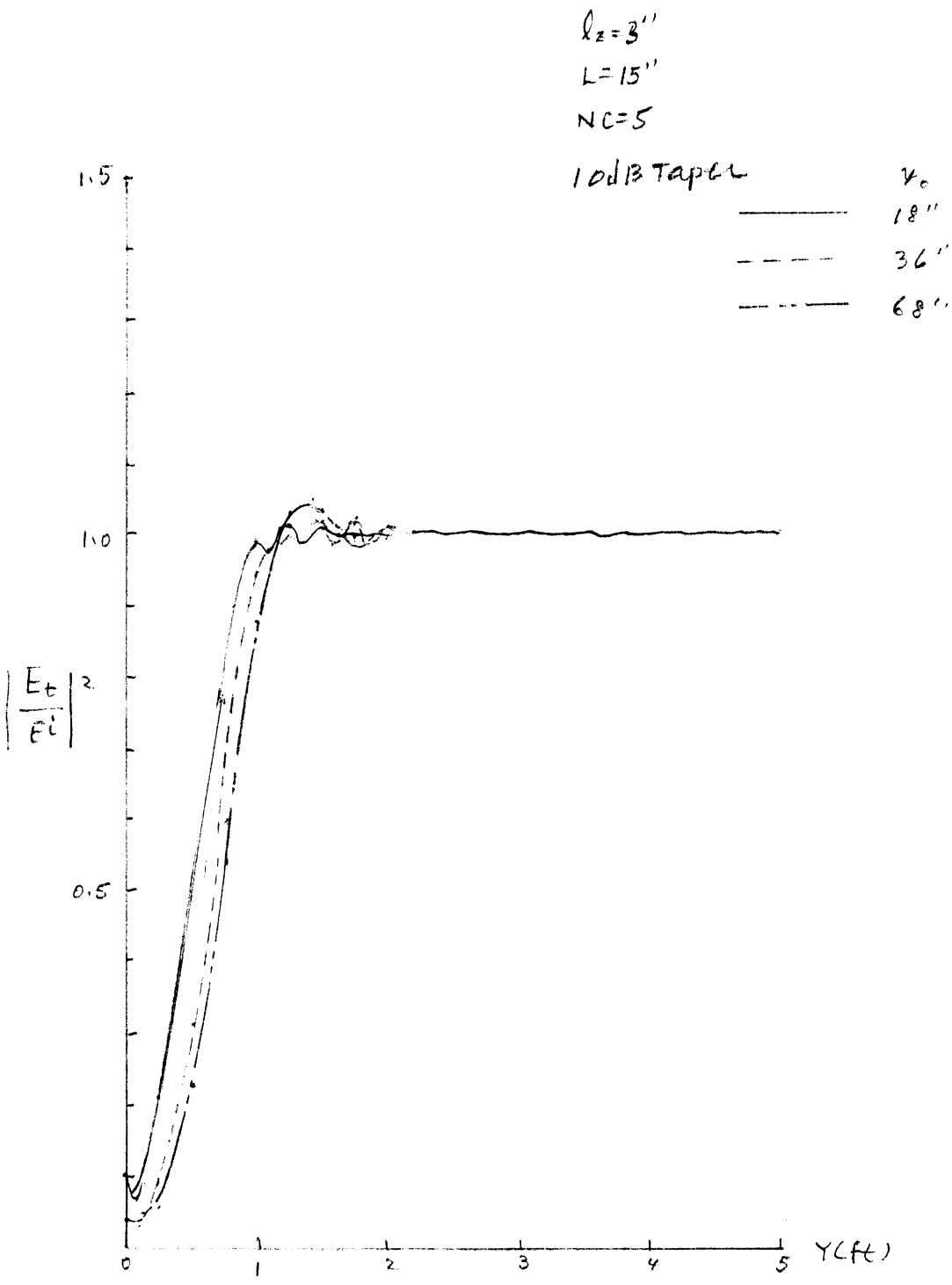

Fig E-3 : Field Variations on Z=30" plane, $a = 2''$, $b = 30''$

$h = 30''$, $d = 100$ ft.

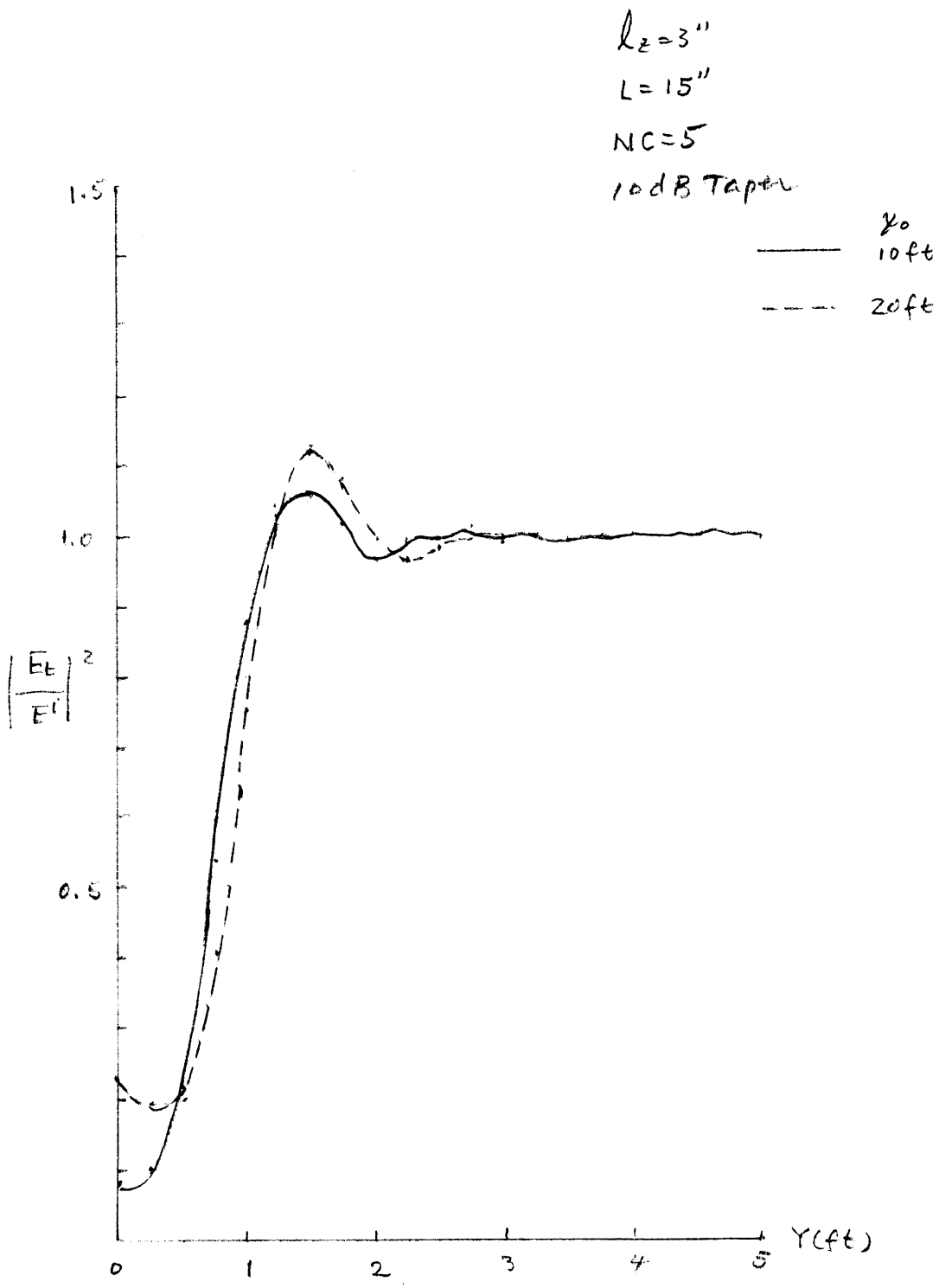

Fig E-9 : Field variations on $z = 30''$-plane, $a = 6''$, $b = 30''$, $h = 30''$, $d = 100$ ft.

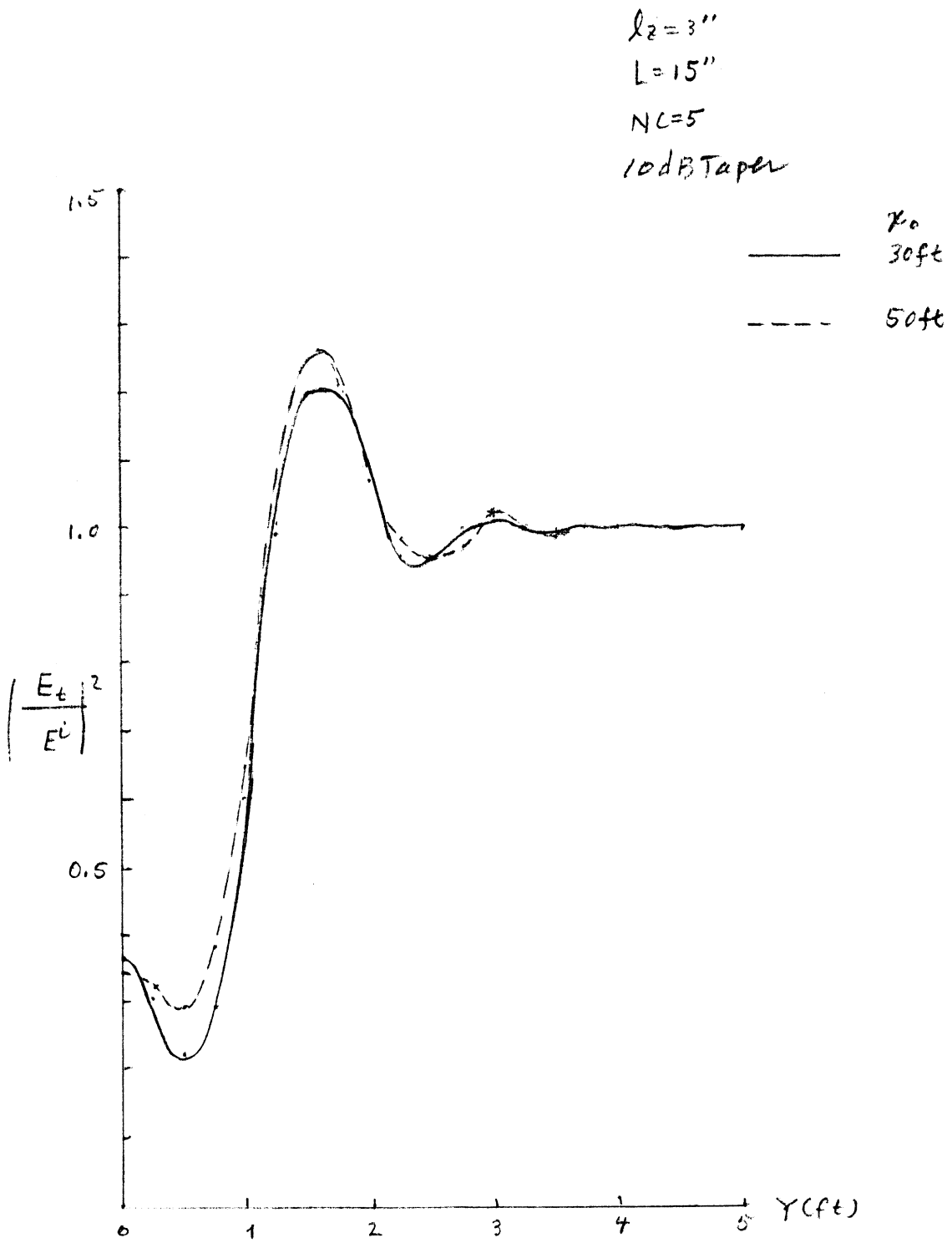

Fig E-10 Field Variations on Z = 30" plane. a=6", b=30"
h=30", d=100ft.

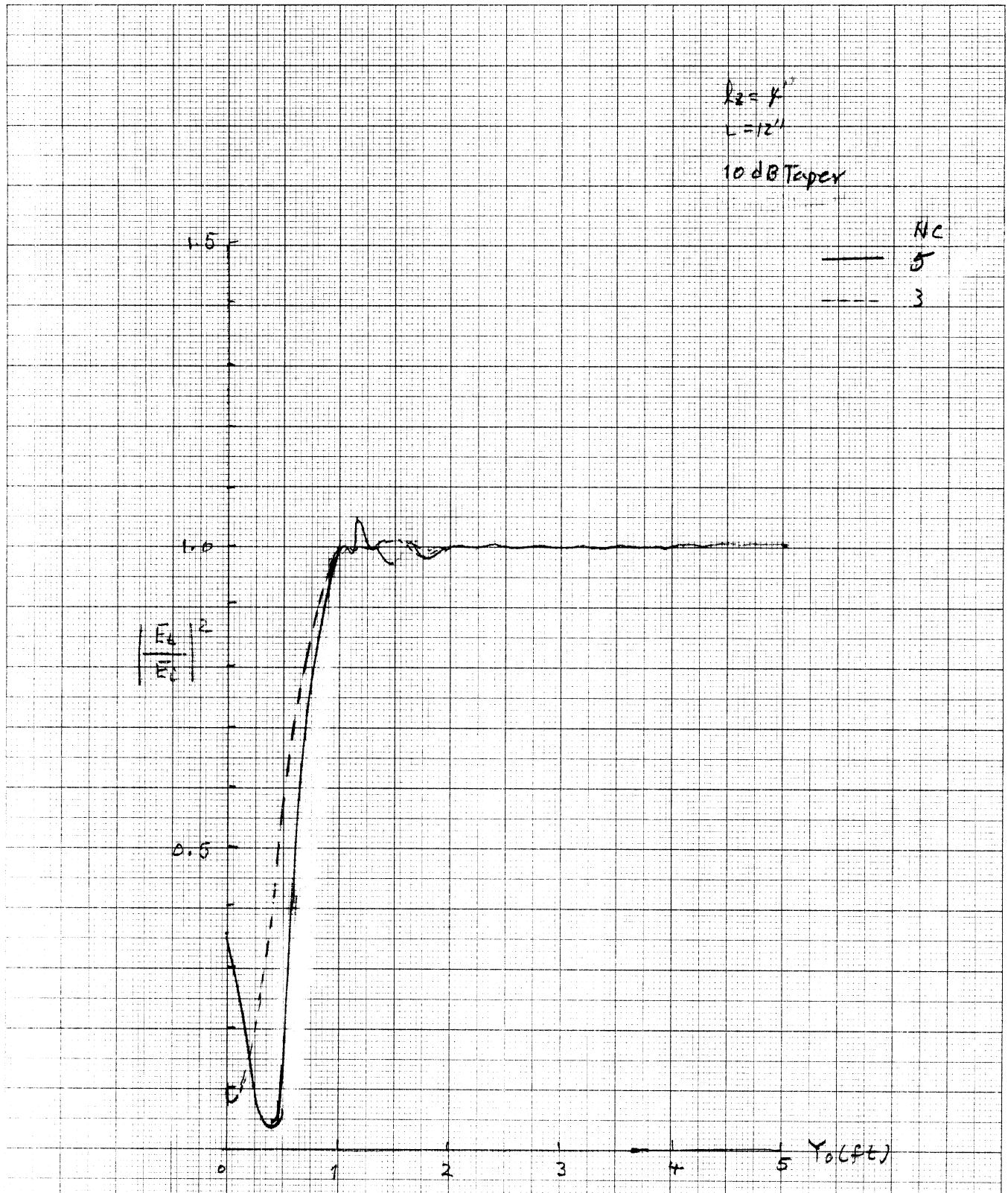

Fig E-11 : Effect of cell sizes on the field variations on $z = 30''$ - plane; $x_0 = 28.54''$. $a = 6''$, $b = 3a''$, $h = 3a''$, $d = \lambda/2$ ft.

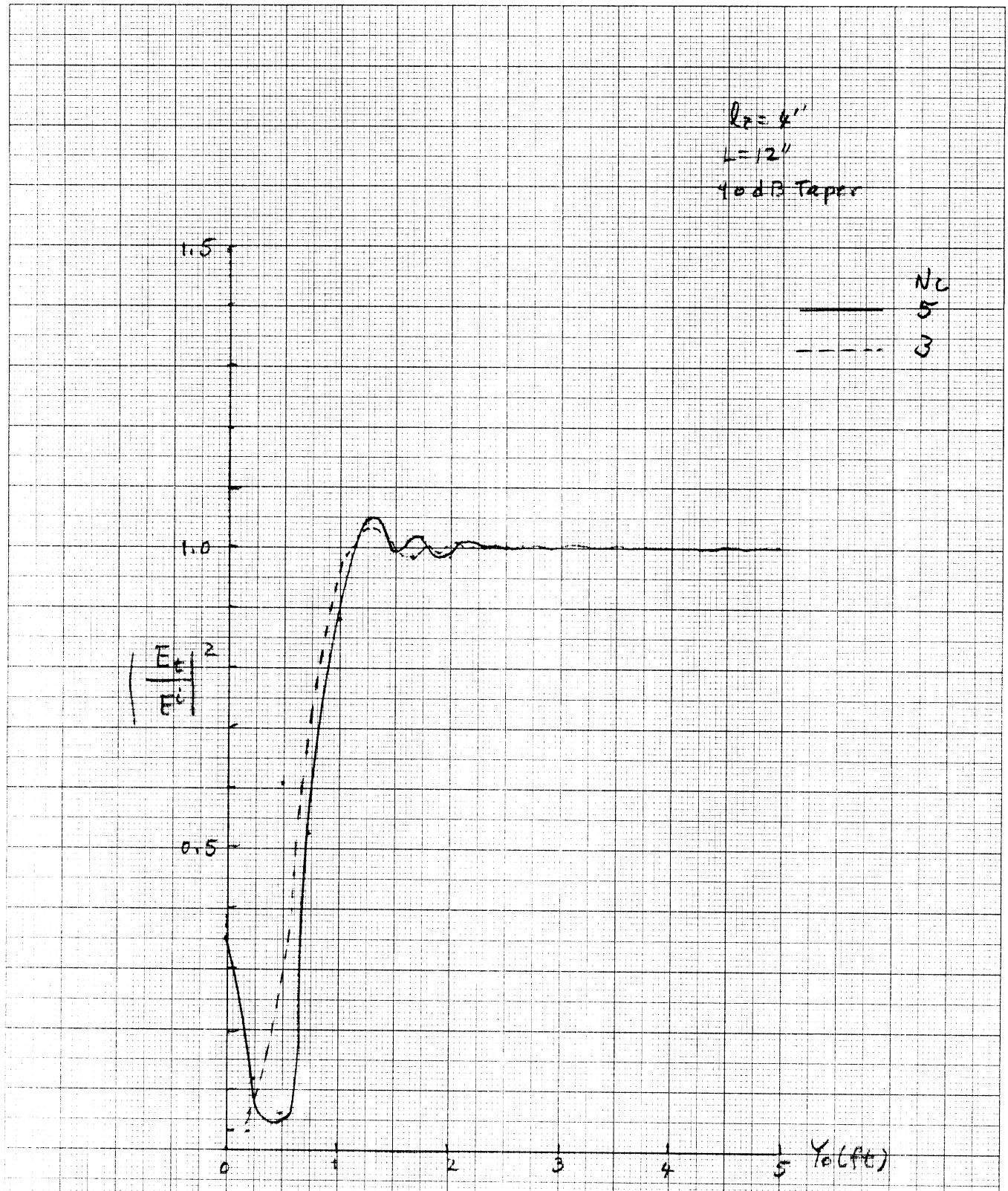

Fig E-12 Effect of Cell Size on Field Variations on $z = 30''$ plane, $X_o = 36''$, $a = 6''$, $b = 30''$, $l_h = 30''$, $d = 10$ ft

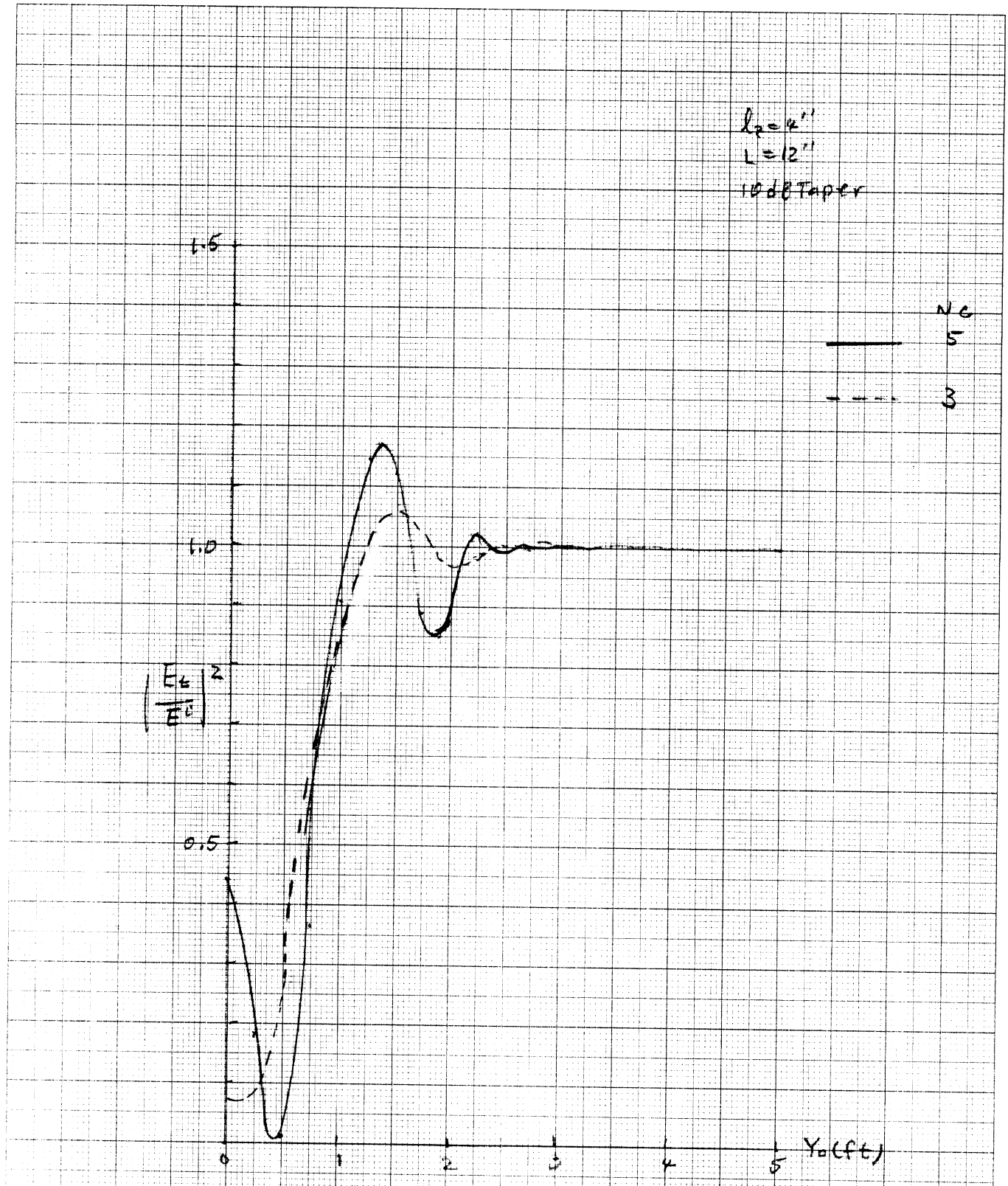

Fig E-13 : Effect of cell sizes on field variations on $z = 30''$ plane, $x_o = 1$ ft. $a = 6''$, $b = 3''$, $h = 30''$, $d = 100$ ft.

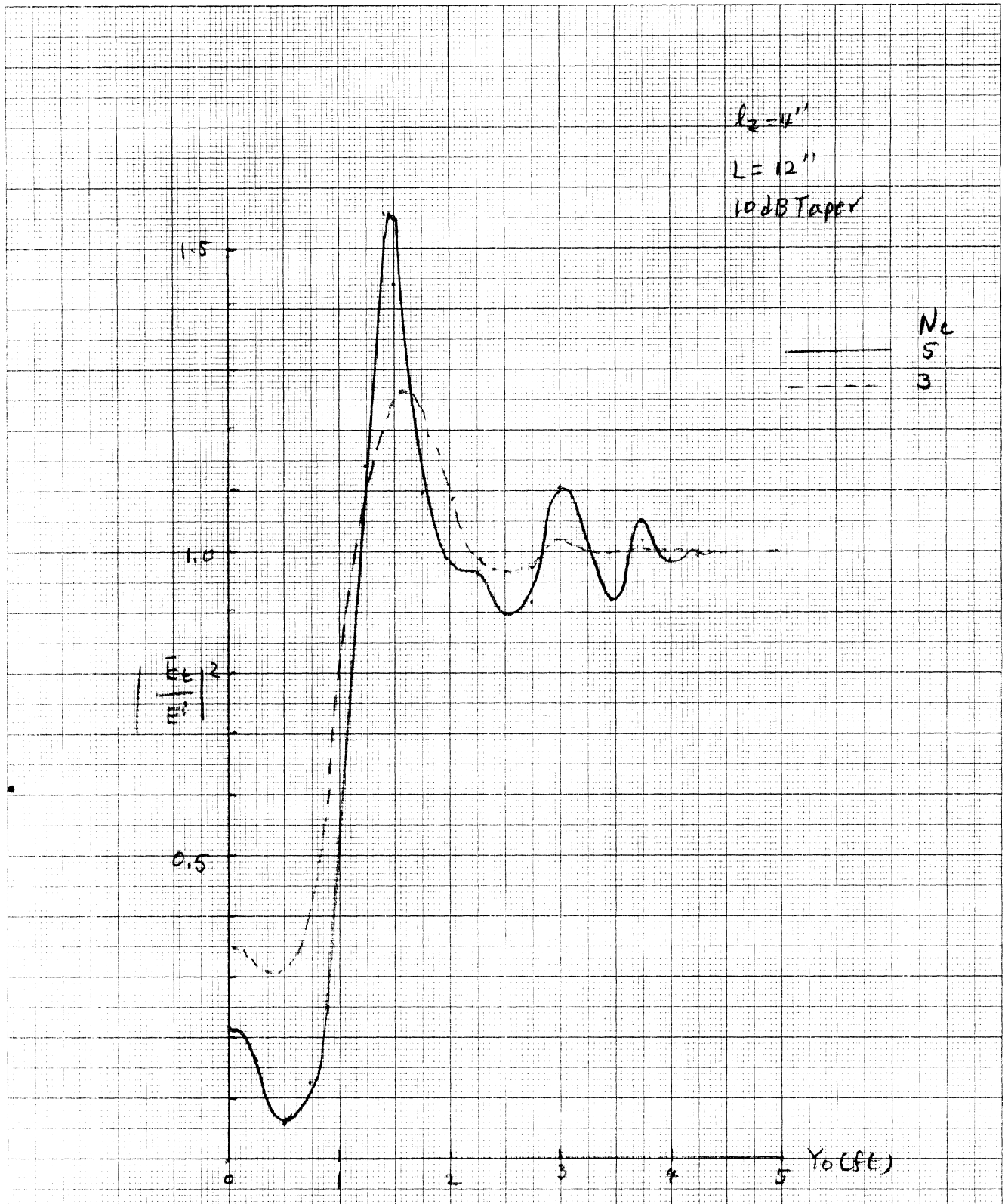

Fig E-14 : Effect of cell sizes on field variations on $z = 30''$-plane, $X_0 = 50$ ft. $a = 6''$, $b = 30''$, $b = 30''$, $d = 100$ ft.

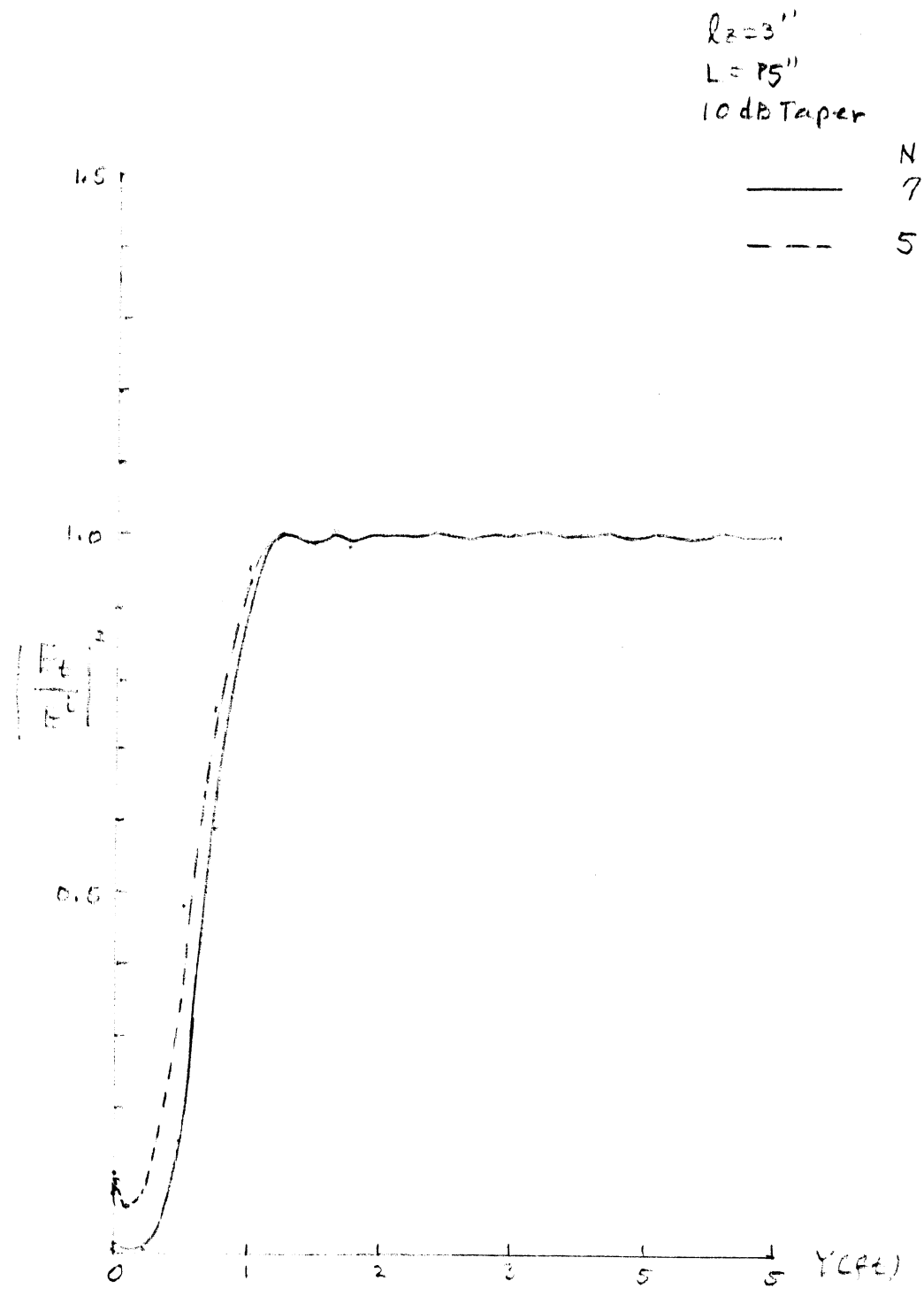

Fig E-15 : Effect of cell sizes of antenna aperture on field variations on z=30" plane, x_0 = 18", a=6", b=36", h=30", d=10ft.

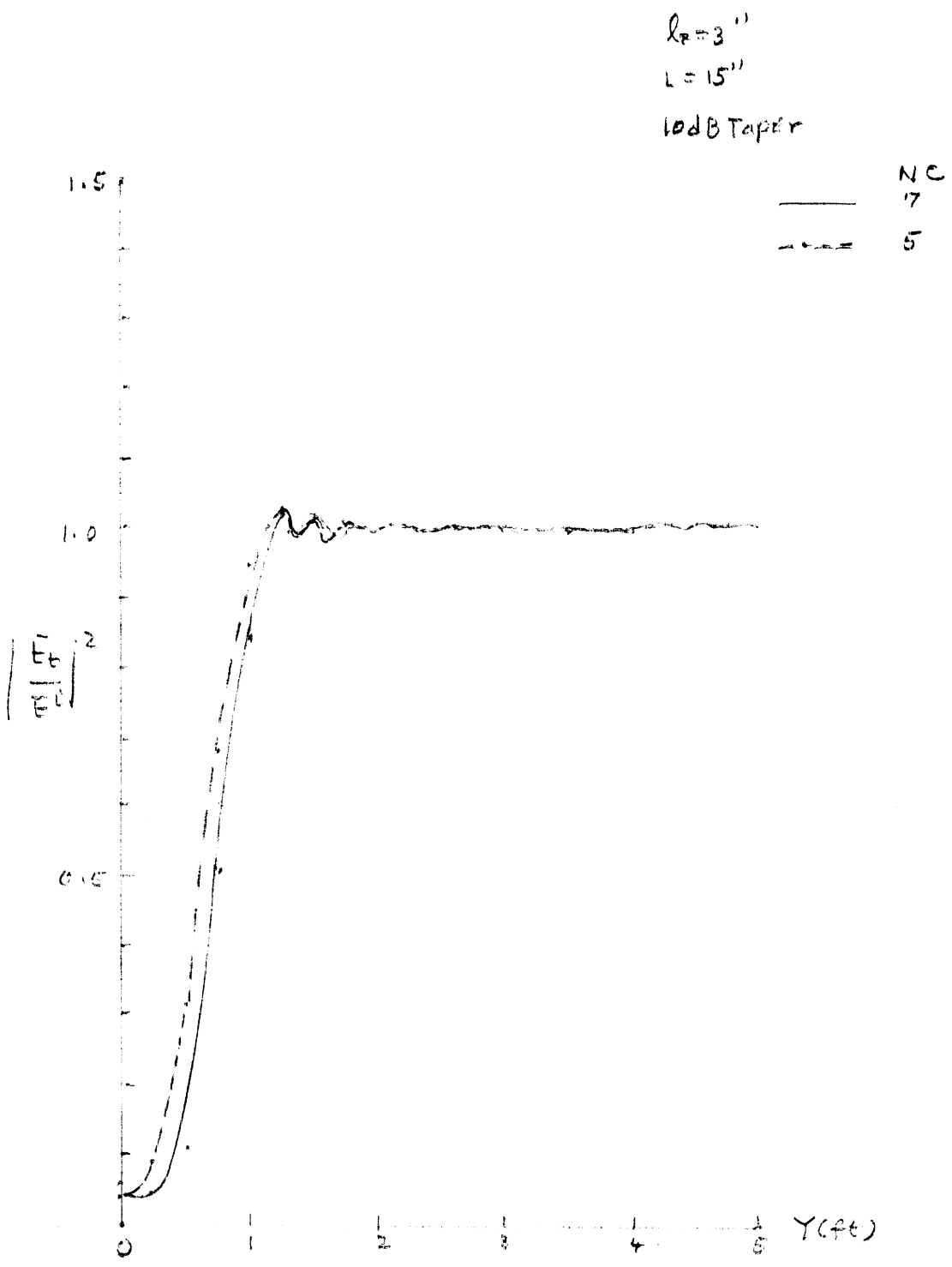

Fig E-16 : Effect of cell size on Field variations on $z = 30''$-plane, $x_0 = 36''$, $a = 6''$, $b = 30''$, $h = 30''$, $d = \infty$ ft.

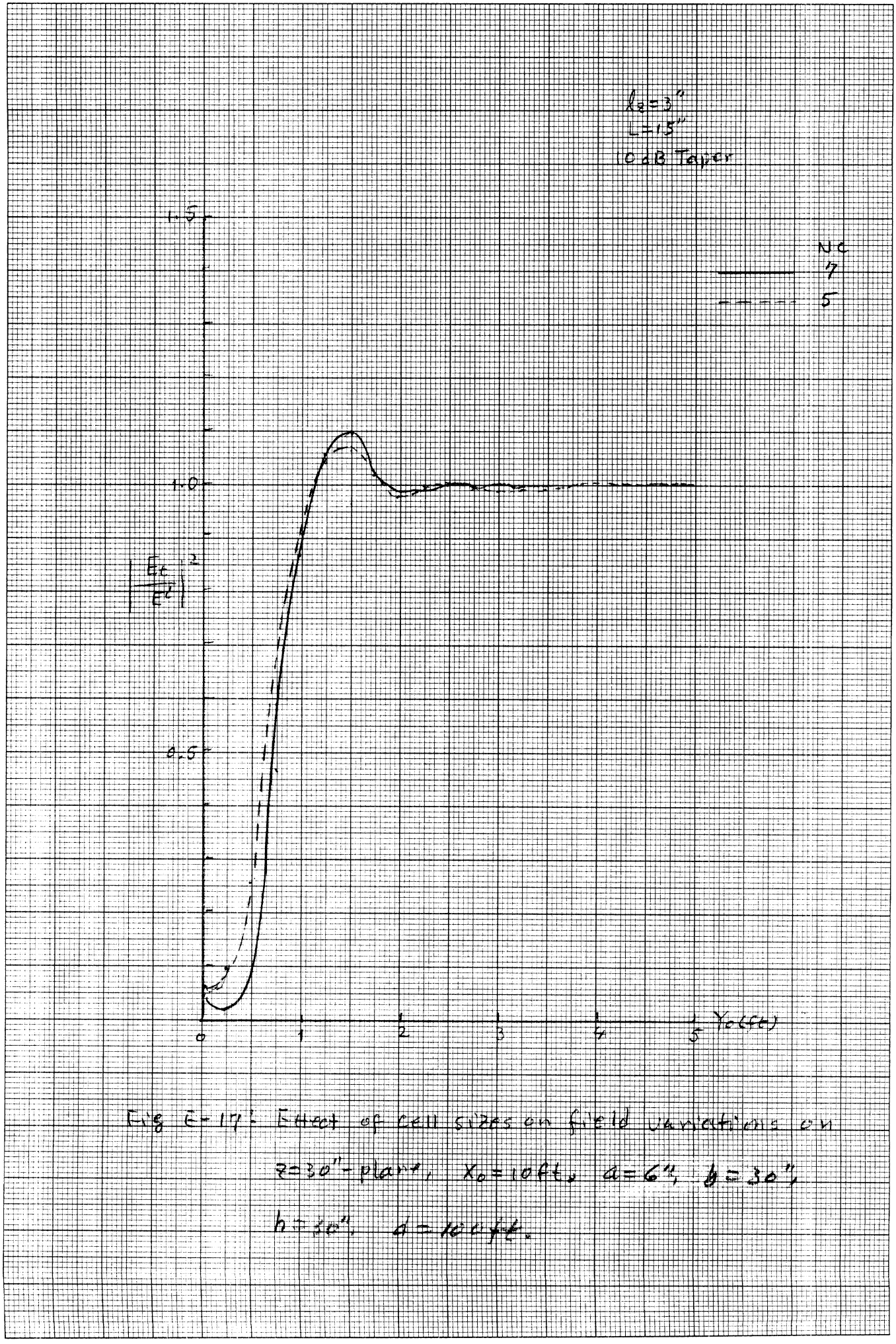

Fig E-17: Effect of cell sizes on field variations on $Z = 30''$ - plane, $X_0 = 10$ ft, $a = 6''$, $b = 30''$, $h = 30''$, $d = 10$ cycles.

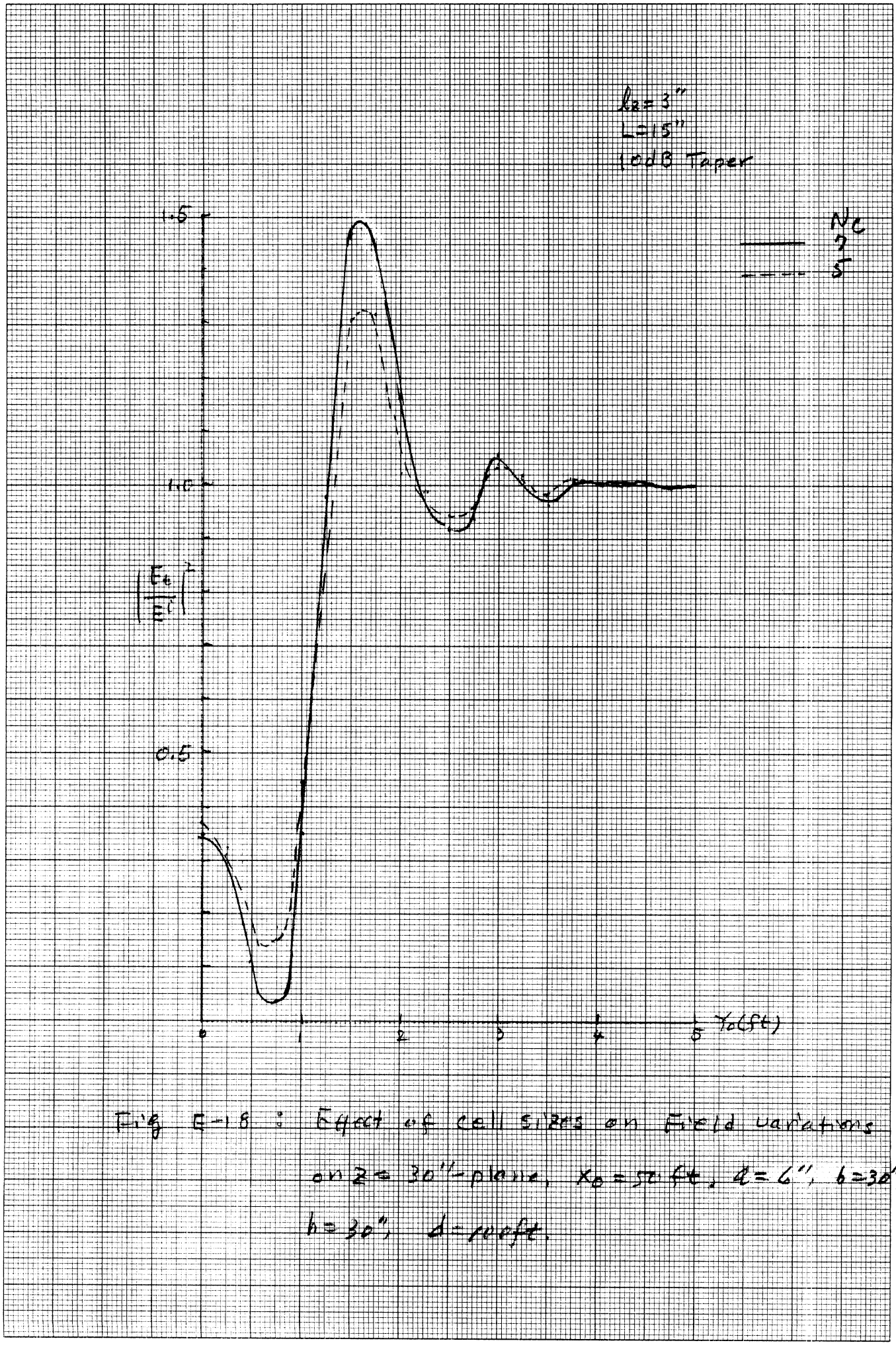

Fig 8 : Effect of cell size on field variations on Z = 30"-plane, $X_0 = 57$ ft, $d = 6''$, $b = 30''$, $h = 30''$, $d = 10$ ft.

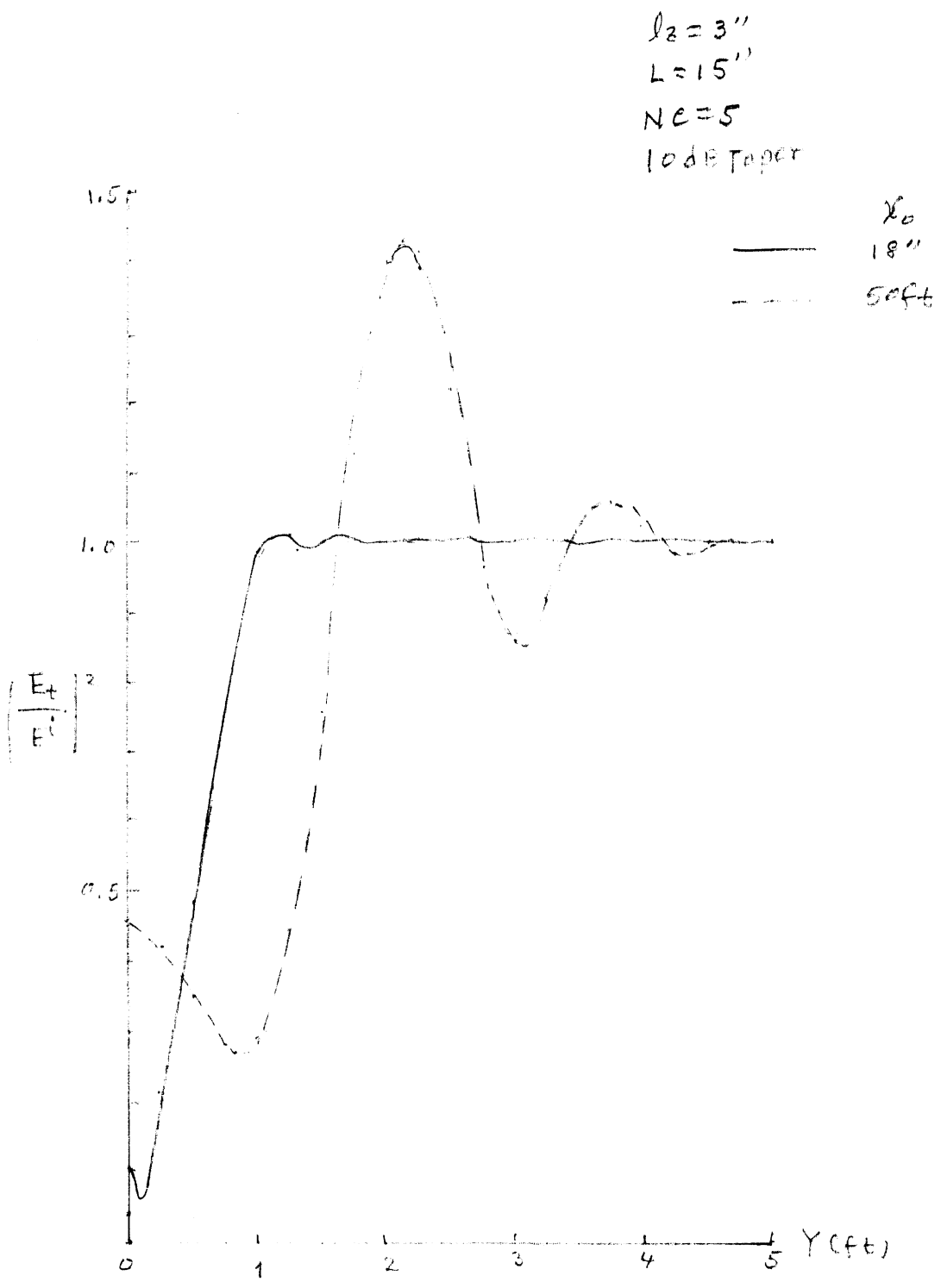

Fig E-19 : Field variations on $z = 30''$ plane, $a = 6''$, $b = 30''$, $h = 30''$, $d = 300$ ft.

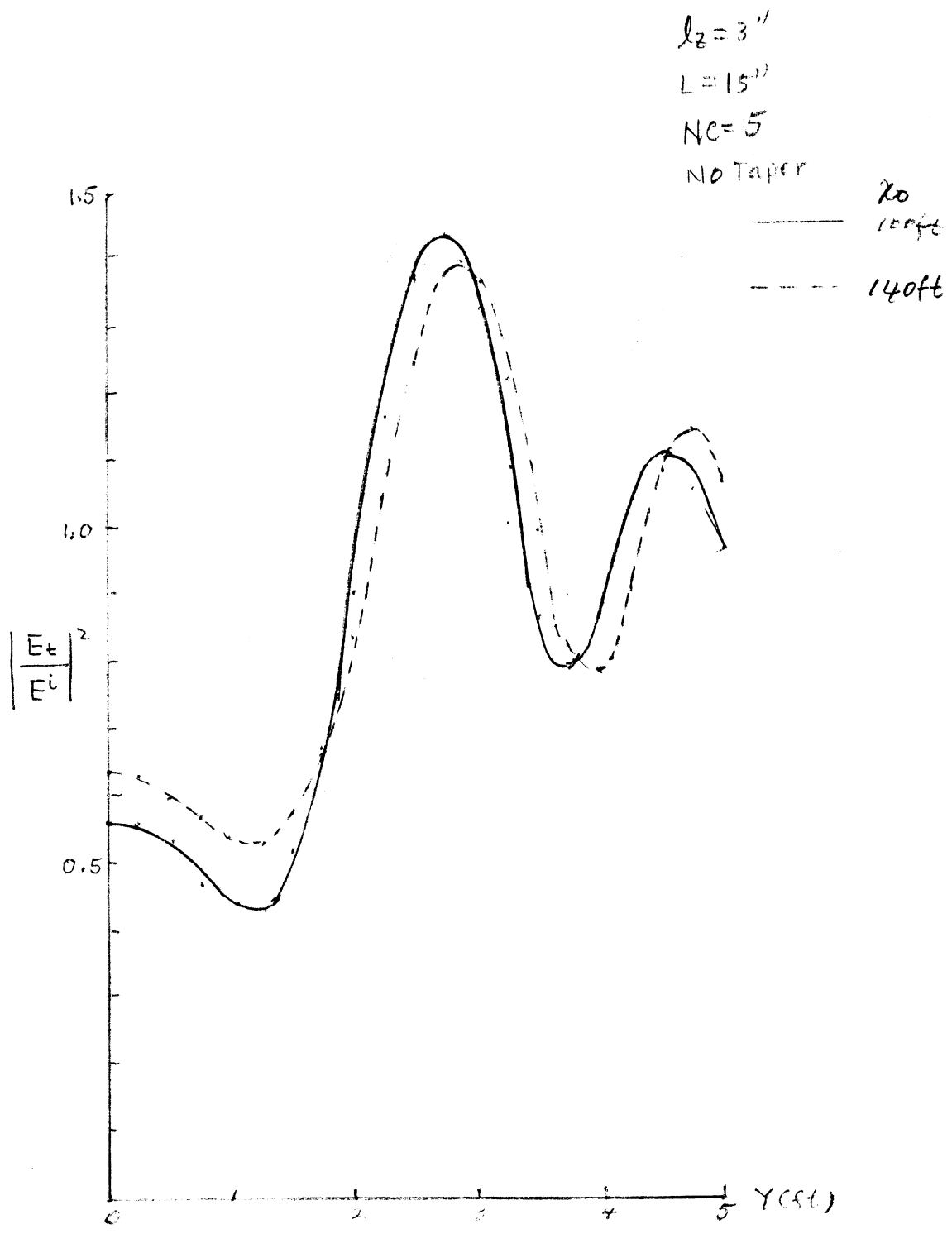

Fig E-20 : Field variations on z=30"-plane, a=6", b=30", h=30", d=300ft.

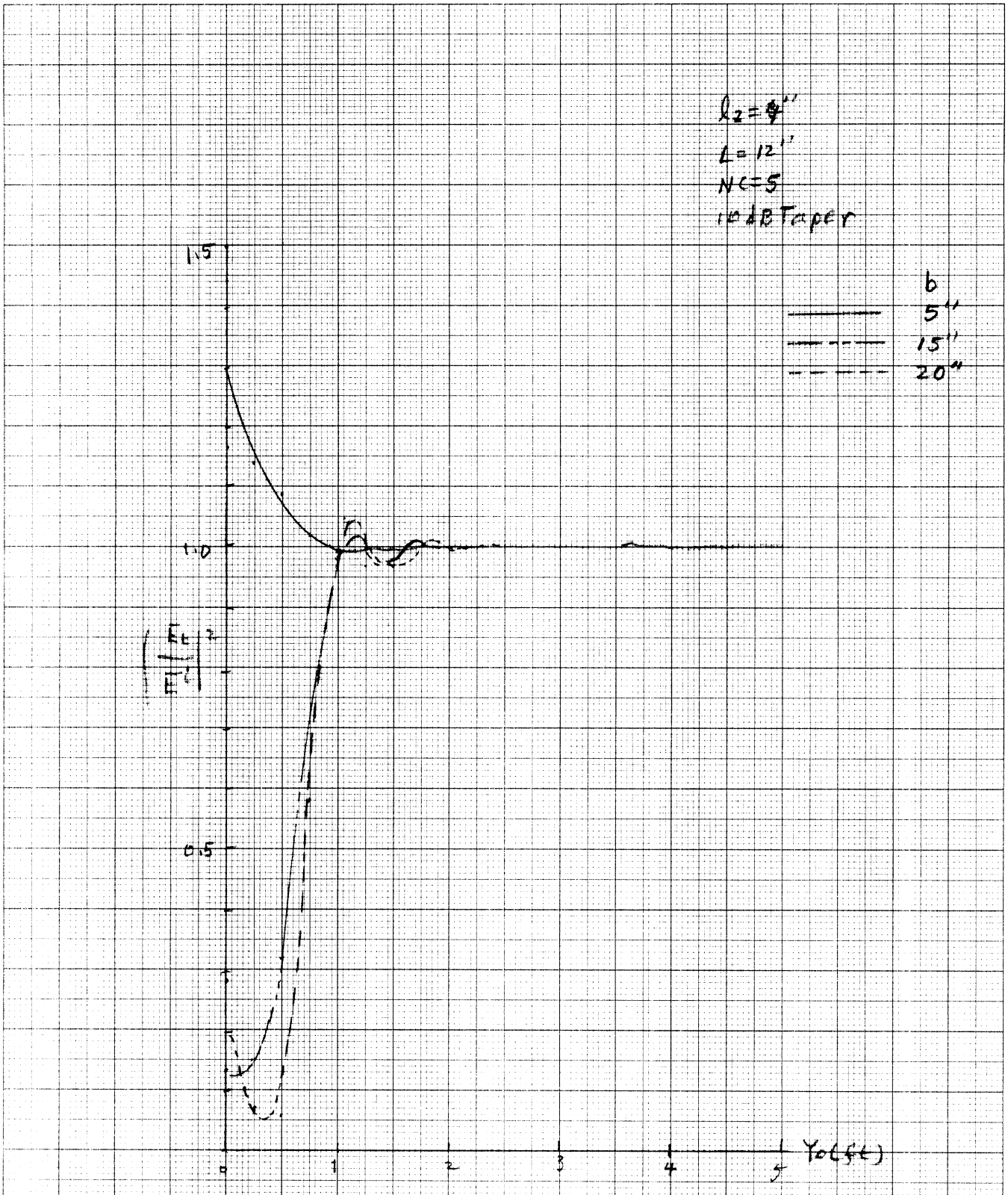

Fig E-2.1 : Field variations on $z = 50''$-plane, $x_o = 28.5''$ for different scattering object heights. $a = 6''$, $h = 30''$, $d = 10$ ft.

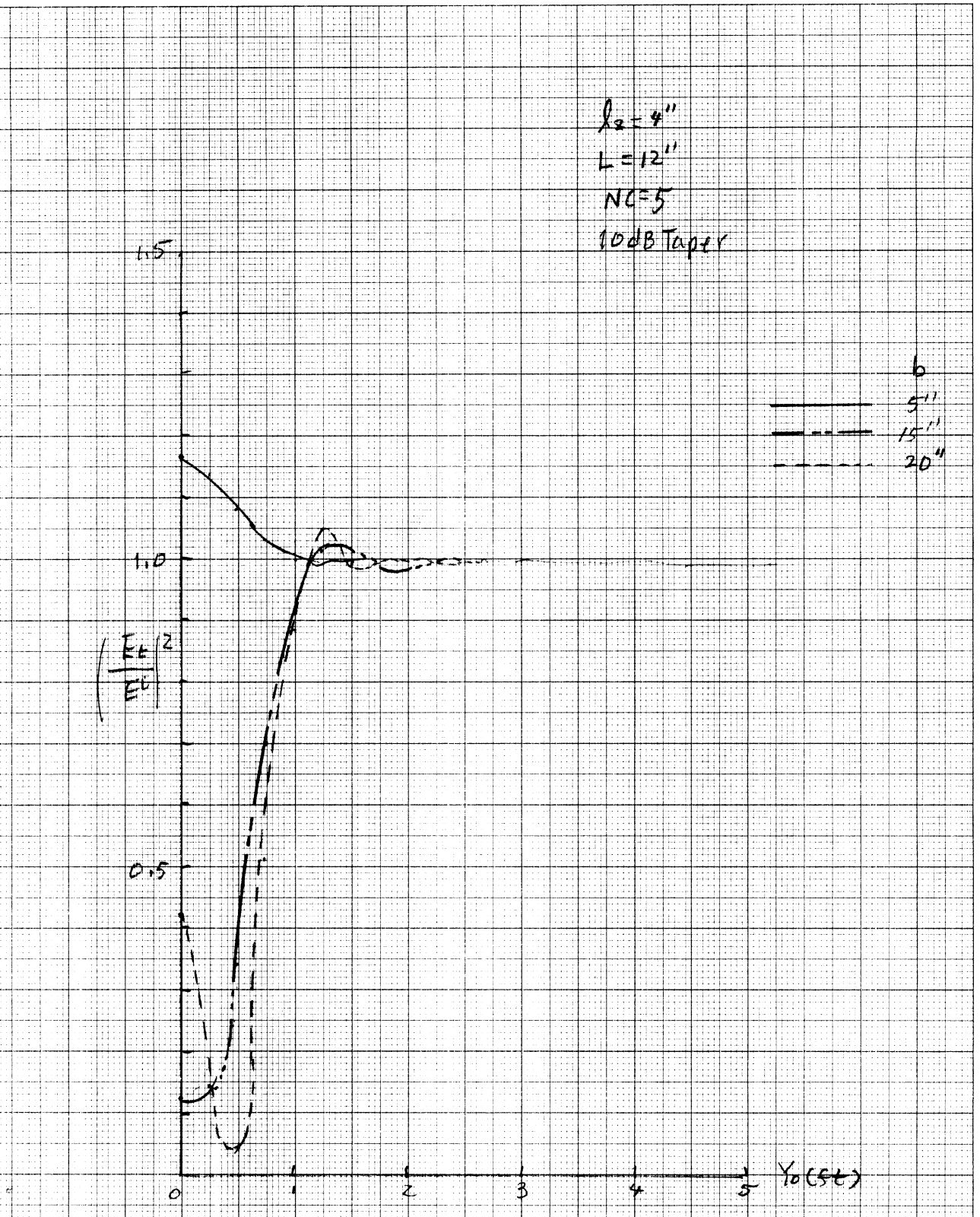

Fig E-24 : Field variations on $z = 30''$-plane, $x_0 = 36''$ for different scattering object heights. $a = 6''$, $h = 30''$, $d = 100$ ft.

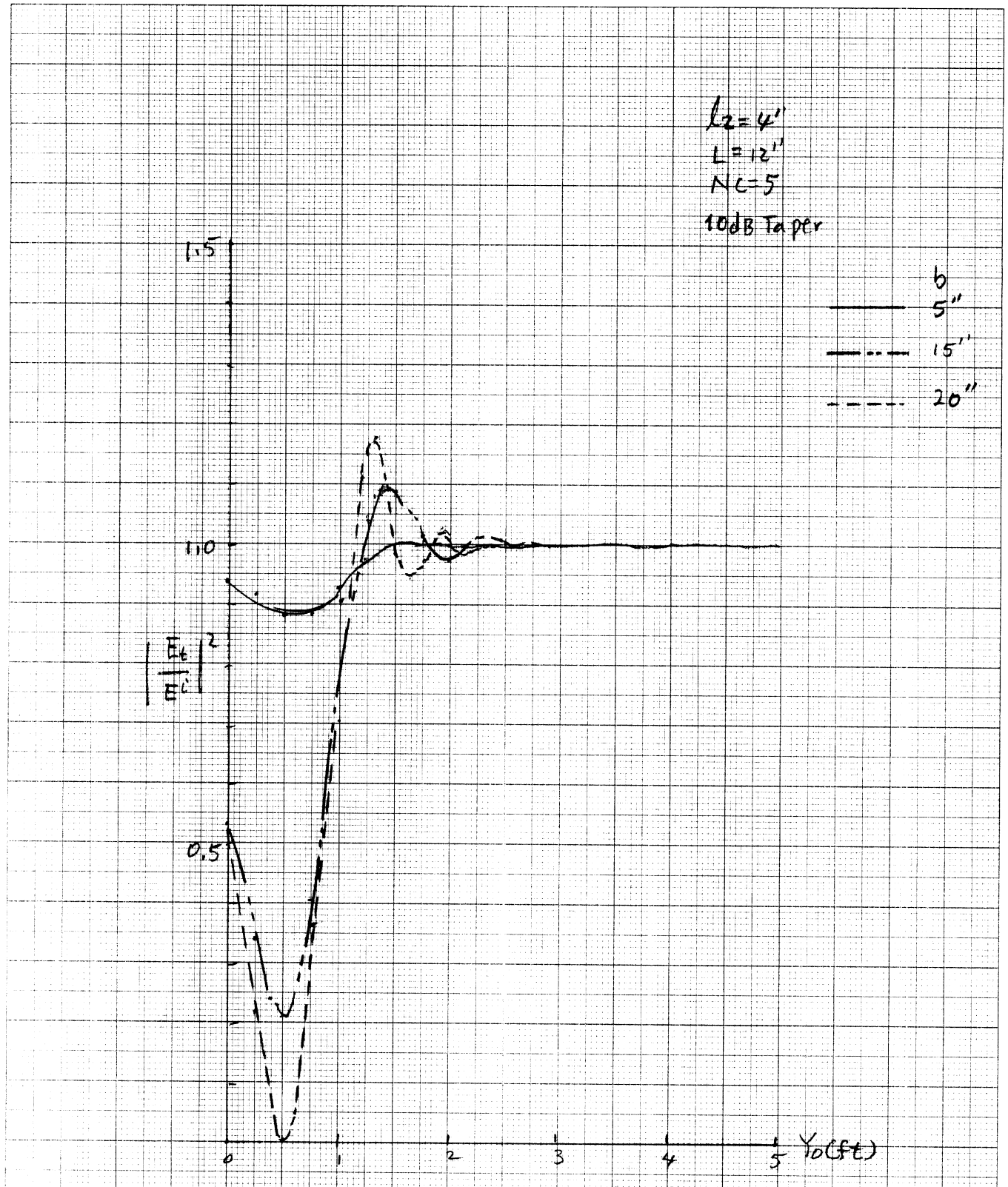

Fig E-23 : Field variations on $z = 30''$-plane, $x_0 = 10$ ft for different scattering object heights.
$a = 6''$, $h = 30''$, $d = 100$ ft.

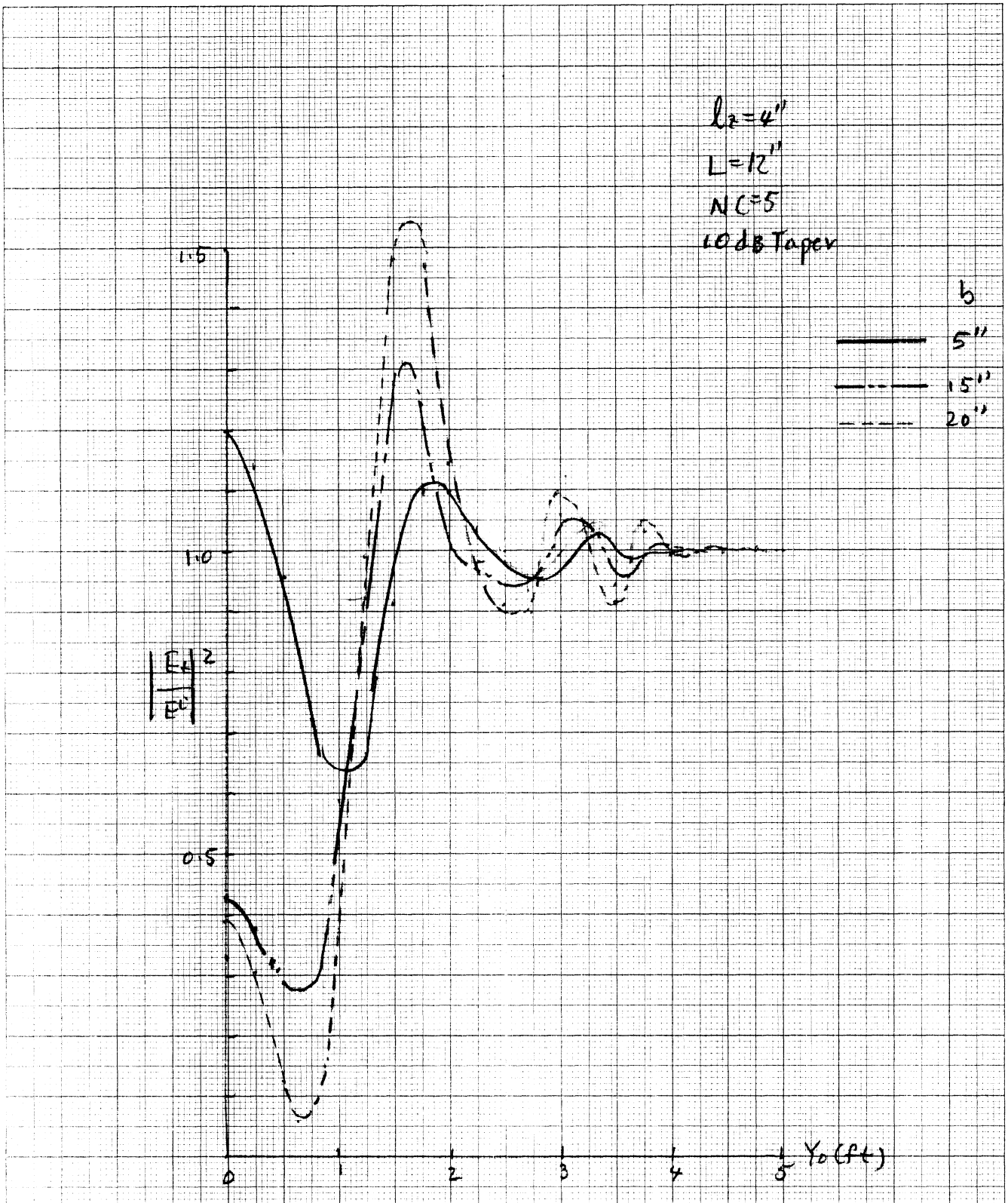

Fig E-24 : Field variations on z = 30'' plane, x_0 = 50ft for different scattering object heights. a = 6'' h = 30'', d = 10 oft.

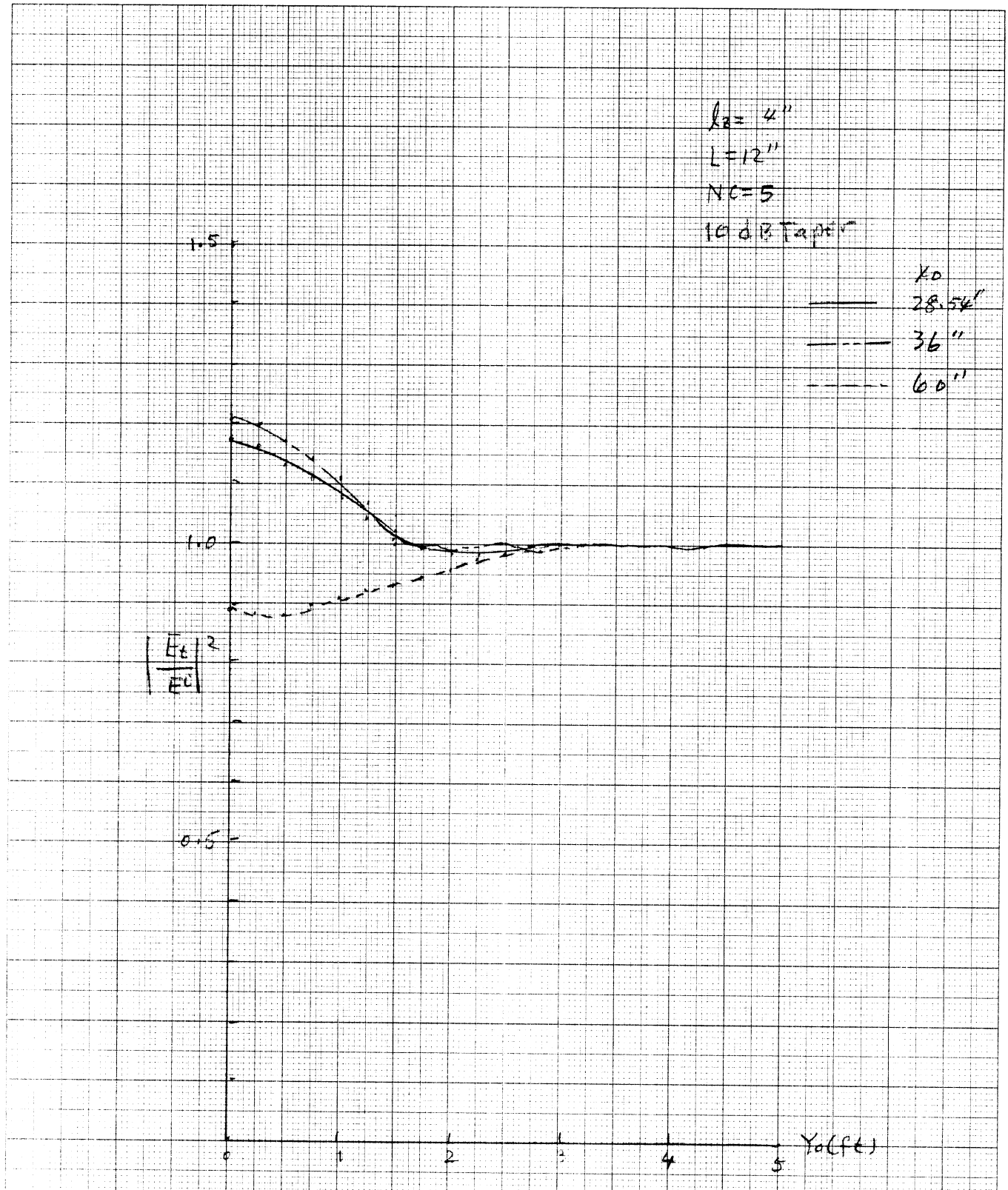

Fig E-25: Field variations for a = 30", b = 6" (a crawling man), h = 30", d = 10 ft.

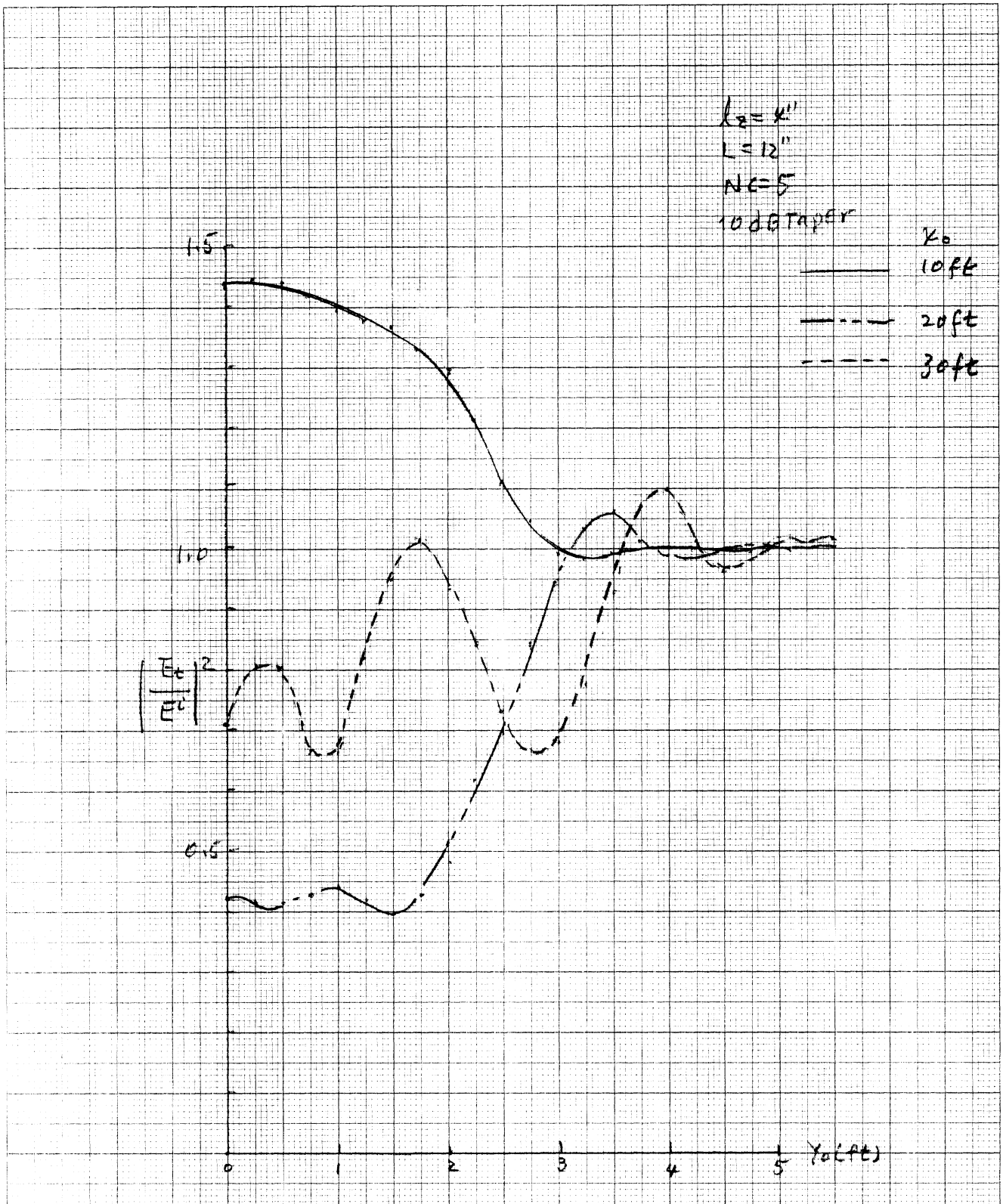

Fig E-26 : Field variation for $a = 30''$, $b = 6''$ (a crawling man), $h = 30''$, $d = 1$ ft.

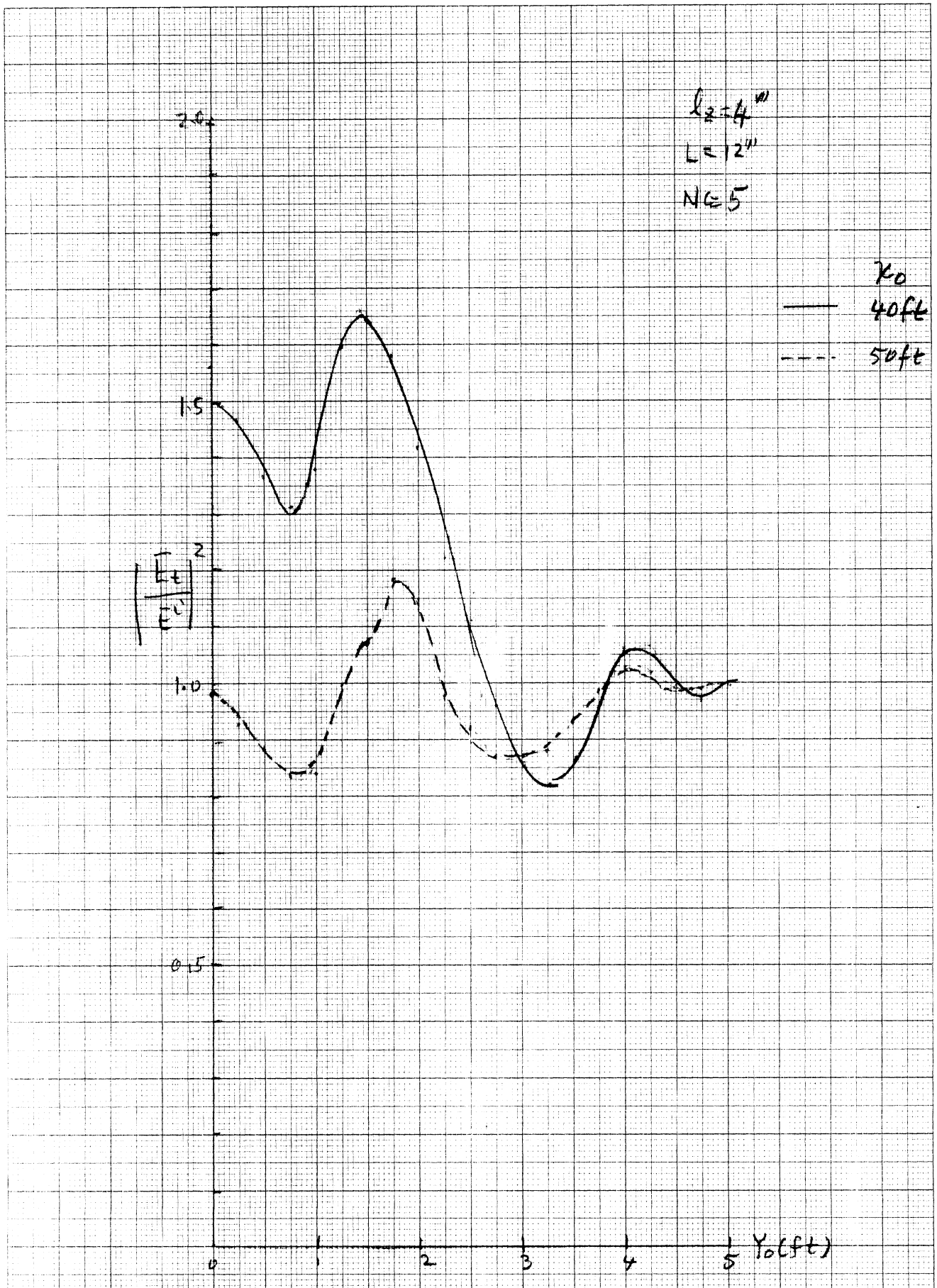

Fig B-27 : Field variations for $a = 30''$, $b = 6''$ (a crawling wall), $h = 30''$, $d = 100$ ft.